

STUDY OF QUANTUM ENTANGLEMENT IN ATOM-PHOTON INTERACTIONS

THESIS SUBMITTED FOR THE DEGREE OF
DOCTOR OF PHILOSOPHY (SCIENCE)
OF THE
JADAVPUR UNIVERSITY



Biplab Ghosh

SATYENDRANATH BOSE NATIONAL CENTRE
FOR BASIC SCIENCES
JD BLOCK, SECTOR III, SALT LAKE CITY
KOLKATA 700 098, INDIA

2007

CERTIFICATE FROM THE SUPERVISORS

This is to certify that the thesis entitled **Study of quantum entanglement in atom-photon interactions** submitted by **Biplab Ghosh**, who got his name registered on **January 13, 2006** for the award of **Ph.D. (Science) degree** of **Jadavpur University**, is absolutely based upon his own work under the supervision of **Dr. Archan S. Majumdar and Dr. Nilkantha Nayak** at **S. N. Bose National Centre For Basic Sciences, Kolkata, India** and that neither this thesis nor any part of it has been submitted for any degree/diploma or any other academic award anywhere before.

Archan S. Majumdar (Reader),
Satyendranath Bose National Centre For Basic Sciences,
JD Block, Sector III, Salt Lake, Kolkata 700 098, India.
Date :

Nilkantha Nayak (Associate Professor),
Satyendranath Bose National Centre For Basic Sciences,
JD Block, Sector III, Salt Lake, Kolkata 700 098, India.
Date :

Acknowledgments

First and foremost I would like to thank my supervisors, Dr. Archan S. Majumdar and Dr. Nilkantha Nayak for their constant guidance, encouragement and support and also for giving me the freedom to investigate topics that truly inspired me. They have been always more than a guide to me.

I would like to thank also Dr. Guruprasad Kar for helpful discussions.

My sincere thanks go to all faculty members of S. N. Bose Centre for their help and discussions throughout this research period.

I am thankful to my friends Debabrata, Mrinal, Malay, Suman, Jayee, Subarna and my seniors Manirul-da, Abhishek-da, Sibasish-da for their help and discussions. My heartiest thanks goes to my friends, seniors and juniors who made my stay at S. N. Bose Centre colourful and enjoyable. I wish to thank all the staff members of this centre for their sincere cooperation and help.

I am grateful to my parents, wife, brother and all of my friends for their constant encouragement and their sacrifice.

Biplab Ghosh

Satyendranath Bose National Centre For Basic Sciences,
JD Block, Sector III, Salt Lake, Kolkata 700 098, India.

List of Publications

1. **Information transfer through a one-atom micromaser**
A. Datta, Biplab Ghosh, A. S. Majumdar and N. Nayak
Europhys. Lett. **67**, 934 (2004).
2. **Information transfer in leaky atom-cavity systems**
Biplab Ghosh, A. S. Majumdar and N. Nayak
Int. J. Quant. Inf. **4**, 665 (2006).
3. **Environment assisted entanglement enhancement**
Biplab Ghosh, A. S. Majumdar and N. Nayak
Physical Review A **74**, 052315 (2006).
4. **Quantum Information transfer in atom-photon interactions in a cavity**
A. S. Majumdar, N. Nayak and Biplab Ghosh
in *Current Topics in Atomic, Molecular and Optical Physics* eds. C. Sinha and S. Bhattacharayya (World Scientific, 2007 p 143).
5. **Effects of cavity-field statistics on atomic entanglement in the Jaynes-Cummings model**
Biplab Ghosh, A. S. Majumdar and N. Nayak
Int. J. Quant. Inf. **5**, 169 (2007).
6. **Atomic entanglement mediated by a squeezed cavity field**
Biplab Ghosh, A. S. Majumdar and N. Nayak
International Journal of Theoretical Physics, Group Theory and Nonlinear Optics ,
12 Issue 2 (2007).
7. **Control of atomic entanglement by dynamic Stark effect**
Biplab Ghosh, A. S. Majumdar and N. Nayak
quant-ph/0708.0770.

Contents

1	Introduction	1
1.1	Quantum entanglement	1
1.2	Criteria for entanglement	2
1.2.1	Schmidt number	5
1.2.2	Partial transposition	6
1.2.3	Bell's inequality	7
1.3	Quantification of entanglement	9
1.3.1	von Neumann entropy	10
1.3.2	Concurrence and Entanglement of formation	11
1.4	Decoherence and its effect on Entanglement	13
1.5	Plan	14
2	Entanglement in the Jaynes-Cummings model with dissipation	19
2.1	The Jaynes-Cummings model	19
2.1.1	The energy eigenstates of the Jaynes-Cummings Hamiltonian	23
2.1.2	Various atom-field evolved states under the Jaynes-Cummings interaction	24
2.2	Dissipative dynamics	25
2.2.1	A model solution	26
2.3	Various types of entanglement and the effect of cavity dissipation on them	30
2.3.1	Atom-cavity entanglement	31
2.3.2	Atom-atom entanglement	34
2.3.3	Cavity-cavity entanglement	37
2.4	Summary	40
3	Quantum entanglement in the micromaser	42
3.1	Introduction	42
3.1.1	The experimental scenario	43
3.2	Micromaser dynamics	44

3.2.1	Steady state photon distribution	46
3.3	The generation of atomic entanglement	47
3.3.1	The entanglement of formation of two successive atoms	47
3.3.2	Information transfer in the micromaser	50
3.4	Summary	52
4	Curious features of entanglement: a quantitative study	54
4.1	Introduction	54
4.2	Monogamy of entanglement in a system of two cavities and a single atom .	56
4.2.1	Pure state of three qubits	56
4.2.2	Effects of cavity dissipation on entanglement	61
4.3	Monogamy of entanglement in a system of two maximally entangled atoms and a single cavity	66
4.3.1	Pure state of three qubits	66
4.3.2	Effects of cavity dissipation on entanglement	69
4.4	Entanglement swapping in a system of two cavities and two atoms	73
4.4.1	Ideal case of four qubits	73
4.4.2	Information transfer with cavity dissipation	75
4.5	Summary	78
5	Effects of cavity field statistics on entanglement	80
5.1	Introduction	80
5.2	Cavity field statistics and atomic entanglement	81
5.2.1	Fock state cavity field	82
5.2.2	Thermal state cavity field	84
5.2.3	Coherent state cavity field	86
5.3	Effects of squeezing on entanglement	91
5.4	Summary	95
6	Environment induced entanglement	99
6.1	Introduction	99
6.2	Enhancement of entanglement in tripartite systems	100

6.2.1	A two-level atom interacting with one of two maximally entangled cavities	100
6.2.2	A single cavity and two two-level atoms	104
6.3	The one-atom micromaser	106
6.4	Summary	109
7	Conclusions	110
	Appendix	114
	Bibliography	116

List of Figures

1.1	Two particles A and B are emitted from a common source S	3
1.2	Schematic experiment for Bell's inequality. Alice can choose to measure either Q or R , and Bob can choose to measure either S or T . They perform their measurement simultaneously. Alice and Bob are assumed to be far apart that performing a measurement on one system can not have any effect on the result of the measurements on the other.	7
2.1	A two-level atom-photon interaction.	19
2.2	A two-level atom taken from the lower to the upper state with the absorption of a photon. It is the term σ^+a	22
2.3	A two-level atom taken from the upper to the lower state with the emission of a photon. It is the term σ^-a^\dagger	22
2.4	A two-level atom taken from the lower to the upper state with the emission of a photon. It is the term σ^+a^\dagger	22
2.5	A two-level atom taken from the upper to the lower state with the absorption of a photon. It is the term σ^-a	22
2.6	A two-level atom prepared in the excited state is traversing through an empty cavity.	31
2.7	Atom-cavity entanglement i.e., concurrence is plotted vs gt	32
2.8	Atom-cavity entanglement i.e., concurrence is plotted vs gt for (i) $\kappa/g = 0.05$ (solid line), (ii) $\kappa/g = 0.1$ (dashed line).	33
2.9	Two two-level atoms, first prepared in the excited state and second prepared in the ground state, traverses an empty cavity one after the other.	34
2.10	Atom-atom entanglement i.e., concurrence is plotted vs gt	36
2.11	Atom-atom entanglement i.e., concurrence is plotted vs gt for (i) $\kappa/g = 0.05$ (solid line) (ii) $\kappa/g = 0.1$ (dashed line).	37

2.12	A two-level atom prepared in the excited state is traversing through two separated cavities one after another.	37
2.13	Cavity-cavity entanglement i.e., concurrence is plotted vs gt	39
2.14	Cavity-cavity entanglement i.e., concurrence is plotted vs gt for (i) $\kappa/g = 0.05$ (solid line) (ii) $\kappa/g = 0.1$ (dashed line).	40
3.1	Atom-atom entanglement i.e., E_F is plotted vs micromaser pump parameter $D = gt\sqrt{N}$ for different values of n_{th} . $\kappa/g = 0.000001$, $N = 1$	49
3.2	Atom-atom entanglement i.e., E_F is plotted vs κ/g for different values of the micromaser pump parameter $D = gt\sqrt{N}$. $n_{th} = 0.01$, $N = 1$	49
3.3	Variance of the photon number distribution of the cavity (V) is plotted vs micromaser pump parameter $D = gt\sqrt{N}$. $\kappa/g = 0.001$ and $n_{th} = 0.01$, $N = 1$	50
3.4	Atom-atom entanglement i.e., E_F (solid line) and difference of the Shannon entropies i.e. $(S\rho_f^{(2)}) - S(\rho_f^{(ss)})/10$ (dashed line) are plotted versus micromaser pump parameter $D = gt\sqrt{N}$. $\kappa/g = 0.001$ and $n_{th} = 0.01$, $N = 1$	51
4.1	The passage of atom B_1 through the cavities C_1 and C_2 successively with different interaction times such as $gt = \pi/4$ and $gt = \pi/2$ respectively.	57
4.2	Two maximally entangled cavities	58
4.3	A two-level Rydberg atom prepared in the ground state is passing through the one of the maximally entangled cavities C_1	58
4.4	$C(\rho(t)_{C_1C_2})$ (solid line), $C(\rho(t)_{C_2A_1})$, (dotted line), $C(\rho_{C_1A_1})$ (broken line) plotted with respect to the Rabi angle gt	61
4.5	$C(\rho(t)_{C_1C_2})$ (solid line), $C(\rho(t)_{C_2A_1})$, (dotted line), $C(\rho(t)_{C_1A_1})$ (broken line) plotted with respect to the Rabi angle gt . $\frac{\kappa_1}{g} = \frac{\kappa_2}{g} = 0.1$	64
4.6	$C_{C_2C_1}^2 + C_{C_2A_1}^2$ (solid line), $C_{C_2(C_1A_1)}^2$ (dotted line) plotted with respect to the Rabi angle gt	65
4.7	$C(\rho(t)_{A_1C_1})$ (solid line) for $gt = \pi/4$, $C(\rho(t)_{A_1C_1})$ (broken line) for $gt = 3\pi/4$, $C(\rho(t)_{A_1C_1})$, (dotted line) for $gt = 5\pi/4$ plotted with respect to $\log(\kappa/g)$, where $\kappa/g = \kappa_1/g = \kappa_2/g$	65
4.8	Two maximally entangled atoms.	66
4.9	One of the maximally entangled atoms A_1 is passing through the cavity C_1	67

4.10	$C(\rho(t)_{A_1A_2})$ (solid line), $C(\rho(t)_{A_2C_1})$, (dotted line), $C(\rho_{A_1C_1})$ (broken line) plotted with respect to the Rabi angle gt	69
4.11	$C(\rho(t)_{A_1A_2})$ (solid line), $C(\rho(t)_{A_2C_1})$, (dotted line), $C(\rho_{A_1C_1})$ (broken line) plotted with respect to the Rabi angle gt . $\kappa/g = 0.1$	72
4.12	$C_{A_1A_2}^2 + C_{A_2C_1}^2$ (solid line), $C_{A_2(A_1C_1)}^2$ (dotted line) plotted with respect to the Rabi angle gt	72
4.13	Two Rydberg atoms A_1 , A_2 prepared in the ground states g_1 , g_2 pass through two maximally entangled cavities C_1 , C_2 respectively.	74
4.14	$C(\rho(t)_{C_1C_2})$ (solid line), $C(\rho(t)_{A_1A_2})$, (dotted line) plotted with respect to the Rabi angle gt	76
4.15	$C(\rho(t)_{C_1C_2})$ (solid line), $C(\rho(t)_{A_1A_2})$, (dotted line) plotted with respect to the Rabi angle gt . $\kappa_1/g = \kappa_2/g = 0.1$	78
5.1	Atom-atom entanglement versus gt . Solid line, dotted line, and dashed line indicate E_F between two atoms when the cavity Fock states are $n = 0$, $n = 10$, and $n = 100$ respectively.	83
5.2	Thermal field distribution function P_n is plotted vs photon number n when (i) average photon number $\langle n \rangle = 0.3$ (solid line), (ii) $\langle n \rangle = 0.5$ (dotted line) and (iii) $\langle n \rangle = 0.7$ (dashed line).	85
5.3	Atom-atom entanglement of formation mediated by the thermal cavity field is plotted versus gt	86
5.4	Coherent field distribution function P_n is plotted vs photon number n when (i) average photon number $\langle n \rangle = 50$ (solid line), (ii) $\langle n \rangle = 100$ (dotted line) and (iii) $\langle n \rangle = 150$ (dashed line).	87
5.5	Two-atom entanglement mediated by the coherent state cavity field at low average photon number is plotted versus gt	89
5.6	Atom-atom entanglement mediated by coherent state cavity field at high average photon number is plotted versus gt	90
5.7	Atom-atom entanglement mediated by coherent state cavity field in the Tavis-Cummings model is plotted vs gt for average photon number (i) $\langle n \rangle = 100$ (solid line), (ii) $\langle n \rangle = 200$ (dotted line), and (iii) $\langle n \rangle = 300$ (dashed line).	90
5.8	Probability distribution function P_n is plotted vs n for (i) sub-Poissonian field (solid line) (ii) super-Poissonian field (dotted line) (iii) coherent state field (dashed line).	92

5.9	Atom-atom entanglement of formation mediated by the squeezed field for different values of α is plotted versus gt for the low photon number case.	93
5.10	E_F mediated by the squeezed field is plotted versus gt for different values of the squeezing parameter r corresponding to the low average photon number case.	94
5.11	E_F mediated by squeezed field for different values of α is plotted versus gt for the high average photon number case.	94
5.12	Atom-atom entanglement mediated by (i) squeezed cavity field (dotted line) when $\langle n \rangle = 0.3$ and $r = 0.5$, and (ii) coherent state field (dashed line) when $\langle n \rangle = 0.3$, plotted vs gt	96
5.13	Atom-atom entanglement mediated by (i) squeezed cavity field (dashed line) for $\langle n \rangle = 50$ and $r = 1$, and (ii) coherent state field (solid line) for $\langle n \rangle = 50$ plotted vs gt	96
5.14	Atom-atom entanglement mediated by squeezed cavity field for (i) $\langle n \rangle = 0.5$ and $r = 0.5$ (solid line), (ii) $\langle n \rangle = 0.5$ and $r = 0$ (dashed line), and (iii) $\langle n \rangle = 0.5$ and $r = -0.5$ (dotted line) plotted vs gt	97
6.1	A two-level Rydberg atom prepared in the ground state is passing through one of two maximally entangled cavities C_1 (same as Figure 4.3)	101
6.2	Two two-level atoms, the first prepared in the excited state and the second prepared in the ground state, traverse an empty cavity one after the other (same as Figure 2.9).	104
6.3	The two-atom concurrence $C_{A_1A_2}$ is plotted versus the κ/g for the atom-field interaction time (i) $gt = 5\pi/2$ (solid line) (ii) $gt = 7\pi/2$ (dotted line) (iii) $gt = 9\pi/2$ (dashed line).	106
6.4	The two-atom concurrence $C_{A_1A_2}$ is plotted versus the Rabi angle gt for various values of the cavity leakage parameter κ . Here we choose $N = 1$ and $\bar{n}_{th} = 0.033$	108

List of Tables

6.1	Steady state photon statistics for the micromaser with the parameter values $n_{th} = 0.033$, $N = 1$, and $gt = 3\pi/4$	107
-----	--	-----

Chapter 1

Introduction

1.1 Quantum entanglement

In 1935 Einstein, Podolsky and Rosen [1] (EPR) presented a paradox that still baffles and surprises us today. They proposed the following two “reasonable” criteria as the basis of any acceptable theory: (i) *Reality*: ‘If, without in any way disturbing a system, we can predict with certainty the value of a physical quantity, then there exists an element of reality corresponding to the physical quantity’, and (ii) *Locality*: *The theory should be local, i.e., there is no action at a distance in nature.* EPR were able to give an example of a quantum mechanical system which did not satisfy these above two conditions and concluded that the quantum description of nature was incomplete. But, as Bell [2] put it, “The reasonable thing just does not work”. The assumption is inconsistent with quantum mechanics and with experiment. The mathematical framework for demonstrating the violation of local realism in quantum mechanics was first provided by Bell through his famous inequality [2].

The essence of nonlocality follows from the property of inseparability of composite quantum systems. Consider two particles that once interacted but are remote from one another now and do not interact. Although they do not interact, they are still *entangled* if *their joint state cannot be written as a product of the states of individual subsystems.* Schrödinger [3] first coined the term ‘entanglement’ for the non-local correlation represented by the inseparable state. Such states are now called entangled states. Quantum entanglement is one of the essential ingredients in the current development of quantum information processing. Now entanglement is treated as a resource in quantum communi-

cation and computation protocols [4, 5]. After Bell's work quantum entanglement became a subject of intensive study among those interested in the foundations of quantum theory. But more recently, entanglement has come to be viewed not just as a tool for exposing the weirdness of quantum mechanics, but as a potentially valuable resource. By exploiting entangled quantum states, we can perform tasks that are otherwise difficult or impossible i.e., typical resources required for cryptography, quantum teleportation and dense-coding [4] are entangled states. For example, in entanglement-assisted teleportation entangled pairs are used (one maximally entangled qubit pair is needed for every qubit teleported).

The arena of atom-photon interactions is a vast and potentially useful physical domain for implementing quantum information protocols. Entanglement has been widely observed in quantum optical systems such as cavity quantum electrodynamics. A number of experiments have been carried out. Several studies have been performed to quantify the entanglement that is obtained in atom-photon interactions in a cavity [6]-[13], which, from the view point of information processing, is considered an important aspect. Practical realization of various features of quantum entanglement are obtained in atom-photon interactions in optical and microwave cavities, using which controlled experiments can be performed with the present state-of-the-art technology. In this thesis we perform the study of several facets of quantum entanglement generated in atom-photon interactions with the viewpoint of obtaining interesting and useful applications in real physical processes and devices.

1.2 Criteria for entanglement

If two systems interact in the past, it is in general not possible to assign a single state vector to either of the two subsystems. This is what is sometimes called the principle of non-separability, or non-locality, and is one of the most evident manifestations of quantum entanglement. We can choose a very simple example of two spin-1/2 particles emitted in opposite directions from a common source. Let A and B be two spin-1/2 particles which are emitted from a common source S . To describe any one of the particles we require a two-dimensional Hilbert space. Let the basis for the two-dimensional Hilbert space for particle A be $|0\rangle_1$ and $|1\rangle_1$ which are the eigenstates of σ_{1z} (Pauli spin operator), where $|0\rangle$

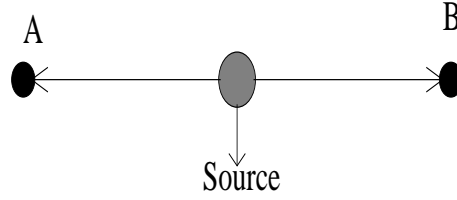


Figure 1.1: Two particles A and B are emitted from a common source S .

represents the spin-down state and $|1\rangle$ represents the spin-up state. Similarly, the basis of the two-dimensional Hilbert space for particle B will be $|0\rangle_2$ and $|1\rangle_2$ for operator σ_{2z} . Now if we are to describe the composite system, we have to consider a Hilbert space of $2 \otimes 2$ dimension, i.e. , a four-dimensional Hilbert space. Here the basis of $H_1 \otimes H_2$ will be

$$\begin{aligned} |00\rangle &= |0\rangle_1 \otimes |0\rangle_2, \\ |01\rangle &= |0\rangle_1 \otimes |1\rangle_2, \\ |10\rangle &= |1\rangle_1 \otimes |0\rangle_2, \\ |11\rangle &= |1\rangle_1 \otimes |1\rangle_2. \end{aligned}$$

These are the eigenstates of the operator $\sigma_{1z} \otimes \sigma_{2z}$. Now, the general states in the composite Hilbert space can be written as

$$|\phi\rangle = \alpha|00\rangle_{12} + \beta|11\rangle_{12} + \gamma|01\rangle_{12} + \delta|10\rangle_{12},$$

where $\alpha, \beta, \gamma, \delta$ are complex quantities with the normalization condition $|\alpha|^2 + |\beta|^2 + |\gamma|^2 + |\delta|^2 = 1$.

Now choosing particular values of $\alpha, \beta, \gamma, \delta$ one can write

$$\begin{aligned} |\phi^+\rangle_{12} &= \frac{1}{\sqrt{2}} (|00\rangle + |11\rangle), \\ |\phi^-\rangle_{12} &= \frac{1}{\sqrt{2}} (|00\rangle - |11\rangle), \\ |\psi^+\rangle_{12} &= \frac{1}{\sqrt{2}} (|01\rangle + |10\rangle), \\ |\psi^-\rangle_{12} &= \frac{1}{\sqrt{2}} (|01\rangle - |10\rangle). \end{aligned}$$

These states are pure entangled states because these states can not be written as $|\Psi\rangle = |\chi\rangle_1 \otimes |\xi\rangle_2$, i.e. , in the separable form. The states $|\phi^+\rangle, |\phi^-\rangle, |\psi^+\rangle, |\psi^-\rangle$ are also maximally

entangled states or Bell states because they violate maximally the Bell's inequality [2] which will be discussed latter. An N -particle entangled state can be written as

$$|\Psi\rangle = \sum_{i>1} \phi_i(1)\psi_i(2)\chi_i(3)\dots\dots\dots\xi_i(N), N > 1. \quad (1.1)$$

For the case of mixed states if the density operator of a bipartite system ρ is not represented by $\rho_{ab} \neq \sum_i \rho_a(i) \otimes \rho_b(i)$, the system is said to be entangled, where ρ_a and ρ_b are density operators for the subsystems a and b respectively. For the above pure states, $\rho^2 = \rho$. However, for mixed states $\text{Tr}\rho^2 < \text{Tr}\rho$. The example of a pure separable and a pure entangled state are, respectively

$$|\Psi\rangle = |00\rangle, \quad (1.2)$$

and

$$|\Phi\rangle = \frac{1}{\sqrt{2}}[|00\rangle \pm |11\rangle]. \quad (1.3)$$

Now the conditions for mixed separable and entangled states are respectively,

$$\rho = \sum_i p_i |a_i\rangle\langle a_i| \otimes |b_i\rangle\langle b_i|, \quad (1.4)$$

and

$$\rho \neq \sum_i p_i |a_i\rangle\langle a_i| \otimes |b_i\rangle\langle b_i|, \quad (1.5)$$

where $0 \leq p_i \leq 1$, $\sum_i p_i = 1$. The example of a mixed separable state is

$$\rho = \frac{1}{2}(|00\rangle\langle 00| + |11\rangle\langle 11|), \quad (1.6)$$

The Werner state is an example of a mixed entangled state [2]:

$$\rho_W = (1-p)\frac{1}{4}I + p|\Phi^+\rangle\langle\Phi^+|, \quad (1.7)$$

with $\frac{1}{3} < p \leq 1$ and $|\Phi^+\rangle = \frac{1}{\sqrt{2}}[|00\rangle + |11\rangle]$

We now know that when the state of a composite system can not be written as a direct product of their individual states, i.e., a state like $|\Psi\rangle \neq |\chi\rangle \otimes |\phi\rangle$, then the state $|\Psi\rangle$ is said to be entangled. But it is not always easy to identify an entangled state in this way. There are systematic procedures to detect entanglement. Let us now describe a few criteria employed in the detection of entanglement as follows (i) Schmidt number (ii) Partial transposition [14, 15] and (iii) Bell's inequality [2].

1.2.1 Schmidt number

With any bipartite pure state as $|\phi\rangle_{AB} = \alpha|0\rangle_A \otimes |1\rangle_B + \beta|1\rangle_A \otimes |0\rangle_B$, we may associate a positive integer, the Schmidt number, which is the number of nonzero eigenvalues of ρ_A or ρ_B , where $\rho_A = \text{Tr}_B(|\phi\rangle_{AB} \langle\phi|)$ ¹. In terms of this quantity, we can define what it means for a bipartite pure state to be entangled. The state $|\phi\rangle_{AB}$ is entangled if its Schmidt number is greater than one, otherwise it is separable. Now

$$\begin{aligned} \rho_A &= \text{Tr}_B(|\phi\rangle_{AB} \langle\phi|), \\ &= \sum_{k=0,1} \langle k|\rho_{AB}|k\rangle, \\ &= |\alpha|^2|0\rangle\langle 0| + |\beta|^2|1\rangle\langle 1|. \end{aligned} \tag{1.8}$$

Therefore the density matrix

$$\rho_A = \begin{pmatrix} |\alpha|^2 & 0 \\ 0 & |\beta|^2 \end{pmatrix} \tag{1.9}$$

has eigenvalues given by

$$\begin{aligned} \lambda_1 &= |\alpha|^2, \\ \lambda_2 &= |\beta|^2. \end{aligned}$$

If α and β are both non zero, the state $|\phi\rangle_{AB}$ will be entangled because it has two positive eigenvalues.

¹Here ρ_A is called reduced density state of ρ_{AB} i.e. $|\phi\rangle_{AB} \langle\phi|$ after taking trace over the system B .

1.2.2 Partial transposition

For a $2 \otimes 2$ and $2 \otimes 3$ dimensional Hilbert space, Peres [14] and Horodecki et al. [15] found a criteria of entanglement for a bipartite system. When the partial transposition of its density matrix has a negative eigenvalue, the bipartite system is entangled. It is a simple but effective criteria. To define partial transposition, we use the density matrix elements of a state in some product basis $\rho_{m\mu, n\nu} = \langle m | \otimes \langle \mu | \rho | n \rangle \otimes | \nu \rangle$, the kets with Latin and Greek letters form an orthogonal basis in the Hilbert space describing the first and second system respectively. Now, the partial transpose of ρ is defined as $\rho_{m\mu, n\nu}^{T_B} = \rho_{m\nu, n\mu}$.

Let us consider a state

$$|\psi\rangle_{AB} = \alpha|0\rangle_A \otimes |1\rangle_B + \beta|1\rangle_A \otimes |0\rangle_B, \quad (1.10)$$

where α and β are not zero. The corresponding density state can be written as

$$\begin{aligned} \rho_{AB} &= |\psi\rangle_{AB} \langle \psi| \\ &= (\alpha|0\rangle_A \otimes |1\rangle_B + \beta|1\rangle_A \otimes |0\rangle_B) \\ &\quad (\alpha^* \langle 0|_A \otimes \langle 1|_B + \beta^* \langle 1|_A \otimes \langle 0|_B) \\ &= |\alpha|^2 |0\rangle_A \langle 0|_A \otimes |1\rangle_B \langle 1|_B + \alpha\beta^* |0\rangle_A \langle 1|_A \otimes |1\rangle_B \langle 0|_B \\ &\quad + \beta\alpha^* |1\rangle_A \langle 0|_A \otimes |0\rangle_B \langle 1|_B + |\beta|^2 |1\rangle_A \langle 1|_A \otimes |0\rangle_B \langle 0|_B. \end{aligned} \quad (1.11)$$

In density matrix form, it is

$$\rho_{AB} = \begin{pmatrix} |\alpha|^2 & 0 & 0 & \alpha\beta^* \\ 0 & 0 & 0 & 0 \\ 0 & 0 & 0 & 0 \\ \alpha^*\beta & 0 & 0 & |\beta|^2 \end{pmatrix}. \quad (1.12)$$

Now, partial transposition on B gives

$$\begin{aligned} \rho_{AB}^{T_B} &= |\alpha|^2 |0\rangle_A \langle 0|_A \otimes |1\rangle_B \langle 1|_B + \alpha\beta^* |0\rangle_A \langle 1|_A \otimes |0\rangle_B \langle 1|_B \\ &\quad + \beta\alpha^* |1\rangle_A \langle 0|_A \otimes |1\rangle_B \langle 0|_B + |\beta|^2 |1\rangle_A \langle 1|_A \otimes |0\rangle_B \langle 0|_B. \end{aligned} \quad (1.13)$$

Therefore its density matrix is given by

$$\rho_{AB}^{T_B} = \begin{pmatrix} |\alpha|^2 & 0 & 0 & 0 \\ 0 & 0 & \alpha\beta^* & 0 \\ 0 & \alpha^*\beta & 0 & 0 \\ 0 & 0 & 0 & |\beta|^2 \end{pmatrix}. \quad (1.14)$$

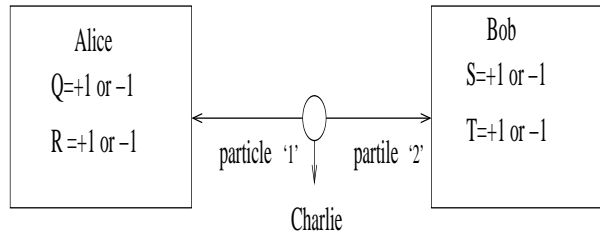


Figure 1.2: Schematic experiment for Bell's inequality. Alice can choose to measure either Q or R , and Bob can choose to measure either S or T . They perform their measurement simultaneously. Alice and Bob are assumed to be far apart that performing a measurement on one system can not have any effect on the result of the measurements on the other.

It has eigen-values

$$\begin{aligned}\lambda_1 &= |\alpha|^2, \\ \lambda_2 &= |\beta|^2, \\ \lambda_3 &= |\alpha\beta|, \\ \lambda_4 &= -|\alpha\beta|.\end{aligned}$$

Since it has a negative eigenvalue, we can say $|\psi\rangle_{AB} = \alpha|0\rangle_A \otimes |1\rangle_B + \beta|1\rangle_A \otimes |0\rangle_B$ is an entangled state. This is useful for both pure and mixed states in $2 \otimes 2$ and $2 \otimes 3$ dimensions only. This is also known as the negative partial transposition test. This test fails in higher dimensions.

1.2.3 Bell's inequality

Violations of Bell's inequalities [2] can also be seen to prove the existence of correlations between quantum systems. The mathematical framework for demonstrating the violation of local realism in quantum mechanics was first provided by Bell through his famous inequality [2]. To obtain Bell's inequality we consider a thought experiment [4], illustrated in Figure 1.2. Here Charlie prepares two particles and he sends one particle to Alice, and the second particle to Bob. Once Alice receives her particle, she performs a measurement on it. She has available to her two different measurement apparatuses, so she could choose to do one of two different measurements. These measurements are of physical properties which are labeled by Q and R respectively and S , T are two physical properties Bob is

capable of measuring. Assume that Q, R, S, T are dichotomic and take the value ± 1 . The timing of the experiment is arranged in such a way that Alice and Bob do their experiment at same time. Therefore, the measurement which Alice performs cannot disturb the result of Bob's measurement (or vice versa) since any physical influence cannot propagate faster than light. Consider the Bell operator defined as

$$(QS + RS + RT - QT) = (Q + R)S + (R - Q)T. \quad (1.15)$$

Because $R = Q = \pm 1$, it follows that $(Q + R)S = 0$ or $(R - Q)T = 0$. In either case, it is easy to see from equation(1) that $(QS + RS + RT - QT) = \pm 2$.

Suppose next, that $p(q, r, s, t)$ is the probability that, before the measurements are performed, the system is in the state where $Q = q, R = r, S = s$, and $T = t$. Letting $E(.)$ denote the mean value of a quantity, we have

$$\begin{aligned} E(QS + RS + RT - QT) &= \sum_{qrst} p(qrst)(qs + rs + rt - qt) \\ &\leq \sum_{qrst} p(qrst) \times 2 \\ &\leq 2. \end{aligned} \quad (1.16)$$

We can also write

$$\begin{aligned} E(QS + RS + RT - QT) &= \sum_{qrst} p(qrst)qs + \sum_{qrst} p(qrst)rs \\ &\quad + \sum_{qrst} p(qrst)rt - \sum_{qrst} p(qrst)qt \\ &= E(QS) + E(RS) + E(RT) - E(QT). \end{aligned} \quad (1.17)$$

Comparing Eq. (1.16) and Eq. (1.17) we obtain the Bell inequality as

$$E(QS) + E(RS) + E(RT) - E(QT) \leq 2. \quad (1.18)$$

This result is also often known as the Clauser, Horn, Shimony, and Holt (CHSH) inequality [16] after the authors who first derived this form of Bell's inequality. Here two assumptions are made, in deriving Eq.(1.16), i.e., (i) the physical properties Q, R, S, T have definite values which exist independent of observation, and (ii) the measurement of Alice does not influence the result of Bob's measurement.

To describe the quantum violation of Bell's inequality, let Charlie prepare a quantum system of two *qubits* (quantum bits)².

$$|\psi\rangle = \frac{1}{\sqrt{2}}(|01\rangle - |10\rangle)$$

which is the spin singlet state. We take the Bell-CHSH operator B as

$$B = \hat{a} \cdot \sigma \otimes (\hat{b} + \hat{b}') \cdot \sigma + \hat{a}' \cdot \sigma \otimes (\hat{b} - \hat{b}') \cdot \sigma.$$

Here $\hat{a}, \hat{a}', \hat{b}, \hat{b}'$ are arbitrary unit vectors. $\hat{a} \cdot \sigma = \sum_{i=1}^3 a_i \sigma_i$, where σ_i are the Pauli matrices. We can show that $\text{Tr}[(\sigma \cdot \hat{a} \otimes \sigma \cdot \hat{b})|\psi\rangle\langle\psi|] = -\hat{a} \cdot \hat{b} = -\cos\theta_{ab}$. Therefore one obtains $\langle\psi|B|\psi\rangle = \text{Tr}[B|\psi\rangle\langle\psi|]$. Thus,

$$\langle\psi|B|\psi\rangle = -\hat{a} \cdot \hat{b} - \hat{a} \cdot \hat{b}' - \hat{a}' \cdot \hat{b} + \hat{a}' \cdot \hat{b}' = -\cos\theta_{ab} - \cos\theta_{ab'} - \cos\theta_{a'b} + \cos\theta_{a'b'}. \quad (1.19)$$

The angles can be chosen in such a way that one gets $\langle\psi|B|\psi\rangle = 2\sqrt{2} \simeq 2.8$, i.e., $\langle B \rangle > 2$. This is the maximal violation Bell's inequality. Therefore, at least one of the above assumptions (i) and (ii) is violated by quantum mechanics. More recently, Gisin [17] proved that all entangled pure states of bipartite systems violate the CHSH inequality. But all mixed entangled states do not violate Bell's inequality as shown by Werner in 1989 [18]. The CHSH inequality was convincingly tested for the first time by Aspect and collaborators in 1982 [19]. There is an experimental proposal to test Bell's inequality in atom-photon interactions using the micromaser in the presence of both atomic decay and cavity dissipation [20].

1.3 Quantification of entanglement

One of the main goals of the theory of entanglement is to develop measures of entanglement. There are some general properties which a reasonable entanglement measure should have [21]. To quantify entanglement means nothing else but to associate a positive real number to each state of a (finite dimensional) bipartite system. For bipartite systems

²The indivisible unit of classical information is the *bit*, which takes one of the two possible values $\{0,1\}$. The corresponding unit of quantum information is called the "quantum bit" or *qubit*. It describes the state in the simplest possible quantum system. A *qubit* state in a two-dimensional Hilbert space that can take any value of the form $a|0\rangle + b|1\rangle$, where a, b are complex numbers that satisfy $|a|^2 + |b|^2 = 1$.

in pure states the quantification problem has been essentially solved. But in multipartite systems additional complications arise, and even the pure state case is not well-understood yet. For bi-partite systems in mixed states the quantification problem has been developed in Hilbert space dimension $2 \otimes 2$. But difficulties arise in the quantification of mixed state entanglement of bipartite systems in higher dimension. Several measures of entanglement have been proposed and studied. We shall review entanglement measures for bipartite systems A and B with Hilbert space dimension $2 \otimes 2$ in case of pure and mixed states. An exhaustive definition of bipartite entanglement exists and is based upon the von Neumann entropy [4] and the entanglement of formation or concurrence [22, 23].

1.3.1 von Neumann entropy

Quantifying bipartite entanglement in pure states is straightforward. If a pure bipartite state is not entangled, when we take partial trace over one subsystem, the state of the remaining sub-system will be pure. However if the state is entangled, the reduced state is necessarily mixed. It thus makes sense to associate the degree of entanglement of the whole bipartite state with how mixed the reduced state is. The measure of mixedness we choose the von Neumann entropy of the reduced state. Let us now consider a pure bipartite state $\rho_{AB} = |\psi\rangle_{AB} \langle\psi|$ shared by two systems A and B . If it is entangled, its partial trace $\rho_A = \text{Tr}_B \rho_{AB}$ or $\rho_B = \text{Tr}_A \rho_{AB}$ is mixed and for a maximally entangled state it is maximally mixed. This suggests the use of the von Neumann entropy of ρ_{AB} , which measures how much a state is mixed, as an entanglement measure for pure states, i.e., we define von Neumann entropy of the reduced density matrix as $E_V(\rho_{AB}) = -\text{Tr}(\rho_A \log_2 \rho_A)$, or $E_V(\rho_{AB}) = -\text{Tr}(\rho_B \log_2 \rho_B)$. If we consider a state

$$|\psi\rangle_{AB} = \alpha|01\rangle_{AB} + \beta|10\rangle_{AB}, \quad (1.20)$$

the reduced state is

$$\begin{aligned} \rho_A &= \text{Tr}_B \rho_{AB} \\ &= \sum_{i=0,1} \langle i | \rho_{AB} | i \rangle \\ &= |\alpha|^2 |0\rangle \langle 0| + |\beta|^2 |1\rangle \langle 1|. \end{aligned} \quad (1.21)$$

Therefore, the von Neumann entropy is

$$\begin{aligned}
E_V &= -\text{Tr}(\rho_A \log_2 \rho_A) \\
&= -\text{Tr} \left[(|\alpha|^2|0\rangle\langle 0| + |\beta|^2|1\rangle\langle 1|) \log_2 (|\alpha|^2|0\rangle\langle 0| + |\beta|^2|1\rangle\langle 1|) \right] \\
&= -\text{Tr} \left[(|\alpha|^2|0\rangle\langle 0| + |\beta|^2|1\rangle\langle 1|) (\log_2 |\alpha|^2|0\rangle\langle 0| + \log_2 |\beta|^2|1\rangle\langle 1|) \right] \\
&= -\text{Tr} \left[(|\alpha|^2 \log_2 |\alpha|^2)|0\rangle\langle 0| + (|\beta|^2 \log_2 |\beta|^2)|1\rangle\langle 1|) \right] \\
&= -|\alpha|^2 \log_2 |\alpha|^2 - |\beta|^2 \log_2 |\beta|^2.
\end{aligned} \tag{1.22}$$

When $\alpha = \beta = 1/\sqrt{2}$, $E_V = 1$.

1.3.2 Concurrence and Entanglement of formation

The above method cannot be used to measure the entanglement in case of mixed states. The difficulties associated with it has been circumvented to some extent by Wootters [22, 23]. However, his prescription is applied to bipartite systems only. He derived a closed-form expression for the entanglement of formation of a pair of qubits in an arbitrary state by introducing a related quantity known as the concurrence. For a pure state of two qubits, the concurrence $C(\psi)$ is given by

$$C(\psi) \equiv |\langle \psi | \tilde{\psi} \rangle| \tag{1.23}$$

where $|\tilde{\psi}\rangle \equiv \sigma_y \otimes \sigma_y |\psi^*\rangle$ represents the ‘spin-flip’ of $|\psi\rangle$, σ_y is the usual Pauli operator, and the ‘*’ denotes complex conjugation in the standard basis. Thus, the concurrence of any product state of the form $|\psi\rangle_{AB} = |01\rangle_{AB}$, is equal to zero, as expected. Conversely, performing the spin-flip operation on a maximally entangled state such as the singlet state in the form $|\psi\rangle_{AB} = \frac{1}{\sqrt{2}}(|01\rangle_{AB} + |10\rangle_{AB})$ leaves the state invariant (up to an overall phase), demonstrating that the concurrence achieves its maximum value for the maximally entangled states. More generally, the following relationship holds between the concurrence and the von Neumann entropy [24]

$$E_V(\psi) = \epsilon(C(\psi)) \tag{1.24}$$

where the function ϵ is defined by

$$\epsilon(C) \equiv h \left(\frac{1 + \sqrt{1 - C^2}}{2} \right) \tag{1.25}$$

and

$$h(x) = -x \log_2 x - (1-x) \log_2(1-x) \quad (1.26)$$

is the binary entropy function. That the concurrence satisfies the requirements for being an entanglement monotone [25] follows immediately from the observation that $\epsilon(C)$ is a monotonically increasing function of C and vice-versa.

For the generalization of the concurrence to a mixed state of two qubits we consider a density matrix ρ of a pair of quantum systems A and B , and consider all possible pure-state decompositions of ρ , i.e., all ensembles of states $|\psi_k\rangle$ with probabilities p_k , such that

$$\rho = \sum_k p_k |\psi_k\rangle \langle \psi_k|. \quad (1.27)$$

The concurrence for a mixed bipartite state is

$$C = \min_{\{p_k, \psi_k\}} \sum p_k C(\psi_k) = \min_{\{p_k, \psi_k\}} \left| \sum_k \langle \psi_k | \tilde{\psi}_k \rangle \right|. \quad (1.28)$$

The analytic solution to this minimization procedure involves finding the eigenvalues of the non-Hermitian operator $\rho \tilde{\rho}$, where the tilde again denotes the spin-flip of the quantum state, i.e., $\tilde{\rho} \equiv (\sigma_y \otimes \sigma_y) \rho^* (\sigma_y \otimes \sigma_y)$. Specifically, the closed form solution for the concurrence of a mixed state of two qubits is given by

$$C(\rho) = \max\{0, \sqrt{\lambda_1} - \sqrt{\lambda_2} - \sqrt{\lambda_3} - \sqrt{\lambda_4}\}, \quad (1.29)$$

where the λ_i are the eigenvalues of $\rho(\sigma_y \otimes \sigma_y) \rho^* (\sigma_y \otimes \sigma_y)$ in descending order. The entanglement of formation E_F of an arbitrary state ρ is related to $C(\rho)$ [23] by a function $E_F(\rho)$ as

$$E_F(\rho) = h\left(\frac{1 + \sqrt{1 - C^2(\rho)}}{2}\right), \quad (1.30)$$

where

$$h(x) = -x \log_2 x - (1-x) \log_2(1-x) \quad (1.31)$$

is the binary entropy function. In case of pure states, the von Neumann entropy E_V and the entanglement of formation E_F are the same, i.e., E_F becomes $\epsilon(C)$ (see Eq.(1.24)).

Now we consider an example to quantify the entanglement using these above mentioned entanglement measures. Consider the state $|\psi\rangle_{AB} = \alpha|01\rangle_{AB} + \beta|10\rangle_{AB}$. The concurrence takes the form

$$C(\rho) = 2|\alpha\beta|. \quad (1.32)$$

If we calculate von Neumann entropy, the concurrence and entanglement of formation for the state $|\psi\rangle = \frac{1}{\sqrt{2}}(|01\rangle - |10\rangle)$, we get the same result which is 1, because the state is a pure and maximally entangled state. Let us consider a mixed entangled state

$$\rho_{AB} = p_1|\Phi^-\rangle_{AB} \langle\Phi^-| + p_2|01\rangle_{AB} \langle 01|$$

where $|\Phi^-\rangle_{AB} = \frac{1}{\sqrt{2}}[|00\rangle_{AB} + |11\rangle_{AB}]$ and $p_1 + p_2 = 1$. The density matrix of ρ_{AB} is given by

$$\rho_{AB} = \begin{pmatrix} p_2 & 0 & 0 & 0 \\ 0 & p_1/2 & p_1/2 & 0 \\ 0 & p_1/2 & p_1/2 & 0 \\ 0 & 0 & 0 & 0 \end{pmatrix}, \quad (1.33)$$

in the basis $|01\rangle, |00\rangle, |11\rangle, |10\rangle$ states. The eigen values of the matrix $\rho_{AB}(\sigma_y \otimes \sigma_y)\rho_{AB}^*(\sigma_y \otimes \sigma_y)$ are given by $\lambda_1 = p_1^2, \lambda_2 = 0, \lambda_3 = 0, \lambda_4 = 0$. Therefore, the concurrence $C(\rho_{AB}) = p_1$ and the entanglement of formation $E_F(\rho_{AB})$ can be obtained from Eq.(1.30). If we choose $p_1 = 1/2$ the above mixed entangled state is given by

$$\rho_{AB} = 1/2[|\Phi^-\rangle_{AB} \langle\Phi^-| + |01\rangle_{AB} \langle 01|].$$

We get $C(\rho_{AB}) = 1/2$ and $E_F(\rho_{AB}) \approx 0.35$.

1.4 Decoherence and its effect on Entanglement

We have defined above measures of entanglement which we will be using in this thesis for several examples of entanglement generated in atom-photon interactions. In the real physical processes that we will study, decoherence plays an important role. When a system

is coupled to a reservoir³ which may be thought of as a collection of a large number of quantum systems (many degrees of freedom) in thermal equilibrium, it loses energy to the reservoir. This mechanism is called damping or decoherence mechanism. In order to recover the state of the system at any time after its interaction with the reservoir, one has to trace out the reservoir variables since it is practically impossible to monitor the behaviour of the large number of degrees of freedom of the reservoir. This process reduces pure states to mixed states, and in general decreases the entanglement of the states of the decohering system.

Decoherence is brought about by both atomic decay as well as cavity photon loss, while the atoms and cavity photons interact with their respective reservoirs. In this thesis work, we do not consider atomic decay because the lifetime of the two-level Rydberg atom that we study in this thesis (see chapter 2) is much longer than the atom-field interaction time inside the cavity. We only consider the cavity photon loss. We study its quantitative action in diminishing the atom-field and the resultant atom-atom secondary correlations discussed in chapter 2. The effects of decoherence on nonlocality can be observed in a controlled manner in actual experiments involving the micromaser discussed in chapter 3. In chapter 4, we observe the effect of cavity dissipation on various systems exhibiting bipartite entanglement. In chapter 6 we analyze a new and counter-intuitive mechanism using various dissipative atom-cavity systems to show that their collective dynamics can be used to maximize entanglement for intermediate values of the cavity leakage parameter.

1.5 Plan

From our introductory discussions, it is apparent that the first task is to generate entangled quantum states in atom-photon interactions and understand their characteristics before making use of them. So with this above motivation the thesis is organised as follows.

In chapter 2 we discuss the Jaynes-Cummings model [26] which is an exactly solvable model describing atom-photon interactions. This model consists of a two-level atom

³In discussion of the master equation (see Appendix 1 on page 114), the environment is typically called the *reservoir*, in deference to the deeply ingrained conventions of statistical physics.

interacting with a single mode radiation field. The resonant Jaynes-Cummings dynamics is considered for simplicity. We describe how the initial atom-photon state evolves under the Jaynes-Cummings interaction. We also discuss the action of dissipative dynamics on atom-photon interactions. We consider only the field-reservoir interaction since the lifetime of the atom is much longer than the atom-photon interaction time. We show a model solution of the complete atom-field evolution equation [27]. When a two-level atom and a photon undergo the Jaynes-Cummings interaction, they become entangled as a rule. We investigate various types of entanglement such as atom-cavity, atom-atom and cavity-cavity entanglements in both the ideal situation, and also in presence of cavity dissipation. We quantify these entanglements with the entanglement measure concurrence [22, 23]. We observe the effects of cavity dissipation on the magnitude of entanglement generated. We see in general that the cavity dissipation reduces the entanglement as the atom-cavity interaction time increases.

In chapter 3 we investigate the entanglement dynamics in the one-atom micromaser [29, 30, 31]. The one-atom micromaser is an experimental realization of Jaynes-Cummings model and has been operational for several years [31, 32]. First we describe the micromaser setup and discuss the micromaser dynamics which is governed by (i) the atom-field interaction, and (ii) the field-reservoir interaction. The steady-state micromaser field distribution function depending on the field-reservoir coupling is obtained [33]. We consider two two-level Rydberg atoms prepared in their excited states which traverse the micromaser cavity one after another such that there is not more than a single atom at any time inside the cavity. Although there is no direct overlap between the two atoms, the emerging atoms will be correlated. The reason behind this correlation is that when the first atom passes through the cavity, it leaves an imprint on the photons inside the cavity, and the second atom interacts with the cavity state which has been modified by the passage of the first atom. In this way a secondary correlation develops between the atoms. We see that two-atom entanglement can be generated by controlling dissipation for experimentally attainable values of the micromaser parameters [9]. We compute this atom-atom entanglement versus time for different micromaser parameters. Such entanglement can also be used to formulate an experimental proposal for testing the violation of Bell's inequality [20]. The steady-state photon statistics of the micromaser field are reflected in the en-

tanglement properties of the emerging atoms. We compute the Shannon entropies of the steady-state micromaser field before and after the passage of two atoms, and investigate the correspondance between the two-atom entanglement and the difference between the Shannon entropies.

Several characteristics of atomic entanglement and quantum information transfer in atom-photon interactions are discussed quantitatively in chapter 3. Entanglement is moreover endowed with certain curious features. Unlike classical correlations, quantum entanglement can not be freely shared among many quantum systems. It has been observed that a quantum system being entangled with another one limits its possible entanglement with a third system. This has been dubbed the “monogamous nature of entanglement” which was first proposed by Bennett [34]. In chapter 4 we perform a quantitative study of the monogamy of quantum entanglement and its swapping both in ideal and dissipative atom-photon interactions. We show the “monogamous nature of entanglement” in different systems. First we consider a tripartite system of two maximally entangled cavities and a single two-level atom prepared in the ground state which passes through the first cavity. In the second case we consider a tripartite system of two maximally entangled two-level atoms and a single empty cavity where the first atom passes through the empty cavity. In the first case we see the monogamous nature between the entanglement of the pair of two cavities and the pair of second cavity and the atom respectively. We further see that this curious behaviour of entanglement is sustained in presence of cavity dissipation [35]. Similarly we get the same result for the pair of two atoms and the pair of the second atom and the cavity. A “monogamy” inequality [36] for these tripartite system is quantitatively studied and verified in the presence of cavity leakage. Another distinctive property of quantum entanglement for multipartite systems is the possibility of entanglement swapping between two or more pairs of qubits. Entanglement swapping is observed between the the two-cavity and the two-atom system. Cavity dissipation leads to the quantitative reduction of information transfer though preserving the basic swapping property [35].

After having discussed the features of entanglement generated by the interaction of two-level atoms with single cavity modes, it is natural to ask the question as to what effect the cavity field properties have on such entanglement. With this aim in mind,

in chapter 5, we study the entanglement properties of a pair of two-level atoms going through a cavity filled with different types of radiation field. We consider the atoms to traverse the cavity one after another as in the micromaser model discussed in chapter 3. The initial joint state of two successive atoms that enter the cavity is unentangled. Interactions mediated by the cavity photon field result in the final two-atom state being of a mixed entangled type. We consider various different kinds of field statistics such as that of the Fock state field, the thermal field, and the coherent state field, respectively, inside the cavity. The entanglement of formation of the joint two-atom state is calculated for both these cases as a function of the Rabi angle gt . We present a comparative study of two-atom entanglement for low and high mean photon number cases corresponding to the different field statistics [12, 13]. We further investigate the consequences on atomic entanglement by squeezing of the radiation field inside the cavity. It is possible to show [13] that squeezing of the cavity field can increase atomic entanglement if the average cavity photon number is held fixed.

As stated earlier, the effects of dissipative dynamics on the magnitude of entanglement generated in atom-photon interactions inside cavities is a focal point of our investigations presented in this thesis. In order to use quantum entanglement as a resource, one has to ensure that it survives long enough for information protocols to be implemented. This can be accomplished, for example, by controlling cavity leakage in the micromaser. However, recently, certain systems have been found [10, 12, 37, 38, 39, 40, 41] where entanglement is seen to be generated through interaction with the environment. In chapter 6 we present some concrete examples of environment induced entanglement in atom-photon interactions. We consider various dissipative atom-cavity systems and show that their collective dynamics can be used to maximize entanglement for intermediate values of the cavity leakage parameter κ [42]. We first consider the interaction of a single two-level atom with one of two coupled microwave cavities and show analytically that the atom-cavity entanglement increases with cavity leakage. We next consider a system of two atoms passing successively through a cavity and derive the expression for the maximum value of κ in terms of the Rabi angle gt , for which the two-atom entanglement can be increased. Further, numerical investigation of micromaser dynamics also reveals the increase of two-atom entanglement with stronger cavity-environment coupling for experimentally

attainable values of the micromaser parameters.

In the final chapter we present a concluding summary of the main results obtained in the various chapters of this thesis. We provide brief discussions of the implications of our results and possible extensions of our investigations with the aim of motivating future directions and associated interesting lines of research that have cropped up from our study.

Chapter 2

Entanglement in the Jaynes-Cummings model with dissipation

2.1 The Jaynes-Cummings model

One of the most fundamental models in quantum mechanics presented in introductory text books is that of the two-level system and the harmonic oscillator. Combining these two into a bipartite system gives many interesting results using one of the most studied models, i.e., the Jaynes Cummings (JC) model [26]. The JC model is the simplest fully quantized model describing the interaction between a two-level atom and a quantized electromagnetic field. The model consists of a single two-level atom interacting with a single quantized electromagnetic cavity field (Figure 2.1).

The Jaynes-Cummings Hamiltonian is obtained by simply imposing the rotating wave approximation RWA [28]. In this approximation exact analytical solutions exist, and in spite of the simplicity of the JC model, the dynamics have turned out to be very rich and complex, describing well several physical phenomena. Among these, atom-field

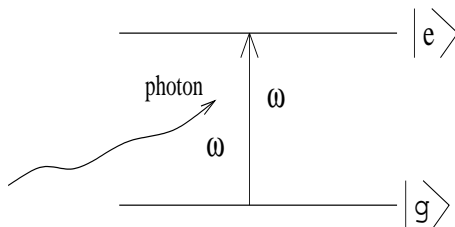


Figure 2.1: A two-level atom-photon interaction.

entanglement [43, 44, 45] is a very interesting subject of research. We have used the Jaynes-Cummings interaction to investigate atom-cavity, atom-atom and cavity-cavity entanglements. In this chapter we will discuss atom-cavity, atom-atom and cavity-cavity entanglement in detail without and with cavity field dissipation.

A two level atom is formally analogous to a spin-1/2 system with two possible states. Let us denote the upper level of the atom as $|e\rangle$ and the lower level as $|g\rangle$. Here we can write the step up and the step down operator as $\sigma^+ = |e\rangle\langle g|$ and $\sigma^- = |g\rangle\langle e|$, with the commutation relation

$$\begin{aligned} [\sigma^+, \sigma^-] &= |e\rangle\langle e| - |g\rangle\langle g| \\ &= \sigma_z. \end{aligned} \tag{2.1}$$

A quantum mechanical field can be represented as (for present purpose, we consider a single mode field)

$$E(t) = \frac{\mathcal{E}}{2}[ae^{-i\omega t} + a^\dagger e^{i\omega t}] \tag{2.2}$$

apart from a mode function which we omit here as it is not required for the present discussion. Here a and a^\dagger are annihilation and creation operators, respectively, ω is the frequency of the field and \mathcal{E} has the dimension of electric field. The graininess of the radiation field is represented by the photon number state $|n\rangle$, $n = 0, 1, 2, \dots$, such that $a|n\rangle = \sqrt{n}|n-1\rangle$ and $a^\dagger|n\rangle = \sqrt{n+1}|n+1\rangle$. It is an eigenstate of the number operator $\hat{n} = a^\dagger a$, $\hat{n}|n\rangle = n|n\rangle$. The field in Eq.(2.2) can be represented by a quantum mechanical state vector $|\psi\rangle$ which is a linear superposition of the number states $|n\rangle$, that is

$$|\psi\rangle = \sum_{n=0}^{\infty} c_n |n\rangle \tag{2.3}$$

where c_n is, in general, complex and gives the probability that the field has n photons by the relation

$$P_n = \langle n|\psi\rangle\langle\psi|n\rangle = |c_n|^2 \tag{2.4}$$

It is now a quantum statistical field and its average photon number is given by

$$\langle n \rangle = \sum_{n=0}^{\infty} n P_n \tag{2.5}$$

with the intensity of the field $I \propto \langle n \rangle$. The statistics brings in a quantum mechanical noise which is represented by the variance

$$V = \frac{\langle n^2 \rangle - \langle n \rangle^2}{\langle n \rangle}. \quad (2.6)$$

$V = 1$ is for coherent state field and $V < 1$ signifies a non-classical state. The parameters $\langle n \rangle$ and V give a fair description of the quantum mechanical nature of the radiation field. The interaction between the two-level atom and the single mode field can be written in the dipole approximation as, $H_{int} = d \cdot E / \hbar$. Here H_{int} is in frequency units, and d is the dipole moment of the atom which can be written as $d = -\langle e|x|g \rangle$. Writing E in terms of operators in Eq.(2.2), and the dipole moment by spin operators in Eq.(2.1), the interacting atom-field system can be represented by the Hamiltonian

$$H = H_0 + H_{int}, \quad (2.7)$$

where the unperturbed Hamiltonian $H_0 = \frac{\Omega \sigma_z}{2} + (a^\dagger a + \frac{1}{2})\omega$ and $H_{int} = g(\sigma^+ + \sigma^-)(a + a^\dagger)$ and $g = -\frac{d \mathcal{E}}{\hbar}$ is the coupling constant. The interaction part contains four terms. The term $\sigma^+ a$ which is an energy conserving term describes the process in which the atom is taken from the lower to the upper state with the absorption of a photon (Figure 2.2). The term $\sigma^- a^\dagger$ which is also an energy conserving term describes the process in which the atom is taken from the upper to the lower state with the emission of a photon (Figure 2.3). The term $\sigma^+ a^\dagger$ which is an energy non-conserving term describes the process in which the atom is taken from the lower to the upper state with the emission of a photon (Figure 2.4). The term $\sigma^- a$, also a non-conserving term, describes the process in which the atom is taken from the upper to the lower state with the absorption of a photon (Figure 2.5). Since the last two terms are energy non-conserving, they have been dropped from the Hamiltonian. This is also known as the rotating-wave approximation in quantum optics.

So the Jaynes-Cummings Hamiltonian reduces to

$$H = \frac{\Omega \sigma_z}{2} + (a^\dagger a + 1/2)\omega + g(\sigma^+ a + \sigma^- a^\dagger). \quad (2.8)$$

Now if we consider resonant atom-field interaction (field frequency and atomic transition frequency are the same), Eq.(2.8) is rewritten as

$$H = \frac{\omega \sigma_z}{2} + (a^\dagger a + 1/2)\omega + g(\sigma^+ a + \sigma^- a^\dagger). \quad (2.9)$$

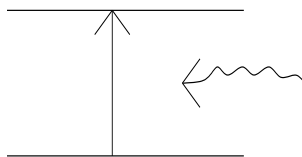


Figure 2.2: A two-level atom taken from the lower to the upper state with the absorption of a photon. It is the term σ^+a .

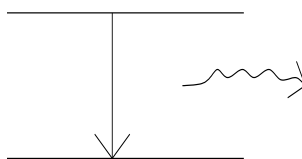


Figure 2.3: A two-level atom taken from the upper to the lower state with the emission of a photon. It is the term σ^-a^\dagger .

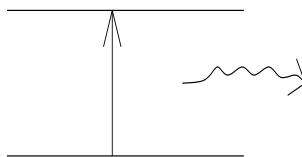


Figure 2.4: A two-level atom taken from the lower to the upper state with the emission of a photon. It is the term σ^+a^\dagger .

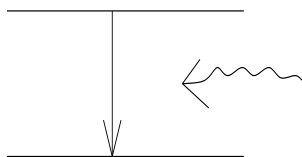


Figure 2.5: A two-level atom taken from the upper to the lower state with the absorption of a photon. It is the term σ^-a .

In a frame rotating at frequency $\omega[\sigma_z/2 + (a^\dagger a + 1)]$, the equation of motion defining the system is

$$i\frac{\partial}{\partial t}|\psi(t)\rangle_I = H_I|\psi(t)\rangle_I, \quad (2.10)$$

where the Hamiltonian H reduces to

$$H_I = g(\sigma^+ a + \sigma^- a^\dagger). \quad (2.11)$$

We deal with this interaction Hamiltonian H_I to investigate the atom-cavity, atom-atom, and cavity-cavity entanglements in this chapter. If we denote an atom-photon state by $|\Psi\rangle$, the dynamics of atom-photon interaction is governed by the equation

$$i|\dot{\Psi}\rangle = H_I|\Psi\rangle. \quad (2.12)$$

Its density operator $\rho = |\Psi\rangle\langle\Psi|$ obeys the equation of motion

$$\begin{aligned} \dot{\rho} &= i(|\dot{\Psi}\rangle\langle\Psi| + |\Psi\rangle\langle\dot{\Psi}|) \\ &= H_I|\Psi\rangle\langle\Psi| - |\Psi\rangle\langle\Psi|H_I \\ &= H_I\rho - \rho H_I = [H_I, \rho]. \end{aligned} \quad (2.13)$$

Therefore

$$\dot{\rho} = -i[H_I, \rho]. \quad (2.14)$$

2.1.1 The energy eigenstates of the Jaynes-Cummings Hamiltonian

Energy conservation considerations indicate that the states $|e, n\rangle$ and $|g, n+1\rangle$ are connected by the interaction Hamiltonian H_I for $n = 0, 1, 2, 3, \dots$. After the interaction, the vectors $|e, n\rangle$ and $|g, n+1\rangle$ form a basis for the atom-field system. Let the eigenstate of the interaction Hamiltonian be written as

$$|\psi\rangle = c_1|e, n\rangle + c_2|g, n+1\rangle, \quad (2.15)$$

with the normalizing condition $|c_1|^2 + |c_2|^2 = 1$. So we can write

$$\begin{aligned} H|\psi\rangle &= \lambda|\psi\rangle \\ &= \lambda(c_1|e, n\rangle + c_2|g, n+1\rangle), \end{aligned} \quad (2.16)$$

where λ is the eigenvalue of Hamiltonian H_I . Also we have

$$g(\sigma^+a + \sigma^-a^\dagger)|\psi\rangle = g\sqrt{n+1}(c_1|a, n\rangle + c_2|g, n+1\rangle). \quad (2.17)$$

Comparing Eq.(2.16) and Eq.(2.17) we get $gc_2\sqrt{n+1} = \lambda c_1$ and $gc_1\sqrt{n+1} = \lambda c_2$. Hence we get the eigen values

$$\lambda = \pm(g\sqrt{n+1}).$$

Now with the normalizing condition $|c_1|^2 + |c_2|^2 = 1$, when $\lambda_1 = (g\sqrt{n+1})$ we choose $c_1 = \frac{1}{\sqrt{2}}$, $c_2 = \frac{i}{\sqrt{2}}$, and for $\lambda_2 = -(g\sqrt{n+1})$ we choose $c_1 = \frac{1}{\sqrt{2}}$, $c_2 = -\frac{i}{\sqrt{2}}$. Therefore the energy eigenstates of the Hamiltonian are given by

$$|\psi^+\rangle = \frac{1}{\sqrt{2}} [|e, n\rangle + i|g, n+1\rangle], \quad (2.18)$$

and

$$|\psi^-\rangle = \frac{1}{\sqrt{2}} [|e, n\rangle - i|g, n+1\rangle]. \quad (2.19)$$

There are also known as dressed states of the system.

2.1.2 Various atom-field evolved states under the Jaynes-Cummings interaction

Suppose the atom-field system is in an initial state

$$|\Psi(t=0)\rangle = |e\rangle \otimes |n\rangle. \quad (2.20)$$

Then, the time evolution of the state vector is

$$\begin{aligned} |\Psi(t)\rangle &= e^{-iH_I t} |\Psi(t=0)\rangle, \\ &= e^{-iH_I t} |e, n\rangle, \\ &= e^{-iH_I t} \left[\frac{1}{\sqrt{2}} (|\psi^+\rangle + |\psi^-\rangle) \right], \end{aligned} \quad (2.21)$$

where we have used

$$|e, n\rangle = \frac{1}{\sqrt{2}} [|\psi^+\rangle + |\psi^-\rangle]. \quad (2.22)$$

Thus,

$$\begin{aligned}
|\Psi(t)\rangle &= \frac{1}{2} \left[\left(e^{i(g\sqrt{n+1})t} + e^{-i(g\sqrt{n+1})t} \right) |e, n\rangle \right. \\
&\quad \left. - i \left(e^{i(g\sqrt{n+1})t} - e^{-i(g\sqrt{n+1})t} \right) |g, n+1\rangle \right] \\
&= \cos(g\sqrt{n+1}t) |e, n\rangle + \sin(g\sqrt{n+1}t) |g, n+1\rangle.
\end{aligned} \tag{2.23}$$

Now let us study the time evolution of the initial state

$$|\Psi(t=0)\rangle = |g\rangle \otimes |n+1\rangle. \tag{2.24}$$

Therefore

$$\begin{aligned}
|\Psi(t)\rangle &= e^{-iH_I t} |\Psi(t=0)\rangle, \\
&= e^{-iH_I t} |g, n+1\rangle, \\
&= e^{-iH_I t} \left[\frac{1}{\sqrt{2}i} (|\psi^+\rangle - |\psi^-\rangle) \right],
\end{aligned} \tag{2.25}$$

where we have used

$$|g, n+1\rangle = \frac{1}{\sqrt{2}i} [|\psi^+\rangle - |\psi^-\rangle]. \tag{2.26}$$

Thus,

$$\begin{aligned}
|\Psi(t)\rangle &= \frac{1}{2} \left[i \left(e^{i(g\sqrt{n+1})t} - e^{-i(g\sqrt{n+1})t} \right) |e, n\rangle \right. \\
&\quad \left. - i \left(e^{i(g\sqrt{n+1})t} + e^{-i(g\sqrt{n+1})t} \right) |g, n+1\rangle \right] \\
&= \cos(g\sqrt{n+1}t) |g, n+1\rangle - \sin(g\sqrt{n+1}t) |e, n\rangle.
\end{aligned} \tag{2.27}$$

However, the time evolution of the state $|\Psi(0)\rangle = |g, 0\rangle$ remains unchanged, i.e.,

$$|\Psi(t)\rangle = e^{-iH_I t} |g, 0\rangle = |g, 0\rangle. \tag{2.28}$$

2.2 Dissipative dynamics

Let us now investigate the dynamics of atom-photon interactions in the presence of cavity dissipation. Since the lifetime of a two-level Rydberg atom is usually much longer compared to the atom-cavity interaction time, we can safely neglect the atomic dissipation. The dynamics of the atom-photon interaction is governed by the evolution equation

$$\dot{\rho} = \dot{\rho}|_{\text{atom-field}} + \dot{\rho}|_{\text{field-reservoir}}, \tag{2.29}$$

where the strength of the couplings are given by the parameters κ (the cavity leakage constant) and g (the atom-field interaction constant). $\dot{\rho}|_{\text{atom-field}} = -i[H_I, \rho_{\text{atom-field}}]$ obtained from Eq.(2.14). The reservoir-induced interactions can be effectively represented by the well-known master equations [46, 47] using Born and Markoff approximations. For the reservoir coupling we have, after tracing over the reservoir variables,

$$\begin{aligned} \dot{\rho}|_{\text{field-reservoir}} &= -\kappa(1 + \langle n \rangle)(a^\dagger a \rho - 2a \rho a^\dagger + \rho a^\dagger a) \\ &\quad - \kappa \langle n \rangle (a a^\dagger \rho - 2a^\dagger \rho a + \rho a a^\dagger), \end{aligned} \quad (2.30)$$

where $\langle n \rangle$ is average thermal photons at the cavity temperature T . A derivation of this equation is given in the Appendix 1 on page 114. At temperature $T = 0K$ the average thermal photon number is zero, and hence one has [47]

$$\dot{\rho}|_{\text{field-reservoir}} = -\kappa(a^\dagger a \rho - 2a \rho a^\dagger + \rho a^\dagger a). \quad (2.31)$$

The total dynamical equation for atom-field density state ρ , is thus given by

$$\dot{\rho} = -i[H_I, \rho_{\text{atom-field}}] - \kappa(a^\dagger a \rho - 2a \rho a^\dagger + \rho a^\dagger a). \quad (2.32)$$

2.2.1 A model solution

In cavity-QED, one usually has $g \gg \kappa$. Hence, in most cases, it is sufficient to get a solution of Eq.(2.32) to the first order in κ . Towards this, we start with the dressed states of H_I given by

$$|+, n\rangle = \frac{1}{\sqrt{2}}[|e, n\rangle + |g, n+1\rangle], \quad (2.33)$$

and

$$|-, n\rangle = \frac{1}{\sqrt{2}}[-|e, n\rangle + |g, n+1\rangle]. \quad (2.34)$$

For $n = 0$ the dressed state basis become

$$|+, 0\rangle = \frac{1}{\sqrt{2}}[|e, 0\rangle + |g, 1\rangle], \quad (2.35)$$

and

$$|-, 0\rangle = \frac{1}{\sqrt{2}}[-|e, 0\rangle + |g, 1\rangle]. \quad (2.36)$$

At $T = 0K$, the only relevant states are $|+, 0\rangle$, $|-, 0\rangle$ and $|g, 0\rangle$. The action of the atom and the field operators on these states yield

$$a|+, 0\rangle = \frac{1}{\sqrt{2}}|g, 0\rangle. \quad (2.37)$$

$$a|-, 0\rangle = \frac{1}{\sqrt{2}}|g, 0\rangle. \quad (2.38)$$

$$a|g, 0\rangle = 0. \quad (2.39)$$

$$a^\dagger|+, 0\rangle = 0. \quad (2.40)$$

$$a^\dagger|-, 0\rangle = 0. \quad (2.41)$$

$$a^\dagger|g, 0\rangle = \frac{1}{\sqrt{2}}[|e, 0\rangle + |g, 1\rangle]. \quad (2.42)$$

$$H_I|e, 0\rangle = g|g, 1\rangle. \quad (2.43)$$

$$H_I|g, 1\rangle = g|e, 0\rangle. \quad (2.44)$$

$$H_I|g, 0\rangle = 0. \quad (2.45)$$

$$H_I|+, 0\rangle = g|+, 0\rangle. \quad (2.46)$$

$$H_I|-, 0\rangle = -g|-, 0\rangle. \quad (2.47)$$

It is straightforward to express the damping equation for the density matrix elements in the dressed state basis.

$$\begin{aligned} \langle +, 0|\dot{\rho}|+, 0\rangle &= -\kappa\langle +, 0|\rho|+, 0\rangle - \frac{\kappa}{2}\langle -, 0|\rho|+, 0\rangle \\ &\quad - \frac{\kappa}{2}\langle +, 0|\rho|-, 0\rangle. \end{aligned} \quad (2.48)$$

$$\begin{aligned} \langle -, 0 | \dot{\rho} | -, 0 \rangle &= -\kappa \langle -, 0 | \rho | -, 0 \rangle - \frac{\kappa}{2} \langle +, 0 | \rho | -, 0 \rangle \\ &\quad - \frac{\kappa}{2} \langle -, 0 | \rho | +, 0 \rangle. \end{aligned} \quad (2.49)$$

$$\begin{aligned} \langle +, 0 | \dot{\rho} | -, 0 \rangle &= -2ig \langle +, 0 | \dot{\rho} | -, 0 \rangle - \kappa \langle +, 0 | \rho | -, 0 \rangle \\ &\quad - \frac{\kappa}{2} \langle +, 0 | \rho | +, 0 \rangle - \frac{\kappa}{2} \langle -, 0 | \rho | -, 0 \rangle. \end{aligned} \quad (2.50)$$

We note that the terms $\langle +, 0 | \rho | +, 0 \rangle$ and $\langle -, 0 | \rho | -, 0 \rangle$ oscillate at zero frequency (or donot oscillate), whereas the terms $\langle +, 0 | \dot{\rho} | -, 0 \rangle$ oscillate at frequency g . The strength of the coupling of these terms are of the order of κ . Hence, for $g \gg \kappa$, it is reasonable to assume that they decouple. In other words, we can neglect their coupling. In the literature, such an approximation is called the ‘‘secular approximation’’. Under this approximation, the equations of motion reduce to

$$\langle +, 0 | \dot{\rho} | +, 0 \rangle = -\kappa \langle +, 0 | \rho | +, 0 \rangle. \quad (2.51)$$

$$\langle -, 0 | \dot{\rho} | -, 0 \rangle = -\kappa \langle -, 0 | \rho | -, 0 \rangle. \quad (2.52)$$

$$\langle +, 0 | \dot{\rho} | -, 0 \rangle = -2ig \langle +, 0 | \dot{\rho} | -, 0 \rangle - \kappa \langle +, 0 | \rho | -, 0 \rangle. \quad (2.53)$$

The obvious solutions of Eq.(2.51), Eq.(2.52) and Eq.(2.53) are

$$\langle +, 0 | \rho | +, 0 \rangle_t = e^{-\kappa t} \langle +, 0 | \rho | +, 0 \rangle_{t=0}, \quad (2.54)$$

$$\langle -, 0 | \rho | -, 0 \rangle_t = e^{-\kappa t} \langle -, 0 | \rho | -, 0 \rangle_{t=0}, \quad (2.55)$$

$$\langle +, 0 | \rho | -, 0 \rangle_t = e^{-2igt} e^{-\kappa t} \langle +, 0 | \rho | -, 0 \rangle_{t=0}. \quad (2.56)$$

We also work under a further approximation (that is justified when the cavity is close to $0K$) that the probability of getting two or more photons inside the cavities is zero, or in other words, the cavity always remains in the two-level state comprising of $|0\rangle$ and $|1\rangle$. For example, the initial state $|e, 0\rangle$ corresponds to the boundary condition

$$\langle +, 0 | \rho | +, 0 \rangle_{t=0} = \langle -, 0 | \rho | -, 0 \rangle_{t=0} = \frac{1}{2}, \quad (2.57)$$

and

$$\langle +, 0 | \rho | -, 0 \rangle_{t=0} = -\frac{1}{2}. \quad (2.58)$$

Therefore

$$\begin{aligned} \langle e, 0 | \rho | e, 0 \rangle_t &= \frac{1}{2} [\langle +, 0 | \rho | +, 0 \rangle_t + \langle -, 0 | \rho | -, 0 \rangle_t \\ &\quad - \langle +, 0 | \rho | -, 0 \rangle_t - \langle -, 0 | \rho | +, 0 \rangle_t] \\ &= \frac{1}{2} e^{-\kappa t} [1 + \cos 2gt] \\ &= e^{-\kappa t} \cos^2 gt, \end{aligned} \quad (2.59)$$

$$\begin{aligned} \langle g, 1 | \rho | g, 1 \rangle_t &= \frac{1}{2} [\langle +, 0 | \rho | +, 0 \rangle_t + \langle -, 0 | \rho | -, 0 \rangle_t \\ &\quad + \langle +, 0 | \rho | -, 0 \rangle_t + \langle -, 0 | \rho | +, 0 \rangle_t] \\ &= \frac{1}{2} e^{-\kappa t} [1 - \cos 2gt] \\ &= e^{-\kappa t} \sin^2 gt, \end{aligned} \quad (2.60)$$

and

$$\begin{aligned} \langle e, 0 | \rho | g, 1 \rangle_t &= \frac{1}{2} [\langle +, 0 | \rho | +, 0 \rangle_t + \langle +, 0 | \rho | -, 0 \rangle_t \\ &\quad - \langle -, 0 | \rho | +, 0 \rangle_t - \langle -, 0 | \rho | -, 0 \rangle_t] \\ &= \frac{i}{2} e^{-\kappa t} [\sin 2gt] \\ &= ie^{-\kappa t} \sin gt \cos gt, \end{aligned} \quad (2.61)$$

$$\langle g, 1 | \rho | e, 0 \rangle_t = -ie^{-\kappa t} \sin gt \cos gt. \quad (2.62)$$

The initial state $|g, 1\rangle$ corresponds to the boundary condition

$$\langle +, 0 | \rho | +, 0 \rangle_{t=0} = \langle -, 0 | \rho | -, 0 \rangle_{t=0} = \frac{1}{2}, \quad (2.63)$$

and

$$\langle +, 0 | \rho | -, 0 \rangle_{t=0} = \frac{1}{2}. \quad (2.64)$$

Therefore

$$\begin{aligned}
\langle e, 0 | \rho | e, 0 \rangle_t &= \frac{1}{2} [\langle +, 0 | \rho | +, 0 \rangle_t + \langle -, 0 | \rho | -, 0 \rangle_t \\
&\quad - \langle +, 0 | \rho | -, 0 \rangle_t - \langle -, 0 | \rho | +, 0 \rangle_t] \\
&= \frac{1}{2} e^{-\kappa t} [1 - \cos 2gt] \\
&= e^{-\kappa t} \sin^2 gt,
\end{aligned} \tag{2.65}$$

$$\begin{aligned}
\langle g, 1 | \rho | g, 1 \rangle_t &= \frac{1}{2} [\langle +, 0 | \rho | +, 0 \rangle_t + \langle -, 0 | \rho | -, 0 \rangle_t \\
&\quad + \langle +, 0 | \rho | -, 0 \rangle_t + \langle -, 0 | \rho | +, 0 \rangle_t] \\
&= \frac{1}{2} e^{-\kappa t} [1 + \cos 2gt] \\
&= e^{-\kappa t} \cos^2 gt,
\end{aligned} \tag{2.66}$$

and

$$\begin{aligned}
\langle e, 0 | \rho | g, 1 \rangle_t &= \frac{1}{2} [\langle +, 0 | \rho | +, 0 \rangle_t + \langle +, 0 | \rho | -, 0 \rangle_t \\
&\quad - \langle -, 0 | \rho | +, 0 \rangle_t - \langle -, 0 | \rho | -, 0 \rangle_t] \\
&= -\frac{i}{2} e^{-\kappa t} [\sin 2gt] \\
&= -ie^{-\kappa t} \sin gt \cos gt,
\end{aligned} \tag{2.67}$$

$$\langle g, 1 | \rho | e, 0 \rangle_t = ie^{-\kappa t} \sin gt \cos gt. \tag{2.68}$$

The above method provides a typical way of solving cavity-QED coupled equations with dissipation. We use them here to study the effect of cavity dissipation on entanglement.

2.3 Various types of entanglement and the effect of cavity dissipation on them

In this section we investigate the various types of entanglement such as atom-cavity entanglement, atom-atom entanglement, and cavity-cavity entanglement in an ideal cavity as well as their evolution in presence cavity dissipation. We quantify the entanglement either with the entanglement measure ‘concurrence’ or ‘entanglement of formation’ [22, 23], through we know that for pure state the von Neumann entropy and ‘entanglement of formation’ are the same.

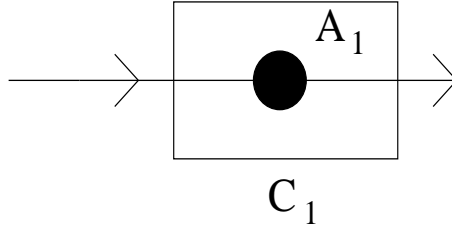


Figure 2.6: A two-level atom prepared in the excited state is traversing through an empty cavity.

2.3.1 Atom-cavity entanglement

Let us first consider a two-level atom A_1 prepared in the excited state $|e\rangle$ passing through an empty cavity C_1 (Figure 2.6). The initial joint state of atom-cavity bipartite system is

$$|\Psi_{A_1C_1}(t=0)\rangle = |e\rangle \otimes |0\rangle. \quad (2.69)$$

The atom-field joint state evolves under the Jaynes-Cummings interaction to

$$|\Psi_{A_1C_1}(t)\rangle = \cos gt|e, 0\rangle + \sin gt|g, 1\rangle, \quad (2.70)$$

which is obtained from Eq.(2.23) by putting $n = 0$. Therefore, the density state can be written as

$$\begin{aligned} \rho_{A_1C_1}(t) &= |\Psi_{A_1C_1}(t)\rangle\langle\Psi_{A_1C_1}(t)| \\ &= \cos^2 gt|e, 0\rangle\langle e, 0| + \cos gt \sin gt|e, 0\rangle\langle g, 1| \\ &\quad + \cos gt \sin gt|g, 1\rangle\langle e, 0| + \sin^2 gt|g, 1\rangle\langle g, 1| \end{aligned} \quad (2.71)$$

The corresponding density matrix $\rho_{A_1C_1}(t)$ can be written as

$$\rho = \begin{pmatrix} 0 & 0 & 0 & 0 \\ 0 & \cos^2 gt & \cos gt \sin gt & 0 \\ 0 & \cos gt \sin gt & \sin^2 gt & 0 \\ 0 & 0 & 0 & 0 \end{pmatrix}, \quad (2.72)$$

in the basis $|e, 1\rangle$, $|e, 0\rangle$, $|g, 1\rangle$ and $|g, 0\rangle$ states. The concurrence C of $\rho_{A_1C_1}(t)$ is $2|\cos gt \sin gt|$. C is maximum ($= 1$) for Rabi angle $gt = (2n+1)\pi/4$. So for an interaction time $gt = (2n+1)\pi/4$, $|\Psi_{A_1C_1}(t)\rangle$ becomes maximally entangled and for an interaction

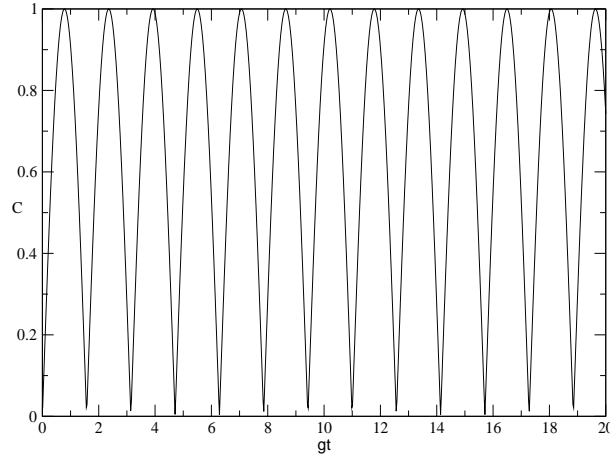


Figure 2.7: Atom-cavity entanglement i.e., concurrence is plotted vs gt

time $gt = n\pi/2$, $|\Psi_{A_1C_1}(t)\rangle$ becomes disentangled. In Figure 2.7 the concurrence C between the atom and the cavity is plotted versus the Rabi angle gt .

Next, we discuss the above case in presence of cavity dissipation. At temperature $T = 0K$, the average thermal photon number is zero, and one has (see, for instance, Ref. [47])

$$\dot{\rho}|_{\text{field-reservoir}} = -\kappa(a^\dagger a \rho - 2a\rho a^\dagger + \rho a^\dagger a), \quad (2.73)$$

as in Eq.(2.31). When $g \gg \kappa$, it is possible to make the secular approximation [27] (discussed in section 2.3) to get the density elements of $\rho_{A_1C_1}(t)$. We also work under a further approximation (which is justified when the cavity is close to $0K$) that the probability of getting two or more photons inside the cavity is zero. The method of solving the dissipation equation has been outlined in section 2.2.1. The joint density state of atom and cavity is then obtained as

$$\begin{aligned} \rho_{A_1C_1}(t) = & (e^{-\kappa t} \cos^2 gt |e, 0\rangle\langle e, 0| + ie^{-\kappa t} \cos gt \sin gt |e, 0\rangle\langle g, 1| \\ & -ie^{-\kappa t} \cos gt \sin gt |g, 1\rangle\langle e, 0| + e^{-\kappa t} \sin^2 gt |g, 1\rangle\langle g, 1|), \end{aligned} \quad (2.74)$$

where κ is leakage constant for cavity C_1 . The corresponding density matrix $\rho_{A_1C_1}(t)$ is

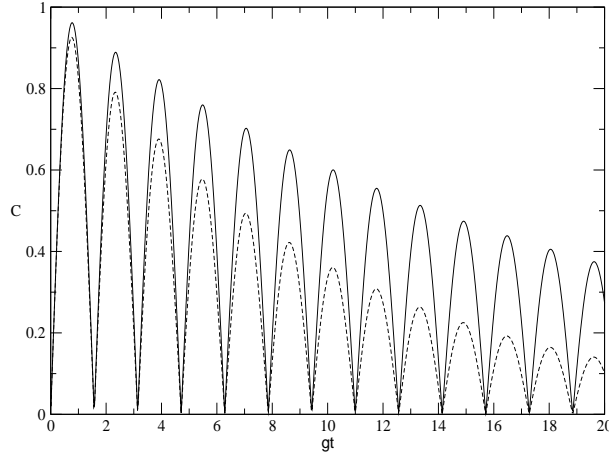


Figure 2.8: Atom-cavity entanglement i.e., concurrence is plotted vs gt for (i) $\kappa/g = 0.05$ (solid line), (ii) $\kappa/g = 0.1$ (dashed line).

given by

$$\rho = \begin{pmatrix} 0 & 0 & 0 & 0 \\ 0 & e^{-\kappa t} \cos^2 gt & ie^{-\kappa t} \cos gt \sin gt & 0 \\ 0 & -ie^{-\kappa t} \cos gt \sin gt & e^{-\kappa t} \sin^2 gt & 0 \\ 0 & 0 & 0 & 0 \end{pmatrix}, \quad (2.75)$$

in the basis of $|e, 1\rangle$, $|e, 0\rangle$, $|g, 1\rangle$ and $|g, 0\rangle$ states.

The concurrence C of $\rho_{A_1 C_1}(t)$ is $|2e^{-\kappa t} \cos gt \sin gt|$. In Figure 2.8 the concurrence C between the atom and the cavity is plotted versus the Rabi angle gt for different values of the cavity leakage constant κ/g . We see clearly the effect of dissipation on entanglement which reduces as we increase the cavity leakage constant κ . This shows that dissipation reduces the atom-cavity entanglement and, ultimately it is destroyed at a later time. If we send an atom prepared in the ground state $|g\rangle$ through the one photon cavity, the initial joint atom-cavity state will be

$$|\Psi(t=0)\rangle = |g\rangle \otimes |1\rangle. \quad (2.76)$$

The time evolved state is

$$|\Psi(t)\rangle = \cos gt |g, 1\rangle - \sin gt |e, 0\rangle. \quad (2.77)$$

In this case the result for entanglement is similar to the case for the state

$$|\Psi(t)\rangle = \cos gt |e, 0\rangle + \sin gt |g, 1\rangle, \quad (2.78)$$

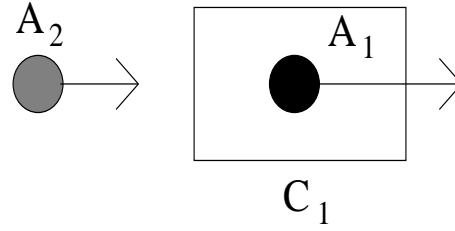


Figure 2.9: Two two-level atoms, first prepared in the excited state and second prepared in the ground state, traverses an empty cavity one after the other.

that we have considered earlier, both with and without dissipation.

2.3.2 Atom-atom entanglement

We consider a system where two two-level atoms, the first prepared in the excited state and the second prepared in the ground state, are sent into a cavity in the vacuum state one after the other (see Figure 2.9). The flight times of both the atoms through the cavity are assumed to be the same.

Let us first consider the passage of the first atom, initially in the excited state $|e\rangle$, through the cavity. The initial joint atom-field state is given by

$$|\Psi(t=0)\rangle_{A_1 C_1} = |e\rangle \otimes |0\rangle. \quad (2.79)$$

The atom-field state evolves with the interaction given by Eqs.(2.70) to

$$|\Psi(t)\rangle_{A_1 C_1} = \cos gt|e, 0\rangle + \sin gt|g, 1\rangle, \quad (2.80)$$

The next atom prepared in $|g\rangle$ which enters the cavity interacts with this “changed” field and thus a correlation develops between the two atoms via the cavity field. The joint tripartite state of the two atoms and the field is given by

$$\begin{aligned} |\Psi(t)\rangle_{A_1 A_2 C_1} &= \cos gt|e_1, g_2, 0\rangle + \cos gt \sin gt|g_1, g_2, 1\rangle \\ &\quad - \sin^2 gt|g_1, e_2, 0\rangle \end{aligned} \quad (2.81)$$

The corresponding atom-atom-field pure density state is

$$\rho(t)_{A_1 A_2 C_1} = |\Psi(t)\rangle_{A_1 A_2 C_1} {}_{A_1 A_2 C_1} \langle \Psi(t)|$$

$$\begin{aligned}
&= \cos^2 gt |e_1, g_2, 0\rangle \langle e_1, g_2, 0| + \cos^2 gt \sin^2 gt |g_1, g_2, 1\rangle \langle g_1, g_2, 1| \\
&+ \sin^4 gt |g_1, e_2, 0\rangle \langle g_1, e_2, 0| + \cos^2 gt \sin gt |e_1, g_2, 0\rangle \langle g_1, g_2, 1| \\
&+ \cos^2 gt \sin gt |g_1, g_2, 1\rangle \langle e_1, g_2, 0| - \cos gt \sin^2 gt |e_1, g_2, 0\rangle \langle g_1, e_2, 0| \\
&- \cos gt \sin^2 gt |g_1, e_2, 0\rangle \langle e_1, g_2, 0| - \cos gt \sin^3 gt |g_1, g_2, 1\rangle \langle g_1, e_2, 0| \\
&- \cos gt \sin^3 gt |g_1, e_2, 0\rangle \langle g_1, g_2, 1|.
\end{aligned} \tag{2.82}$$

The reduced density state of the pair A_1A_2 is obtained by tracing out the field variables, and is given by

$$\begin{aligned}
\rho(t)_{A_1A_2} &= \text{Tr}_{C_1}(\rho_{A_1A_2C_1}) \\
&= \cos^2 gt |e_1, g_2\rangle \langle e_1, g_2| + \cos^2 gt \sin^2 gt |g_1, g_2\rangle \langle g_1, g_2| \\
&+ \sin^4 gt |g_1, e_2\rangle \langle g_1, e_2| - \cos gt \sin^2 gt |g_1, e_2\rangle \langle e_1, g_2| \\
&- \cos gt \sin^2 gt |e_1, g_2\rangle \langle g_1, e_2|
\end{aligned} \tag{2.83}$$

The corresponding density matrix $\rho_{A_1A_2}(t)$ is given by

$$\rho = \begin{pmatrix} \cos^2 gt \sin^2 gt & 0 & 0 & 0 \\ 0 & \sin^4 gt & -\cos gt \sin^2 gt & 0 \\ 0 & -\cos gt \sin^2 gt & \cos^2 gt & 0 \\ 0 & 0 & 0 & 0 \end{pmatrix}, \tag{2.84}$$

in the basis $|g_1, g_2\rangle$, $|g_1, e_2\rangle$, $|e_1, g_2\rangle$ and $|e_1, e_2\rangle$ states.

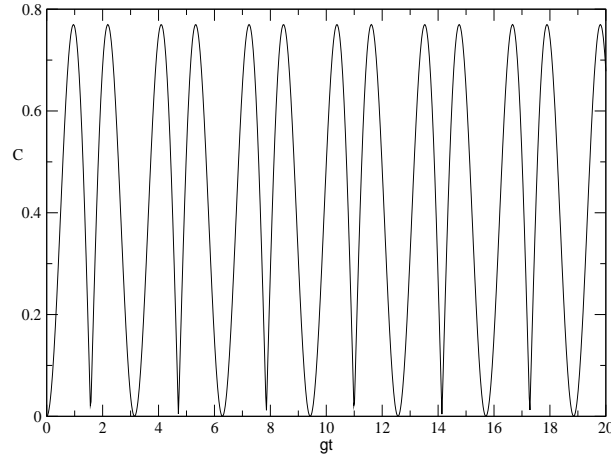
We compute the concurrence for $\rho(t)_{A_1A_2}$ that is

$$C(\rho(t)_{A_1A_2}) = |2 \cos gt \sin^2 gt|. \tag{2.85}$$

The concurrence between the two atoms is plotted versus the Rabi angle gt in Figure 2.10.

We now investigate the above study in presence of the cavity dissipation. Like in the previous section, in the presence of cavity dissipation the evolved state of the system $A_1A_2C_1$ is a mixed state and is obtained with the above approximations (see section 2.2.1). The reduced density state of the pair A_1A_2 is

$$\begin{aligned}
\rho(t)_{A_1A_2} &= \text{Tr}_{C_1}(\rho_{A_1A_2C_1}) \\
&= \gamma_1 |e_1g_2\rangle \langle e_1g_2|
\end{aligned}$$

Figure 2.10: Atom-atom entanglement i.e., concurrence is plotted vs gt

$$\begin{aligned}
& + \gamma_2 |g_1 g_2\rangle \langle g_1 g_2| \\
& + \gamma_3 |g_1 e_2\rangle \langle g_1 e_2| \\
& - \gamma_4 |e_1 g_2\rangle \langle g_1 e_2| \\
& - \gamma_4 |g_1 e_2\rangle \langle e_1 g_2|,
\end{aligned} \tag{2.86}$$

where the γ_i are given by

$$\begin{aligned}
\gamma_1 &= (1 - \sin^2 gte^{-\kappa t}), \\
\gamma_2 &= \cos^2 gt \sin^2 gte^{-2\kappa t}, \\
\gamma_3 &= \sin^4 gte^{-2\kappa t}, \\
\gamma_4 &= \left(\sin gte^{-\kappa t/2} - \frac{\kappa}{2g} \cos gte^{-\kappa t/2} + \frac{\kappa}{2g} \right) \cos gt \sin gte^{-\kappa t},
\end{aligned}$$

κ is the leakage constant of cavity C_1 . The corresponding density matrix $\rho_{A_1 A_2}(t)$ is

$$\rho = \begin{pmatrix} \gamma_2 & 0 & 0 & 0 \\ 0 & \gamma_3 & -\gamma_4 & 0 \\ 0 & -\gamma_4 & \gamma_1 & 0 \\ 0 & 0 & 0 & 0 \end{pmatrix}, \tag{2.87}$$

in the basis of $|g_1, g_2\rangle$, $|g_1, e_2\rangle$, $|e_1, g_2\rangle$ and $|e_1, e_2\rangle$ states.

We compute the concurrence for $\rho(t)_{A_1 A_2}$, i.e.,

$$C(\rho(t)_{A_1 A_2}) = |2 \sin^2 gte^{-\kappa t} \sqrt{(1 - \sin^2 gte^{-\kappa t})}| \tag{2.88}$$

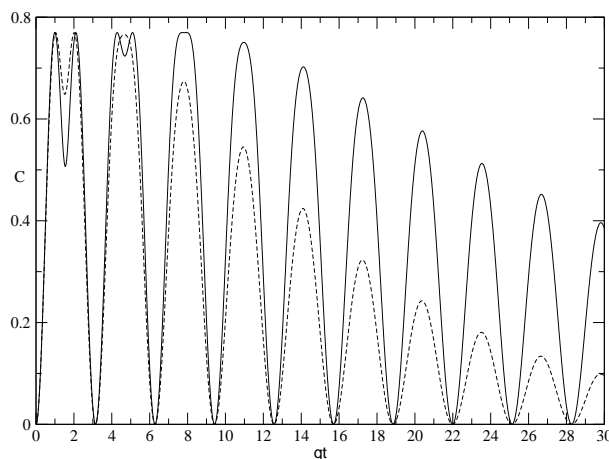


Figure 2.11: Atom-atom entanglement i.e., concurrence is plotted vs gt for (i) $\kappa/g = 0.05$ (solid line) (ii) $\kappa/g = 0.1$ (dashed line).

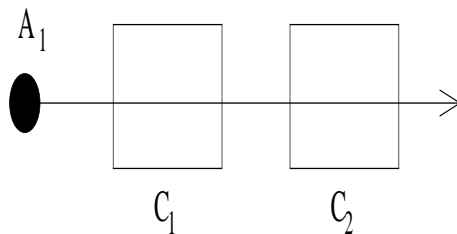


Figure 2.12: A two-level atom prepared in the excited state is traversing through two separated cavities one after another.

The concurrence between the two atoms is plotted versus the Rabi angle gt in Figure 2.11 for different values of the cavity dissipation parameter κ . The entanglement reduces as we increase κ . The effect of κ gets more and more pronounced as time increases.

2.3.3 Cavity-cavity entanglement

Here we consider two initially separated empty cavities C_1 , C_2 and a two-level atom prepared in the excited state passing through C_1 and C_2 such that the times of flight of the atom through the two cavities are the same (see Figure 2.12). The initial joint state of the atom and the two cavities is

$$|\Psi(t)\rangle_{A_1 C_1 C_2} = |e_1\rangle \otimes |0_1\rangle \otimes |0_2\rangle. \quad (2.89)$$

The joint state of the two cavities and the atom undergoing the Jaynes-Cummings interaction at a later time is

$$\begin{aligned} |\Psi(t)\rangle_{A_1 C_1 C_2} &= \cos^2 gt |e_1, 0_2, 0_2\rangle + \cos gt \sin gt |g_1, 0_1, 1_2\rangle \\ &\quad - \sin gt |g_1, 1_1, 0_2\rangle. \end{aligned} \quad (2.90)$$

The corresponding cavity-cavity-atom tripartite pure density state is

$$\begin{aligned} \rho(t)_{A_1 C_1 C_2} &= |\Psi(t)\rangle_{A_1 C_1 C_2} {}_{A_1 C_1 C_2} \langle \Psi(t)| \\ &= \cos^4 gt |e_1, 0_1, 0_2\rangle \langle e_1, 0_1, 0_2| + \cos^2 gt \sin^2 gt |g_1, 0_1, 1_2\rangle \langle g_1, 0_1, 1_2| \\ &\quad + \sin^2 gt |g_1, 1_1, 0_2\rangle \langle g_1, 1_1, 0_2| + \cos^3 gt \sin gt |e_1, 0_1, 0_2\rangle \langle g_1, 0_1, 1_2| \\ &\quad + \cos^2 gt \sin gt |e_1, 0_1, 0_2\rangle \langle g_1, 1_1, 0_2| + \cos^3 gt \sin gt |g_1, 0_1, 1_2\rangle \langle e_1, 0_1, 0_2| \\ &\quad + \cos gt \sin^2 gt |g_1, 0_1, 1_2\rangle \langle g_1, 1_1, 0_2| + \cos^2 gt \sin gt |g_1, 1_1, 0_2\rangle \langle e_1, 0_1, 0_2| \\ &\quad + \cos gt \sin^2 gt |g_1, 1_1, 0_2\rangle \langle g_1, 0_1, 1_2|. \end{aligned} \quad (2.91)$$

The reduced density state of the pair $C_1 C_2$ is

$$\begin{aligned} \rho(t)_{C_1 C_2} &= \text{Tr}_{A_1}(\rho_{A_1 C_1 C_2}) \\ &= \cos^4 gt |0_1, 0_2\rangle \langle 0_1, 0_2| + \cos^2 gt \sin^2 gt |0_1, 1_2\rangle \langle 0_1, 1_2| \\ &\quad + \sin^2 gt |1_1, 0_2\rangle \langle 1_1, 0_2| + \cos gt \sin^2 gt |1_1, 0_2\rangle \langle 0_1, 1_2| \\ &\quad + \cos gt \sin^2 gt |0_1, 1_2\rangle \langle 1_1, 0_2|. \end{aligned} \quad (2.92)$$

The corresponding density matrix $\rho_{C_1 C_2}(t)$ is given by

$$\rho = \begin{pmatrix} \cos^4 gt & 0 & 0 & 0 \\ 0 & \sin^2 gt \cos^2 gt & \cos gt \sin^2 gt & 0 \\ 0 & \cos gt \sin^2 gt & \sin^2 gt & 0 \\ 0 & 0 & 0 & 0 \end{pmatrix}, \quad (2.93)$$

in the basis of $|0_1, 0_2\rangle$, $|0_1, 1_2\rangle$, $|1_1, 0_2\rangle$ and $|1_1, 1_2\rangle$ states. We find that the concurrence for $\rho(t)_{C_1 C_2}$ has the form

$$C(\rho(t)_{C_1 C_2}) = |2 \cos gt \sin^2 gt|. \quad (2.94)$$

The concurrences of the two atoms (see earlier section) and the two cavities are similar functions of the Rabi angle. The concurrence between two cavities is plotted versus the

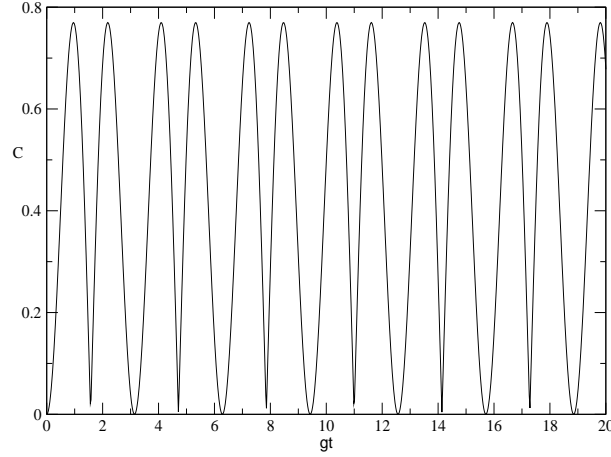


Figure 2.13: Cavity-cavity entanglement i.e., concurrence is plotted vs gt

Rabi angle gt in Figure 2.13.

The time evolution of the reduced density state of two cavities in presence of dissipation is, following the method outlined earlier,

$$\begin{aligned}
 \rho(t)_{C_1 C_2} &= \text{Tr}_{A_1}(\rho_{A_1 C_1 C_2}) \\
 &= e^{-2\kappa t} \cos^4 gt |0_1, 0_2\rangle \langle 0_1, 0_2| + e^{-2\kappa t} \cos^2 gt \sin^2 gt |0_1, 1_2\rangle \langle 0_1, 1_2| \\
 &+ (1 - e^{-\kappa t} \cos^2 gt) |1_1, 0_2\rangle \langle 1_1, 0_2| + e^{-\frac{3\kappa t}{2}} \cos gt \sin^2 gt |1_1, 0_2\rangle \langle 0_1, 1_2| \\
 &+ e^{-\frac{3\kappa t}{2}} \cos gt \sin^2 gt |0_1, 1_2\rangle \langle 1_1, 0_2|.
 \end{aligned} \tag{2.95}$$

The corresponding density matrix $\rho_{A_1 A_2}(t)$ is given by

$$\rho = \begin{pmatrix} e^{-2\kappa t} \cos^4 gt & 0 & 0 & 0 & 0 \\ 0 & e^{-2\kappa t} \sin^2 gt \cos^2 gt & e^{-\frac{3\kappa t}{2}} \cos gt \sin^2 gt & 0 & 0 \\ 0 & e^{-\frac{3\kappa t}{2}} \cos gt \sin^2 gt & (1 - e^{-\kappa t} \cos^2 gt) & 0 & 0 \\ 0 & 0 & 0 & 0 & 0 \end{pmatrix}, \tag{2.96}$$

in the basis of $|0_1, 0_2\rangle$, $|0_1, 1_2\rangle$, $|1_1, 0_2\rangle$ and $|1_1, 1_2\rangle$ states. We compute the concurrence for $\rho(t)_{C_1 C_2}$, that is given by

$$C(\rho(t)_{C_1 C_2}) = |2 \cos gt \sin^2 gte^{-\frac{3\kappa t}{2}}|. \tag{2.97}$$

The concurrence between two cavities is plotted versus the Rabi angle gt in Figure 2.14 for different values of the cavity dissipation parameter κ . The effect of κ gradually reduces the entanglement as it evolves in time.

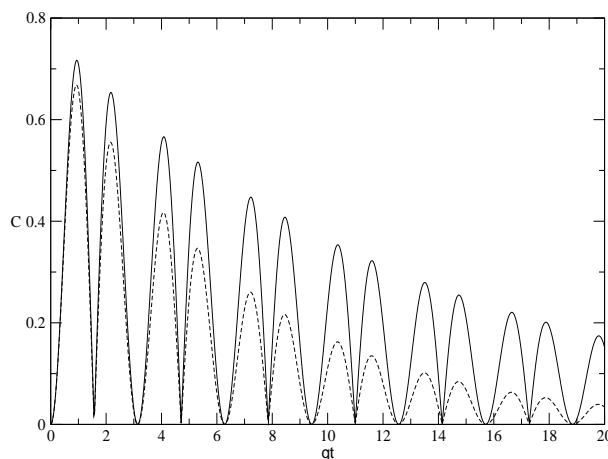


Figure 2.14: Cavity-cavity entanglement i.e., concurrence is plotted vs gt for (i) $\kappa/g = 0.05$ (solid line) (ii) $\kappa/g = 0.1$ (dashed line).

2.4 Summary

In this chapter we have discussed the Jaynes-Cummings model which consists of a two-level atom interacting with a single mode cavity field. This is an exactly solvable model. We have considered resonant interaction between the atom and the cavity field. We saw that the Jaynes-Cummings interaction Hamiltonian takes a simple form in the rotating wave approximation. We then discussed the time evolution of atom-field states evolving under the Jaynes-Cummings interaction. Next we discussed dissipative dynamics of cavity field. Here we considered only cavity dissipation as the lifetime of two-level atoms (we are considering two-level Rydberg atoms) is much longer than the atom-field interaction time. Basically, the dynamical equation of the atom-field density state evolves under (i) the simple atom-field interaction, and (ii) the field-reservoir interaction. We solved the equations of motion under the secular approximation by using the fact that $g \gg \kappa$.

We investigated the various types of entanglement which originates from the Jaynes-Cummings interaction both in ideal and dissipative systems. We showed how the atom-cavity, atom-atom, and cavity-cavity entanglement can be generated in atom-photon interactions. We studied quantitatively the atom-cavity, atom-atom, and cavity-cavity entanglement as functions of the Rabi angle gt in the ideal situation and also in presence of cavity dissipation. We have used the entanglement measure, concurrence [22, 23] to quan-

tify the entanglement. We observed that the cavity dissipation kills the entanglement in all cases as we increase the atom-field interaction time. In this chapter we have set up the framework of generating and quantifying various types of entanglement in atom-photon interactions governed by the Jaynes-Cummings model, which will be applied in the subsequent chapters for performing different studies such as the generation of entanglement in realistic devices, investigating characteristic properties of entanglement, etc.

Chapter 3

Quantum entanglement in the micromaser

3.1 Introduction

The generation of quantum entanglement in atomic systems is being vigorously pursued in recent years. The primary motivation for this upsurge of interest is to test the applicability of the ongoing conceptual developments in quantum information theory and through them the implementation of current quantum communication and computation protocols [4]. Several schemes have been proposed recently to engineer the entanglement of two [48] or more atoms [49, 50]. Many of these proposals are for generating entanglement in a probabilistic manner. Since a large number of these proposals rely on the trapping or slow passage of cold atoms through optical cavities [6], the efficient control of cavity leakage and atomic dissipation is a major concern [51]. As we have seen in chapter 2, decoherence effects are significant even in the time $O(1/g)$ needed for perceptible entanglement. The micromaser, is appreciated as a practical device for processing quantum information, where such dissipative effects can be experimentally monitored.

The one-atom micromaser [29, 30, 31], in which at best one atom at a time is allowed to interact with the radiation field high Q microwave cavity maintained at sub-Kelvin temperatures, has been widely examined as this is now capable of answering a variety of fundamental questions [52]. Moreover, it is now hoped that the radiation field in the cavity may evolve to a Fock state. It is well known that this can be very sensitive to noisy mechanisms, however small, accompanying the coherent atom-field interaction. The decoherence due to atom-reservoir interaction does not affect the individual single-atom dynamics since we consider Rydberg atoms whose lifetime is much longer compared

to the interaction time of the atom and field inside the micromaser.

To find out how these noise creep into the evolution of the cavity radiation field while interacting with a single atom (represented by its two Rydberg levels with transition frequency ω_0 in resonance with the cavity eigenmode) with a random time duration between their successive arrivals at the cavity, let us examine the micromaser mechanism starting from the very first atom that enters the cavity. The radiation field of frequency ω inside the cavity is in equilibrium at its temperature $T(K)$ and has average thermal photons \bar{n}_{th} with which the very first atom interacts for a duration τ , fixed for every atom. The next atom sees the radiation field left in the cavity after the interaction with previous atom. The cavity field evolves under its own dynamics for the duration t_{cav} between two successive atoms. The process repeats itself after every \bar{t}_c seconds where $\bar{t}_c = 1/R$ with R being the number of atoms passing through the cavity per second. Thus we have a repetition time $t_c = \tau + t_{cav}$. \bar{t}_c is the average of t_c with respect to the distribution in time of the incoming atoms which we consider to be Poissonian (random) such as in the experimental setup [29, 31]. From this mechanism, we find that the cavity radiation field is in interaction with its reservoir all the time.

Naturally, the dynamics will carry the signatures of the reservoir to the steady-state situation of the cavity field. In an earlier work [30], the effect of the reservoir was neglected during τ . Although the setting is to have $\tau \ll t_{cav}$ as in the experiments [29, 31], the duration τ can itself be long enough to make the influence of the reservoir crucial. We describe below a micromaser dynamics [33] that includes the influence of the cavity reservoir during the crucial atom-field interaction. The evolution of the cavity field when it is empty of atoms is, of course, included in the dynamics.

3.1.1 The experimental scenario

Before discussing the dynamics, let us briefly describe of the experimental scenario which we model in our analysis. A two-level atom initially in its upper excited state $|e\rangle$ traverses a high-Q single mode cavity. The cavity is in a steady state built up by the dynamics described in the previous section. The emerging single-atom wavefunction is a superposition of the upper $|e\rangle$ and lower $|g\rangle$ state and it leaves an imprint on the photonic

wavefunction in the cavity. During this process, cavity leakage takes place, and is taken into account. Next, a second experimental atom, prepared also in state $|e\rangle$, encounters the cavity photons whose state has been now modified by the passage of the first atom. This atom too emerges in a superposition with either of the above two outcomes possible. Although there is no direct interaction between the atoms, correlations develop between their states mediated by the cavity photons [20, 53]. The effects of dissipation on these correlations can be computed [20]. After emanating from the cavity, each of the atoms encounters a $\pi/2$ pulse through an electromagnetic field whose phase may be varied for different atoms. The effect of the $\pi/2$ pulse is to transform the state $\frac{1}{\sqrt{2}}(|e\rangle + |g\rangle)$ to $|g\rangle$ and the state $\frac{1}{\sqrt{2}}(|e\rangle - |g\rangle)$ to $|e\rangle$. These resultant states may now be detected, and the corresponding outcomes used to signify the states emanating from the cavity.

3.2 Micromaser dynamics

The Hamiltonian for the resonant interaction between the single atom and the single mode of the radiation field described by the Jaynes-Cummings model (as in Eq.(2.11) is

$$H_I = g(\sigma^+ a + \sigma^- a^\dagger). \quad (3.1)$$

The equation of motion of the composite atom-field density state ρ due to the interaction in Eq.(3.1) is

$$\dot{\rho}|_{\text{atom-field}} = -i[H_I, \rho]. \quad (3.2)$$

The reservoir-induced interactions can be effectively represented by the well-known master equation [46, 47] (see Appendix 1 on page 114). For the field-reservoir coupling, after tracing over the reservoir variables, we have

$$\begin{aligned} \dot{\rho}|_{\text{field-reservoir}} &= -\kappa(1 + \bar{n}_{th})(a^\dagger a \rho - 2a \rho a^\dagger + \rho a^\dagger a) \\ &\quad - \kappa \bar{n}_{th}(a a^\dagger \rho - 2a^\dagger \rho a + \rho a a^\dagger), \end{aligned} \quad (3.3)$$

where $\kappa = \frac{\omega}{2Q}$ is the cavity bandwidth and \bar{n}_{th} is the average photon number representing the reservoir. The cavity photon lifetime t_p is related to the bandwidth by $t_p = \frac{1}{2\kappa}$. Hence

the equation of motion of ρ due to the above interactions of the system in Eqs.(3.2) and (3.3), is

$$\dot{\rho} = \dot{\rho}|_{\text{atom-field}} + \dot{\rho}|_{\text{field-reservoir}}. \quad (3.4)$$

This governs the equation of motion during τ while the dynamics is solely represented by Eq.(3.3) during t_{cav} . Hence we divide the process during the repetition time t_c into two regimes, i.e., (i) *atom-field interaction duration*, and (ii) *cavity empty of atoms*. We now solve Eq.(3.4) to evaluate the change in ρ during τ . It has been found convenient to work in a picture [54] represented by the so-called dressed state [27] (Eq.(2.32) and Eq.(2.33)) These are

$$|+, n\rangle = \frac{1}{\sqrt{2}}[|e, n\rangle + |g, n+1\rangle], \quad (3.5)$$

and

$$|-, n\rangle = \frac{1}{\sqrt{2}}[-|e, n\rangle + |g, n+1\rangle]. \quad (3.6)$$

The equation of motion in Eq.(3.4), written in the dressed state basis, reduces to four coupled equations governing the time evolution of $\langle +, n|\dot{\rho}|+, n\rangle$, $\langle -, n|\dot{\rho}|-, n\rangle$, $\langle +, n|\dot{\rho}|-, n\rangle$ and $\langle -, n|\dot{\rho}|+, n\rangle$. The coupled equations have been solved using the experimental condition, $\kappa \ll g$, known as the secular approximation. A time derivative of the density matrix in photon number representation, that is $\rho_{n,n} = \langle n|\rho|n\rangle$, has been obtained after tracing over the atomic states. The resulting equation of motion is

$$\dot{P}_n|_{\text{gain-cum-loss}} = X_n P_{n-1} + (Y_n - R)P_n + Z_n P_{n+1}, \quad (3.7)$$

where,

$$\begin{aligned} X_n &= R \sin^2(g\sqrt{n}\tau) \exp\{-(2n-1)\kappa\tau\} \\ Y_n &= \frac{1}{2}R \left(\{2 \cos^2[g\sqrt{n+1}\tau] - \frac{1}{2}(2n+1) \right. \\ &\quad \left. + F_1(n-1)\} \exp\{-(2n+1)\kappa\tau\} + \left[\frac{1}{2}(2n+1) \right. \right. \\ &\quad \left. \left. - F_2(n-1) \right] \exp\{-(2n-1)\kappa\tau\} \right), \end{aligned} \quad (3.8)$$

and

$$Z_n = \frac{1}{2}R\left(\left[\frac{1}{2}(2n+3) + F_2(n)\right] \exp\{-(2n+1)\kappa\tau\} - \left[\frac{1}{2}(2n+3) + F_1(n)\right] \exp\{-(2n+3)\kappa\tau\}\right).$$

The functions F_i are

$$F_i(n) = \frac{\kappa/4g}{(\sqrt{n+2} - \sqrt{n+1})^2} \left[-[2n+3 + 2\sqrt{(n+1)(n+2)}](\sqrt{n+2} - \sqrt{n+1}) \sin(2g\sqrt{m}\tau) \right] + \frac{\kappa/4g}{(\sqrt{n+2} + \sqrt{n+1})^2} \left[\mp[2n+3 - 2\sqrt{(n+1)(n+2)}](\sqrt{n+2} + \sqrt{n+1}) \sin(2g\sqrt{m}\tau) \right] \quad (3.9)$$

where $m = n+2$ and $n+1$ for $i = 1$ and 2 , respectively, with the upper sign for $i = 1$. The time evolution of $P_{n,n}$ during t_{cav} , cavity empty of atom, can be easily obtained by writing Eq.(3.3) in $|n\rangle$ basis :

$$\dot{P}_n|_{\text{dissipation}} = A_n P_{n-1} + B_n P_n + C_n P_{n+1}, \quad (3.10)$$

where $A_n = 2n\kappa\bar{n}_{th}$, $B_n = -2\kappa(n + \bar{n}_{th} + 2n\bar{n}_{th})$ and $C_n = 2(n+1)(\bar{n}_{th} + 1)\kappa$.

3.2.1 Steady state photon distribution

We now derive $P_{n,n}$ in a steady-state in which gain and loss in Eqs. (3.7) and (3.10) respectively, compensate each other. So, we can write

$$\begin{aligned} \dot{P}_n &= \dot{P}_n|_{\text{gain-cum-loss}} + \dot{P}_n|_{\text{dissipation}} \\ &= 0. \end{aligned} \quad (3.11)$$

This gives a tri-diagonal equation

$$-f_3^{(n)} P_{n-1} + f_2^{(n)} P_n + f_1^{(n)} P_{n+1} = 0. \quad (3.12)$$

We define

$$v_n = \frac{P_n}{P_{n-1}}. \quad (3.13)$$

Eq.(3.12) then gives v_n in the form of a continued fraction.

$$v_m = f_3^{(m)} / (f_2^{(m)} + f_1^{(m)} v_{m+1}). \quad (3.14)$$

We obtain all the P_n s from

$$P_n = P_0 \prod_{m=1}^n v_m \quad (3.15)$$

P_0 is obtained from the normalization $\sum_{n=0}^{\infty} P_n = 1$. The above distribution function describes the micromaser cavity in a steady state on which the experimental atoms impinge one after another.

3.3 The generation of atomic entanglement

The formation of atom-photon entanglement and the subsequent generation of correlations between spatially separated atoms has been shown using the micromaser [9]. Englert et al [55] have also shown using a non-separability criterion, the generation of entanglement between two atoms that pass through a one-atom micromaser one after the other, in immediate succession. The nonlocal correlations developed in this fashion between two or more atoms can be used to test the violation of Bell-type inequalities [8, 20, 53, 55]. For Rydberg atoms tuned with microwave frequencies, atomic damping is negligible, and it does not crucially affect the individual single atom dynamics. However, cavity dissipation does build up over the passage of a number of atoms through the micromaser, and is revealed in the photonic statistics of the steady-state cavity field, as was discussed in the previous section. The entanglement between a pair of atoms pumped at the same time through a micromaser has been analysed in Ref. [8]. It is rather difficult to practically realize such a set-up though. The genuine one-atom micromaser, on the other hand, can be operated over a reasonably large region of parameter space, and is thus a feasible device [31] for generating entanglement between two or more atoms.

3.3.1 The entanglement of formation of two successive atoms

Since the joint state of the two atoms emanating from the cavity is not a pure state, we quantify the entanglement using the well known measure appropriate for mixed states, i.e.,

the entanglement of formation [22, 23]. We compute the atomic entanglement generated between two experimental atoms that pass successively through the micromaser cavity. The tripartite joint state of the cavity and the two atoms is obtained by summing over all n . The reduced density state of the two atoms after passing through the cavity field after tracing over the field (we display the non-vanishing terms only) is given by

$$\begin{aligned}
\rho(t)_{A_1 A_2} &= \text{tr}_f(\rho(t)_{A_1 A_2 f}) \\
&= \beta_1 |e_1 e_2\rangle \langle e_1 e_2| + \beta_2 |e_1 g_2\rangle \langle e_1 g_2| \\
&\quad + \beta_3 |g_1 e_2\rangle \langle g_1 e_2| + \beta_4 |e_1 g_2\rangle \langle g_1 e_2| \\
&\quad + \beta_4 |g_1 e_2\rangle \langle e_1 g_2| + \beta_5 |g_1 g_2\rangle \langle g_1 g_2|,
\end{aligned} \tag{3.16}$$

where the β_i are given by

$$\begin{aligned}
\beta_1 &= \sum_n P_n^{ss} \cos^4(\sqrt{n+1}gt), \\
\beta_2 &= \sum_n P_n^{ss} \cos^2(\sqrt{n+1}gt) \sin^2(\sqrt{n+1}gt), \\
\beta_3 &= \sum_n P_n^{ss} \cos^2(\sqrt{n+2}gt) \sin^2(\sqrt{n+1}gt), \\
\beta_4 &= \sum_n P_n^{ss} \sin^2(\sqrt{n+1}gt) \cos(\sqrt{n+1}gt) \cos(\sqrt{n+2}gt), \\
\beta_5 &= \sum_n P_n^{ss} \sin^2(\sqrt{n+1}gt) \sin^2(\sqrt{n+2}gt).
\end{aligned} \tag{3.17}$$

The corresponding reduced density matrix is obtained to be

$$\rho(t)_{A_1 A_2} = \begin{pmatrix} \beta_5 & 0 & 0 & 0 \\ 0 & \beta_3 & \beta_4 & 0 \\ 0 & \beta_4 & \beta_2 & 0 \\ 0 & 0 & 0 & \beta_1 \end{pmatrix} \tag{3.18}$$

in the basis of $|g_1 g_2\rangle$, $|g_1 e_2\rangle$, $|e_1 g_2\rangle$ and $|e_1 e_2\rangle$ states.

We compute numerically the values of $E_F(\rho_a)$ [22, 23] for a range of micromaser parameters. We plot the entanglement of formation E_F of the two-atom state versus the micromaser pump parameter $D = gt\sqrt{N}$ for different values of the average thermal photons number n_{th} for fixed $\kappa/g = 0.000001$ in Figure 3.1. We also plot E_F vs κ/g for different values of the micromaser pump parameter D in Figure 3.2. The steady-state photon statistics of the cavity field [20, 33] depending on the cavity parameters are reflected in the entanglement properties of the emerging atoms.

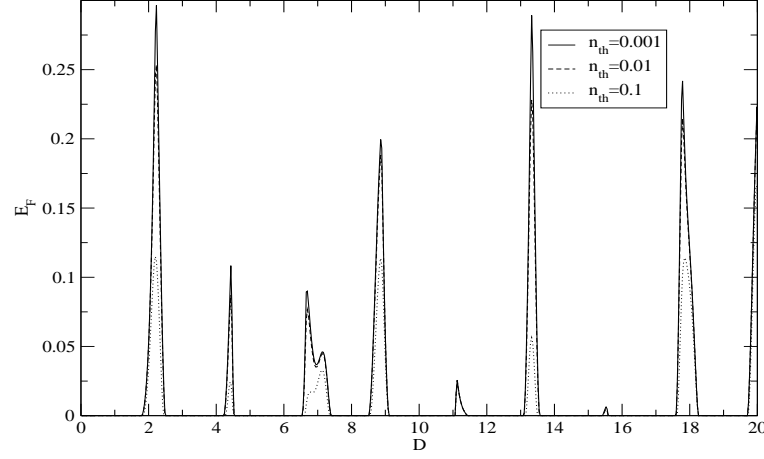


Figure 3.1: Atom-atom entanglement i.e., E_F is plotted vs micromaser pump parameter $D = gt\sqrt{N}$ for different values of n_{th} . $\kappa/g = 0.000001$, $N = 1$.

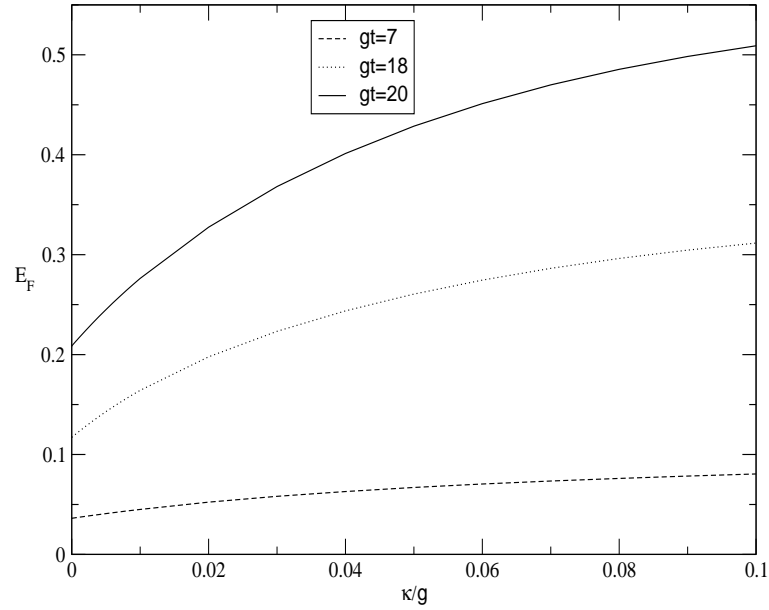


Figure 3.2: Atom-atom entanglement i.e., E_F is plotted vs κ/g for different values of the micromaser pump parameter $D = gt\sqrt{N}$. $n_{th} = 0.01$, $N = 1$.

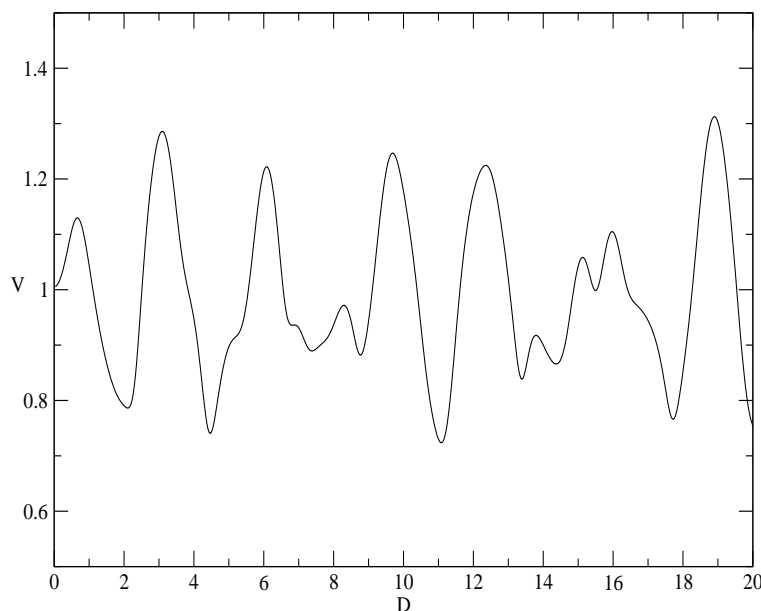


Figure 3.3: Variance of the photon number distribution of the cavity (V) is plotted vs micromaser pump parameter $D = gt\sqrt{N}$. $\kappa/g = 0.001$ and $n_{th} = 0.01$, $N = 1$.

3.3.2 Information transfer in the micromaser

Information is transferred from the cavity to the atoms in order to build up entanglement. The amount of information transferred is expected to depend on the available information content of the cavity. The variance of the photon number distribution of the cavity is an indicator of the information content of the cavity field, and we compute the variance (Figure 3.3) over a range of atom-photon interaction times. The total information inside the cavity is however measured by its Shannon entropy [56] which has contributions from higher moments of the photon statistics as well. We therefore calculate the Shannon entropy of the photon distribution function in the cavity before and after the passage of the two atoms. The role of photon statistics on information transfer is further revealed by the computation of the Shannon entropy which for the cavity in a steady state is

$$S(\rho_f^{(ss)}) = - \sum_{n=1}^{\infty} P_n^{(ss)} \log P_n^{(ss)} \quad (3.19)$$

using the expression for the steady-state photon number distribution with the normalization $\sum_n P_n = 1$ (See Eq.(3.2.1)). It is straightforward to derive the expression for the

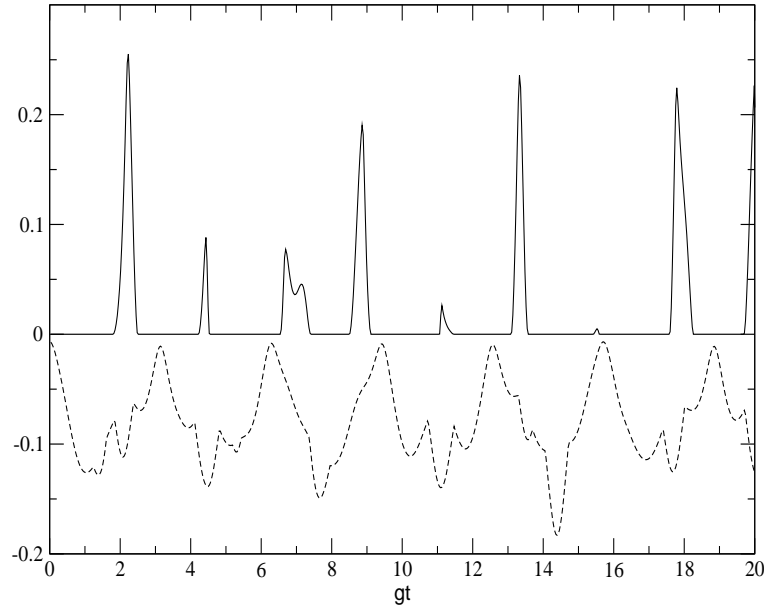


Figure 3.4: Atom-atom entanglement i.e., E_F (solid line) and difference of the Shannon entropies i.e. $(S(\rho_f^{(2)}) - S(\rho_f^{(ss)}))/10$ (dashed line) are plotted versus micromaser pump parameter $D = gt\sqrt{N}$. $\kappa/g = 0.001$ and $n_{th} = 0.01$, $N = 1$.

density operator of the cavity field after passage of the two experimental atoms [20]. We denote this cavity state as $\rho_f^{(2)}$, given by

$$\begin{aligned}
 \rho_f^{(2)} &= \sum_n P_n^{ss} \cos^4(\sqrt{n+1}gt)|n\rangle\langle n| + \sum_n P_n^{ss} \cos^2(\sqrt{n+1}gt) \sin^2(\sqrt{n+1}gt)|n+1\rangle\langle n+1| \\
 &+ \sum_n P_n^{ss} \cos^2(\sqrt{n+2}gt) \sin^2(\sqrt{n+1}gt)|n+1\rangle\langle n+1| \\
 &+ \sum_n P_n^{ss} \sin^2(\sqrt{n+1}gt) \sin^2(\sqrt{n+2}gt)|n+2\rangle\langle n+2|.
 \end{aligned} \tag{3.20}$$

We then compute its Shannon entropy given by

$$S(\rho_f^{(2)}) = - \sum_{n=1}^{\infty} P_n^{(2)} \log P_n^{(2)} \tag{3.21}$$

as well, through the corresponding photon number distribution $P_n^{(2)} = \langle n|\rho_f^{(2)}|n\rangle$. We also calculate the difference of these Shannon entropies i.e., $S(\rho_f^{(2)}) - S(\rho_f^{(ss)})$. We plot E_F and $(S(\rho_f^{(2)}) - S(\rho_f^{(ss)}))$ versus $D = gt\sqrt{N}$ for $\kappa/g = 0.001$ and $n_{th} = 0.01$ in Figure 3.4.

3.4 Summary

In this chapter we have described the one-atom micromaser and its dynamics. We obtained the steady-state micromaser field which evolves under the field-reservoir coupling. We show here that entanglement between two atoms can be generated in the one-atom micromaser device. We have proposed a scheme to measure the entanglement generated between two successive atoms that stream through a real one-atom micromaser in such a manner that their flights through the cavity do not overlap. There is always a time gap between one atom leaving the cavity and the next atom entering the cavity. We show that successive atoms that emerge out of the cavity are entangled. This scheme does not require the spatial overlap between the two atoms at any stage. In the theory for the micromaser used by us [33], the interaction of the cavity with its reservoir is taken into account at all times. We indeed compute the effect of photon leakage on the entanglement measure. Such a model was earlier used by us [20] to show the violation of a Bell-type inequality between two spatially non-overlapping atoms correlated via atom-photon interactions. The generation of nonlocal correlations between the two atomic states emerging from the cavity can in general be understood using the Horodecki theorem [57].

We have studied the entanglement of formation between two atoms as a function of the various micromaser parameters. We have plotted E_F between two atoms versus the Rabi angle gt for different values of average thermal photons n_{th} keeping κ/g fixed. We have also plotted E_F as a function of cavity dissipation κ/g . In the first case entanglement decreases with increasing average thermal photon number providing an example of environment-induced entanglement that we will study in detail in chapter 6. In the second case we see two-atom entanglement increases with increasing κ/g , the explanation for which will also be apparent in chapter 6. Next we have calculated the initial Shannon entropy of the steady-state micromaser field and the final Shannon entropy of the steady-state micromaser field after the passage of the two atoms. We have compared E_F with the difference of the Shannon entropies versus as a function of the Rabi angle gt . The difference in the Shannon entropies is seen to exhibit some correspondence with the entanglement of formation of the atoms for certain values of the atom-photon interaction time. Thus this scheme provides a concrete quantitative example of information transfer

between the microwave cavity and the two atoms in a realistic set-up. The micromaser is an experimentally operational real physical device where abstract quantum information theoretic concepts can be revealed in the presence of dissipative interactions. The quantitative study of information transfer in the micromaser calls for the future study of channel capacity [21] of the entangling atoms as functions of the various micromaser parameters.

Chapter 4

Curious features of entanglement: a quantitative study

4.1 Introduction

We have seen that entanglement between separate quantum systems is a distinctive feature of quantum mechanics [1, 3]. Quantum entanglement is moreover endowed with certain curious features. Unlike classical correlations, quantum entanglement cannot be freely shared among many quantum systems. It has been observed that a quantum system being entangled with another one limits its possible entanglement with a third system. This has been dubbed the “monogamous nature of entanglement” which was first proposed by Bennett [34]: “.....*you can't become entangled simply by talking on the telephone. Entanglement is monogamous-the more entangled Bob is with the Alice, the less entangled he can be*”. For example, if a pair of qubits A and B have a perfect quantum correlation, namely, if they are in a maximally entangled state $\Psi^- = (|01\rangle - |10\rangle)/\sqrt{2}$, then the system A cannot be entangled with a third system C . This is because if A were entangled with C , then the pair AB would also be entangled with C , and would therefore have a mixed-state density matrix (the reduced density state ρ_{AB} after taking trace over C from a pure tripartite entangled state ρ_{ABC} always is a mixed density state i.e. $\rho_{AB} = \text{Tr}_C(\rho_{ABC})$ would be a mixed density state), whereas the singlet state is pure. In general, there is trade-off between the amount of entanglement between qubits A and B and the same qubit A and C . This property is purely quantum.

In the classical world if A and B bits are perfectly correlated, then there is no con-

straints in the correlation between bits A and C . The trade-off is described by the Coffman-Kundu-Wootters (CKW) monogamy inequality [36] $C_{AB}^2 + C_{AC}^2 \leq C_{(AB)C}^2$, where C_{AB} is the concurrence [22, 23] between A and B , C_{AC} is the concurrence between A and C , and $C_{(AB)C}$ is the concurrence between AB and C . There was a conjecture [36] that the above inequality can be extended to n -qubits which has been proved recently [58]. This indicates that there is a limitation in the distribution of entanglement, and several efforts have been devoted to capture this unique property of “monogamy of quantum entanglement” in a quantitative way for tripartite and multipartite systems ([36],[58]-[65]). In the present chapter we investigate the “monogamy of quantum entanglement” for tripartite systems.

Another distinctive property of quantum entanglement for multipartite systems is the possibility of “entanglement swapping” between two or more pairs of qubits. Using this property, two parties that never interacted in their history can be entangled [66, 67]. Usually quantum entanglement originates in certain direct interactions between two particles placed closed together. But it is possible to entangle two particles which have never interacted in the past as we saw in the case of two successive atoms in the micromaser in chapter 3, and also via entanglement swapping [68, 69]. There may indeed exist a deeper connection between the characteristics of “monogamy” and entanglement “swapping” since the features of the distribution and transfer of quantum information is essentially reflected in the both these properties. We show these interesting characteristics of entanglement in details for given systems discussed below. In this chapter we will present these features of entanglement i.e. “monogamy of quantum entanglement” and “entanglement swapping” both in ideal and dissipative cases with three qubits (two cavities and a two-level atom and two two-level atom and a single cavity) and four qubits (two cavities and two two-level atoms) respectively.

In the next section (4.2) we first consider a tripartite pure system (two ideal cavities and one atom) and study the features of “monogamy” exhibited between the atom-cavity and the cavity-cavity entanglements. In section 4.3 we consider another system of two two-level maximally entangled atoms i.e. an EPR pair [6] and a single-mode cavity. We then consider the passage of one of two maximally entangled atoms through the vacuum cavity and study the features of “monogamy” exhibited between the atom-atom

and the atom-cavity entanglements. In particular, we demonstrate the applicability of the Coffman-Kundu-Wootters (CKW) [36] “monogamy” inequality to this system. We consider in section 4.2.2 a realistic cavity with photon leakage, and repeat the above analysis keeping in mind the recently conjectured validity of the CKW inequality extended to mixed states [58]. We find that cavity dissipation could lead to interesting possibilities, such as the enhancement of the entanglement between the atom and the cavity mode that it interacts with, a feature that could be understood by the “monogamous” behaviour of entanglement in section 4.2.2. Finally in section 4.4 we consider a four-qubit system (two cavities and two atoms) where our goal is to observe entanglement swapping, or the transfer of entanglement from the initially entangled two cavities to the two atoms. Here again, we first perform the analysis with ideal cavities, and then consider the effects of cavity leakage on entanglement swapping.

4.2 Monogamy of entanglement in a system of two cavities and a single atom

4.2.1 Pure state of three qubits

We first discuss how a system of two maximally entangled single-mode cavities (C_1 and C_2) which are empty initially is prepared. This system of two maximally entangled single-mode cavities is called a teleportation machine [70, 71, 72]. We send the atom B_1 prepared in the excited state $|e\rangle$ through two separated vacuum cavities C_1 and C_2 successively, and we have to take different passage times for the passage of the atom through the cavities (Figure 4.1).

The initial joint state of C_1 , C_2 and B_1 is

$$|\Psi\rangle_{C_1 C_2 B_1} = |0_1, 0_2, e\rangle. \quad (4.1)$$

We assume the resonant interaction between the two-level atom and cavity mode frequency. The interaction Hamiltonian in the rotating frame approximation for the atom-cavity system, as discussed in chapter 2, [Eq.(2.11)], is

$$H_I = g(\sigma^+ a + \sigma^- a^\dagger), \quad (4.2)$$

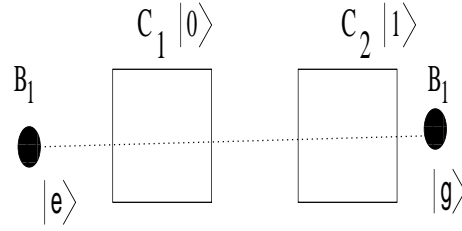


Figure 4.1: The passage of atom B_1 through the cavities C_1 and C_2 successively with different interaction times such as $gt = \pi/4$ and $gt = \pi/2$ respectively.

and the dynamics of the atom-photon interaction is governed by the equation

$$\dot{\rho} = -i[H_I, \rho]. \quad (4.3)$$

First we send the atom B_1 through the cavity C_1 . The resulting atom-cavity state at time t is

$$|\Psi\rangle_{C_1 C_2 c} = (\cos gt |0_1 e\rangle + \sin gt |1_1 g\rangle) \otimes 0_2. \quad (4.4)$$

If we take $gt = \pi/4$, the resulting atom-cavity state becomes

$$|\Psi\rangle_{C_1 C_2 c} = \frac{1}{\sqrt{2}}(|0_1 e\rangle + |1_1 g\rangle) \otimes 0_2. \quad (4.5)$$

After emerging from the cavity C_1 the atom B_1 passes through the cavity C_2 . The resulting atom-cavity state at time t is

$$|\Psi\rangle_{C_1 C_2 B_1} = \frac{1}{\sqrt{2}}(\cos gt |0_1 0_2 e\rangle + \sin gt |0_1 1_2 g\rangle + |1_1 0_2 g\rangle). \quad (4.6)$$

If we take $gt = \pi/2$ the resulting atom-cavity state becomes

$$|\Psi\rangle_{C_1 C_2 c} = \frac{1}{\sqrt{2}}(|0_1 1_2\rangle + |1_1 0_2\rangle) \otimes |g\rangle. \quad (4.7)$$

Thus, we get two ideal cavities which are maximally entangled (Figure 4.2) by sending a single circular Rydberg atom prepared in the excited state through two identical and initially empty ideal cavities (C_1 and C_2) [70, 71, 72].

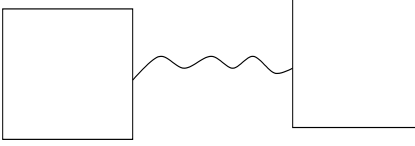
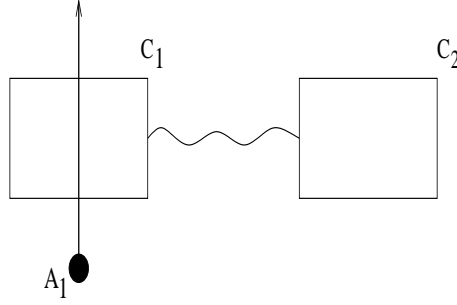
$$C_1 C_2 = \frac{1}{\sqrt{2}} (|0_1 1_2\rangle + |1_1 0_2\rangle)$$


Figure 4.2: Two maximally entangled cavities

Figure 4.3: A two-level Rydberg atom prepared in the ground state is passing through the one of the maximally entangled cavities C_1

We now consider this maximally entangled bipartite system of two cavities having the state

$$|\Psi\rangle_{C_1 C_2} = \frac{1}{\sqrt{2}} (|0_1 1_2\rangle + |1_1 0_2\rangle), \quad (4.8)$$

as the initial state for our purpose of investigating the monogamy of entanglement. Let another two-level Rydberg atom A_1 prepared in the ground state $|g\rangle$ pass through the cavity C_1 (see Figure 4.3). The initial atom-field system is

$$|\Psi(t=0)\rangle_{C_1 C_2 A_1} = \frac{1}{\sqrt{2}} (|0_1 1_2\rangle + |1_1 0_2\rangle) \otimes |g_1\rangle. \quad (4.9)$$

After a time t the joint atom-field system has the state given by

$$|\Psi(t)\rangle_{C_1 C_2 A_1} = \frac{1}{\sqrt{2}} (|0_1 1_2 g_1\rangle + \cos gt |1_1 0_2 g_1\rangle - \sin gt |0_1 0_2 e_1\rangle) \quad (4.10)$$

The corresponding density state is

$$\rho(t)_{C_1 C_2 A_1} = |\Psi(t)_{C_1 C_2 A_1}\rangle \langle \Psi(t)_{C_1 C_2 A_1}|$$

$$\begin{aligned}
&= \frac{1}{2}|0_1 1_2 g_1\rangle\langle 0_1 1_2 g_1| \\
&+ \frac{\cos^2 gt}{2}|1_1 0_2 g_1\rangle\langle 1_1 0_2 g_1| \\
&+ \frac{\sin^2 gt}{2}|0_1 0_2 e_1\rangle\langle 0_1 0_2 e_1| \\
&+ \frac{\cos gt}{2}|0_1 1_2 g_1\rangle\langle 1_1 0_2 g_1| \\
&+ \frac{\cos gt}{2}|1_1 0_2 g_1\rangle\langle 0_1 1_2 g_1| \\
&- \frac{\cos gt \sin gt}{2}|1_1 0_2 g_1\rangle\langle 0_1 0_2 e_1| \\
&- \frac{\cos gt \sin gt}{2}|0_1 0_2 e_1\rangle\langle 1_1 0_2 g_1| \\
&- \frac{\sin gt}{2}|0_1 0_2 e_1\rangle\langle 0_1 1_2 g_1| \\
&- \frac{\sin gt}{2}|0_1 1_2 g_1\rangle\langle 0_1 0_2 e_1|. \tag{4.11}
\end{aligned}$$

The reduced density states of the pairs $C_1 C_2$, $C_2 A_1$, $C_1 A_1$ are obtained by taking the appropriate traces and are given by

$$\begin{aligned}
\rho(t)_{C_1 C_2} &= \text{Tr}_{A_1}(\rho(t)_{C_1 C_2 A_1}), \\
&= \frac{1}{2}|0_1 1_2\rangle\langle 0_1 1_2| + \frac{\cos^2 gt}{2}|1_1 0_2\rangle\langle 1_1 0_2| \\
&+ \frac{\sin^2 gt}{2}|0_1 0_2\rangle\langle 0_1 0_2| + \frac{\cos gt}{2}|0_1 1_2\rangle\langle 1_1 0_2| \\
&+ \frac{\cos gt}{2}|1_1 0_2\rangle\langle 0_1 1_2|. \tag{4.12}
\end{aligned}$$

$$\begin{aligned}
\rho(t)_{C_2 A_1} &= \text{Tr}_{C_1}(\rho(t)_{C_1 C_2 A_1}), \\
&= \frac{1}{2}|1_2 g_1\rangle\langle 1_2 g_1| + \frac{\cos^2 gt}{2}|0_2 g_1\rangle\langle 0_2 g_1| \\
&+ \frac{\sin^2 gt}{2}|0_2 e_1\rangle\langle 0_2 e_1| - \frac{\sin gt}{2}|1_2 g_1\rangle\langle 0_2 e_1| \\
&- \frac{\sin gt}{2}|0_2 e_1\rangle\langle 1_2 g_1|. \tag{4.13}
\end{aligned}$$

$$\begin{aligned}
\rho(t)_{C_1 A_1} &= \text{Tr}_{C_2}(\rho(t)_{C_1 C_2 A_1}), \\
&= \frac{1}{2}|0_1 g_1\rangle\langle 0_1 g_1| + \frac{\cos^2 gt}{2}|1_1 g_1\rangle\langle 1_1 g_1|
\end{aligned}$$

$$\begin{aligned}
& + \frac{\sin^2 gt}{2} |0_1 e_1\rangle \langle 0_1 e_1| - \frac{\sin gt \cos gt}{2} |1_1 g_1\rangle \langle 0_1 e_1| \\
& - \frac{\sin gt \cos gt}{2} |0_1 e_1\rangle \langle 1_1 g_1|.
\end{aligned} \tag{4.14}$$

The reduced density matrix of the pair of atoms $C_1 C_2$ is thus given by

$$\rho(t)_{C_1 C_2} = \begin{pmatrix} \frac{\sin^2 gt}{2} & 0 & 0 & 0 \\ 0 & \frac{1}{2} & \frac{\cos gt}{2} & 0 \\ 0 & \frac{\cos gt}{2} & \frac{\cos^2 gt}{2} & 0 \\ 0 & 0 & 0 & 0 \end{pmatrix} \tag{4.15}$$

in the basis of $|0_1 0_2\rangle$, $|0_1 1_2\rangle$, $|1_1 0_2\rangle$, and $|1_1 1_2\rangle$ states. Similarly, the reduced density matrix of the pair of atoms $C_2 A_1$ is given by

$$\rho(t)_{C_2 A_1} = \begin{pmatrix} \frac{\cos^2 gt}{2} & 0 & 0 & 0 \\ 0 & \frac{\sin^2 gt}{2} & -\frac{\sin gt}{2} & 0 \\ 0 & -\frac{\sin gt}{2} & \frac{1}{2} & 0 \\ 0 & 0 & 0 & 0 \end{pmatrix} \tag{4.16}$$

in the basis of $|0_2 g_1\rangle$, $|0_2 e_1\rangle$, $|1_2 g_1\rangle$, and $|1_2 e_1\rangle$ states. The reduced density matrix of the pair of atoms $C_1 A_1$ is given by

$$\rho(t)_{C_1 A_1} = \begin{pmatrix} \frac{1}{2} & 0 & 0 & 0 \\ 0 & \frac{\sin^2 gt}{2} & -\frac{\sin gt \cos gt}{2} & 0 \\ 0 & -\frac{\sin gt \cos gt}{2} & \frac{\cos^2 gt}{2} & 0 \\ 0 & 0 & 0 & 0 \end{pmatrix} \tag{4.17}$$

in the basis of $|0_1 g_1\rangle$, $|0_1 e_1\rangle$, $|1_1 g_1\rangle$, and $|1_1 e_1\rangle$ states.

We now compute the mixed-state bipartite entanglement measure (concurrence) [22, 23] for different pairs. These are given by

$$C(\rho(t)_{C_1 C_2}) = |\cos gt|, \tag{4.18}$$

$$C(\rho(t)_{C_2 A_1}) = |\sin gt|, \tag{4.19}$$

$$C(\rho(t)_{C_1 A_1}) = |\cos gt \sin gt| \tag{4.20}$$

and are plotted in Figure 4.4 for varying Rabi angle. The monogamous nature of entanglement between the pairs $C_1 C_2$ and $C_2 A_1$, is clearly reflected.

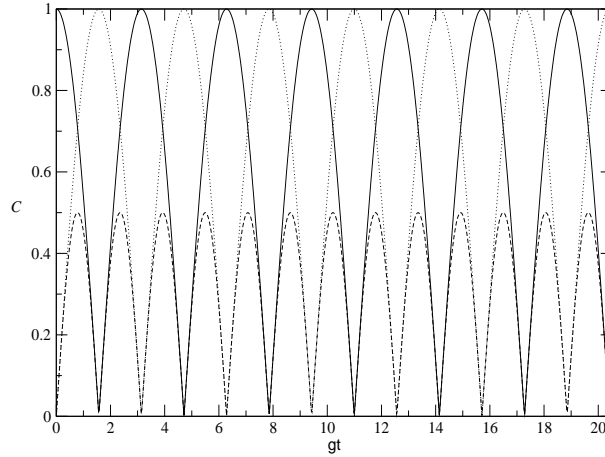


Figure 4.4: $C(\rho(t)_{C_1 C_2})$ (solid line), $C(\rho(t)_{C_2 A_1})$, (dotted line), $C(\rho_{C_1 A_1})$ (broken line) plotted with respect to the Rabi angle gt .

The CKW inequality [36] for the tripartite pure state $\rho(t)_{C_2 C_1 A_1}$ is given by $C_{C_2 C_1}^2 + C_{C_2 A_1}^2 \leq C_{C_2(C_1 A_1)}^2$ or $C_{C_2 C_1}^2 + C_{C_2 A_1}^2 \leq 4 \det \rho(t)_{C_2}$ (since $C_{C_2(C_1 A_1)} = 2\sqrt{\det \rho(t)_{C_2}}$). So the CKW inequality reduces to $\cos^2 gt + \sin^2 gt = 1$ in this case since $\det \rho(t)_{C_2} = 1/4$. More interesting is the case if we consider the following pure state of $C_2 C_1 A_1$:

$$|\psi\rangle_{C_2 C_1 A_1} = \alpha|1_2 0_1 g_2\rangle + \beta|0_2 1_1 g_1\rangle + \gamma|0_2 0_1 e_1\rangle, \quad (4.21)$$

where the three positions in the kets refer to qubits C_2 , C_1 , and A_1 in that order. Then $C_{C_2 C_1}^2 + C_{C_2 A_1}^2 = C_{C_2(C_1 A_1)}^2$, i.e., the CKW inequality is saturated.

4.2.2 Effects of cavity dissipation on entanglement

Let us now investigate the above case in presence of cavity dissipation. The dynamics of the flight of the atom can be represented by the equation

$$\dot{\rho} = \dot{\rho}|_{\text{atom-field}} + \dot{\rho}|_{\text{field-reservoir}}, \quad (4.22)$$

where the strength of the couplings are given by the parameters κ (the cavity leakage constant) and g (the atom-field interaction constant). At temperature $T = 0K$ the average thermal photon number is zero, and hence one has [47]

$$\dot{\rho}|_{\text{field-reservoir}} = -\kappa(a^\dagger a \rho - 2a \rho a^\dagger + \rho a^\dagger a). \quad (4.23)$$

Since $g \gg \kappa$, we again make the secular approximation [27] (see chapter 2) while solving the complete evolution equation by combining Eqs.(4.3) and (4.25) in order to get the density elements of $\rho(t)_{C_1C_2A_1}$. We further assume (that is justified when the cavity is close to $0K$) that the probability of getting two or more photons inside the cavities is zero, or in other words, a cavity always remains in the two level state comprising of $|0\rangle$ and $|1\rangle$. The tripartite (mixed) state is then obtained to be

$$\begin{aligned}
\rho(t)_{C_1C_2A_1} &= \alpha_1|0_11_2g_1\rangle\langle 0_11_2g_1| \\
&+ \alpha_2|1_10_2g_1\rangle\langle 1_10_2g_1| \\
&+ \alpha_3|0_10_2e_1\rangle\langle 0_10_2e_1| \\
&+ \alpha_4|0_11_2g_1\rangle\langle 1_10_2g_1| \\
&+ \alpha_4|1_10_2g_1\rangle\langle 0_11_2g_1| \\
&+ \alpha_5|1_10_2g_1\rangle\langle 0_10_2e_1| \\
&- \alpha_5|0_10_2e_1\rangle\langle 1_10_2g_1| \\
&+ \alpha_6|0_10_2e_1\rangle\langle 0_11_2g_1| \\
&- \alpha_6|0_11_2g_1\rangle\langle 0_10_2e_1|,
\end{aligned} \tag{4.24}$$

where the α_i are given by

$$\begin{aligned}
\alpha_1 &= \left(1 - \frac{e^{-\kappa_1 t}}{2}\right)e^{-2\kappa_2 t}, \\
\alpha_2 &= \cos^2 gte^{-\kappa_1 t} \left(1 - \frac{e^{-2\kappa_2 t}}{2}\right), \\
\alpha_3 &= \sin^2 gte^{-\kappa_1 t} \left(1 - \frac{e^{-2\kappa_2 t}}{2}\right), \\
\alpha_4 &= \frac{\cos gte^{-\frac{\kappa_1 t}{2}}e^{-\kappa_2 t}}{2}, \\
\alpha_5 &= i \sin gt \cos gte^{-\kappa_1 t} \left(1 - \frac{e^{-2\kappa_2 t}}{2}\right), \\
\alpha_6 &= i \left(\frac{e^{-\frac{\kappa_1 t}{2}} \sin gt}{2} - \frac{\kappa_1 e^{-\frac{\kappa_1 t}{2}} \cos gt}{4g} + \frac{\kappa_1}{4g} \right) e^{-\kappa_2 t},
\end{aligned}$$

and κ_1 and κ_2 are the leakage constants for cavity C_1 and C_2 respectively. The reduced density states of the pairs C_1C_2 , C_2A_1 , C_1A_1 are thus given by

$$\rho(t)_{C_1C_2} = \text{Tr}_{A_1}(\rho_{C_1C_2A_1}),$$

$$\begin{aligned}
&= \alpha_1|0_11_2\rangle\langle 0_11_2| + \alpha_2|1_10_2\rangle\langle 1_10_2| \\
&+ \alpha_3|0_10_2\rangle\langle 0_10_2| + \alpha_4|0_11_2\rangle\langle 1_10_2| \\
&+ \alpha_4|1_10_2\rangle\langle 0_11_2|.
\end{aligned} \tag{4.25}$$

$$\begin{aligned}
\rho(t)_{C_2A_1} &= \text{Tr}_{C_1}(\rho_{C_1C_2A_1}), \\
&= \alpha_1|1_2g_1\rangle\langle 1_2g_1| + \alpha_2|0_2g_1\rangle\langle 0_2g_1| \\
&+ \alpha_3|0_2e_1\rangle\langle 0_2e_1| - \alpha_6|1_2g_1\rangle\langle 0_2e_1| \\
&+ \alpha_6|0_2e_1\rangle\langle 1_2g_1|.
\end{aligned} \tag{4.26}$$

$$\begin{aligned}
\rho(t)_{C_1A_1} &= \text{Tr}_{C_2}(\rho_{C_1C_2A_1}), \\
&= \alpha_1|0_1g_1\rangle\langle 0_1g_1| + \alpha_2|1_1g_1\rangle\langle 1_1g_1| \\
&+ \alpha_3|0_1e_1\rangle\langle 0_1e_1| + \alpha_5|1_1g_1\rangle\langle 0_1e_1| \\
&- \alpha_5|0_1e_1\rangle\langle 1_1g_1|.
\end{aligned} \tag{4.27}$$

The reduced density matrix of the pair of cavities C_1C_2 can thus be written as

$$\rho(t)_{C_1C_2} = \begin{pmatrix} \alpha_3 & 0 & 0 & 0 \\ 0 & \alpha_1 & \alpha_4 & 0 \\ 0 & \alpha_4 & \alpha_2 & 0 \\ 0 & 0 & 0 & 0 \end{pmatrix} \tag{4.28}$$

in the basis of $|0_10_2\rangle$, $|0_11_2\rangle$, $|1_10_2\rangle$, and $|1_11_2\rangle$ states. Similarly,

$$\rho(t)_{C_2A_1} = \begin{pmatrix} \alpha_2 & 0 & 0 & 0 \\ 0 & \alpha_3 & -\alpha_6 & 0 \\ 0 & \alpha_6 & \alpha_1 & 0 \\ 0 & 0 & 0 & 0 \end{pmatrix} \tag{4.29}$$

in the basis of $|0_2g_1\rangle$, $|0_2e_1\rangle$, $|1_2g_1\rangle$, and $|1_2e_1\rangle$ states, and

$$\rho(t)_{C_1A_1} = \begin{pmatrix} \alpha_1 & 0 & 0 & 0 \\ 0 & \alpha_3 & -\alpha_5 & 0 \\ 0 & \alpha_5 & \alpha_2 & 0 \\ 0 & 0 & 0 & 0 \end{pmatrix} \tag{4.30}$$

in the basis of $|0_1g_1\rangle$, $|0_1e_1\rangle$, $|1_1g_1\rangle$, and $|1_1e_1\rangle$ states.

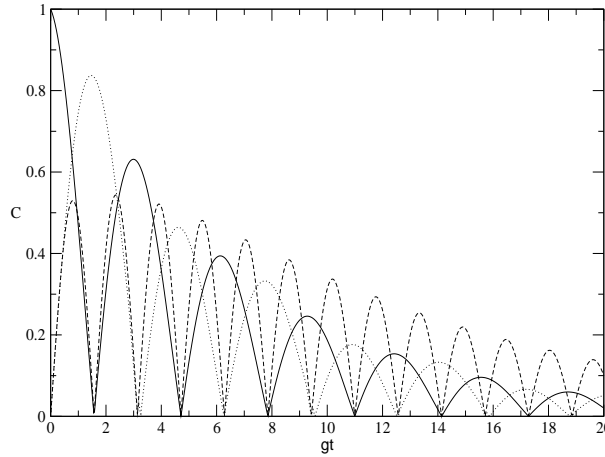


Figure 4.5: $C(\rho(t)_{C_1 C_2})$ (solid line), $C(\rho(t)_{C_2 A_1})$ (dotted line), $C(\rho(t)_{C_1 A_1})$ (broken line) plotted with respect to the Rabi angle gt . $\frac{\kappa_1}{g} = \frac{\kappa_2}{g} = 0.1$.

One can then obtain the respective concurrences. These, namely, $C(\rho(t)_{C_1 C_2})$, $C(\rho(t)_{C_2 A_1})$, and $C(\rho(t)_{C_1 A_1})$ are given by

$$C(\rho(t)_{C_1 C_2}) = |\cos gte^{-\frac{\kappa_1 t}{2}} e^{-\kappa_2 t}| \quad (4.31)$$

$$C(\rho(t)_{C_2 A_1}) = \left| \left(e^{-\frac{\kappa_1 t}{2}} \sin gt - \frac{\kappa_1 e^{-\frac{\kappa_1 t}{2}} \cos gt}{2g} + \frac{\kappa_1}{2g} \right) e^{-\kappa_2 t} \right| \quad (4.32)$$

$$C(\rho(t)_{C_1 A_1}) = \left| 2 \cos gt \sin gte^{-\kappa_1 t} \left(1 - \frac{e^{-2\kappa_2 t}}{2} \right) \right| \quad (4.33)$$

These concurrences are plotted with respect to the Rabi angle gt in Figure 4.5. As expected, dissipation reduces the respective concurrences. However, the ‘‘monogamous’’ character, or the ‘complementarity’ between $C(\rho(t)_{C_1 C_2})$ and $C(\rho(t)_{C_2 A_1})$ is maintained even with cavity leakage.

To verify the CKW inequality for the mixed state $\rho(t)_{C_1 C_2 A_1}$, one has to average $C(\rho(t)_{C_2(C_1 A_1)})$ over all pure state decompositions [58]. We however, adopt an utilitarian point of view, and for small κ take $C(\rho(t)_{C_2(C_1 A_1)}) \approx 2\sqrt{\det \rho_{C_2}}$. Note that this result holds exactly for a pure state [36]. Nevertheless, for a small value of κ and for a bipartite photon field, one stays very close to a pure state. In Figure 4.6 we plot the left and the right hand sides ($C_{C_2 C_1}^2 + C_{C_2 A_1}^2$ and $C_{C_2(C_1 A_1)}^2$, respectively) of the corresponding CKW inequality and observe that it always holds under the above approximation. An interesting

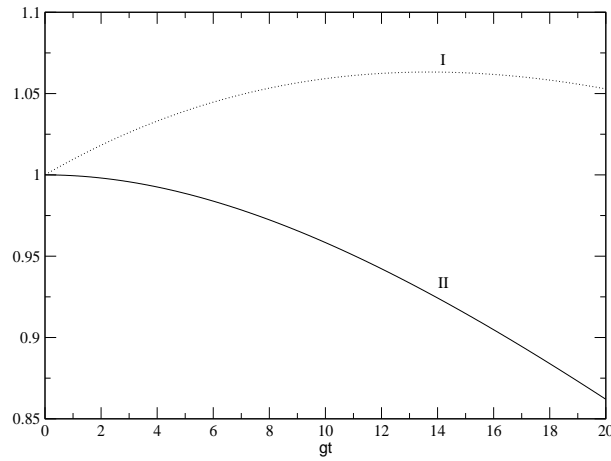


Figure 4.6: $C_{C_2C_1}^2 + C_{C_2A_1}^2$ (solid line), $C_{C_2(C_1A_1)}^2$ (dotted line) plotted with respect to the Rabi angle gt .

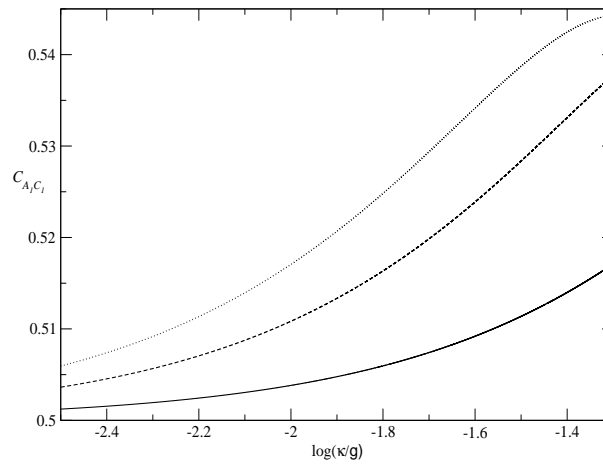


Figure 4.7: $C(\rho(t)_{A_1C_1})$ (solid line) for $gt = \pi/4$, $C(\rho(t)_{A_1C_1})$ (broken line) for $gt = 3\pi/4$, $C(\rho(t)_{A_1C_1})$ (dotted line) for $gt = 5\pi/4$ plotted with respect to $\log(\kappa/g)$, where $\kappa/g = \kappa_1/g = \kappa_2/g$.

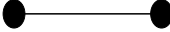
$$A_1 A_2 = \frac{1}{\sqrt{2}} (|e_1 g_2\rangle + |g_1 e_2\rangle)$$


Figure 4.8: Two maximally entangled atoms.

feature of the entanglement obtained between the atom A_1 and the cavity C_1 through which it interacts directly is displayed in Figure 4.7 where $C(\rho(t)_{A_1 C_1})$ is plotted versus the dissipation parameter κ . Note that the concurrence increases for increasing cavity loss. This happens because the cavity leakage reduces the initial entanglement between C_1 and C_2 , and hence makes room for the subsequent entanglement between C_1 and A_1 to form. The dissipative mechanism is thus a striking confirmation of the “monogamous” character of entanglement. The role of the dissipative environment in creating desired forms of entanglement has been revealed earlier in the literature [40, 41], and forms an important part of this thesis, which will be studied in details in chapter 6. The present case can be also viewed as a further example of this kind.

4.3 Monogamy of entanglement in a system of two maximally entangled atoms and a single cavity

4.3.1 Pure state of three qubits

In this section we discuss another example where we see the monogamous behaviour of entanglement. We consider the initial state of two maximally entangled atoms A_1 and A_2 (Figure 4.8) (that can be generated by passing the atoms one after the other through a vacuum cavity with suitably chosen different interaction times, in a manner similar to the generation of two maximally entangled cavities discussed in the previous section), and a single cavity C_1 . Now consider the atom A_1 to pass through the cavity C_1 . The atom A_2 remains undisturbed (See Figure 4.9). The initial joint state of A_1 , A_2 and C_1 is

$$|\Psi\rangle_{A_1 A_2 C_1} = \frac{1}{\sqrt{2}} (|e_1 g_2\rangle + |g_1 e_2\rangle) \otimes |0_1\rangle \quad (4.34)$$

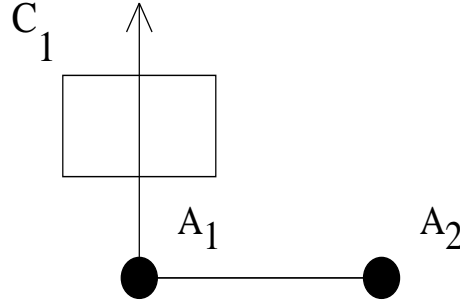


Figure 4.9: One of the maximally entangled atoms A_1 is passing through the cavity C_1 .

In a similar fashion as discussed in section 4.3.1 we get the evolved state at any time t to be

$$\begin{aligned}
 |\Psi(t)\rangle_{A_1 A_2 C_1} = & \frac{1}{\sqrt{2}}(\cos gt|e_1 g_2 0_1\rangle + \sin gt|g_1 g_2 1_1\rangle \\
 & + |g_1 e_2 0_1\rangle). \tag{4.35}
 \end{aligned}$$

The corresponding density state is

$$\begin{aligned}
 \rho(t)_{A_1 A_2 C_1} = & |\Psi(t)_{A_1 A_2 C_1}\rangle\langle\Psi(t)_{A_1 A_2 C_1}| \\
 = & \frac{\cos^2 gt}{2}|e_1 g_2 0_1\rangle\langle e_1 g_2 0_1| \\
 & + \frac{\sin^2 gt}{2}|g_1 g_2 1_1\rangle\langle g_1 g_2 1_1| \\
 & + \frac{1}{2}|g_1 e_2 0_1\rangle\langle g_1 e_2 0_1| \\
 & + \frac{\cos gt}{2}|e_1 g_2 0_1\rangle\langle g_1 e_2 0_1| \\
 & + \frac{\cos gt}{2}|g_1 e_2 0_1\rangle\langle e_1 g_2 0_1| \\
 & - \frac{\sin gt}{2}|g_1 g_2 1_1\rangle\langle g_1 e_2 0_1| \\
 & - \frac{\sin gt}{2}|g_1 e_2 0_1\rangle\langle g_1 g_2 1_1| \\
 & + \frac{\cos gt \sin gt}{2}|e_1 g_2 0_1\rangle\langle g_1 g_2 1_1| \\
 & + \frac{\cos gt \sin gt}{2}|g_1 g_2 1_1\rangle\langle e_1 g_2 0_1|. \tag{4.36}
 \end{aligned}$$

The reduced density states of the pairs $A_1 A_2$, $A_2 C_1$, $A_1 C_1$ are given by

$$\rho(t)_{A_1 A_2} = \text{Tr}_{C_1}(\rho(t)_{A_1 A_2 C_1}),$$

$$\begin{aligned}
&= \frac{\cos^2 gt}{2} |e_1 g_2\rangle \langle e_1 g_2| + \frac{\sin^2 gt}{2} |g_1 g_2\rangle \langle g_1 g_2| \\
&+ \frac{1}{2} |g_1 e_2\rangle \langle g_1 e_2| + \frac{\cos gt}{2} |e_1 g_2\rangle \langle g_1 e_2| \\
&+ \frac{\cos gt}{2} |g_1 e_2\rangle \langle e_1 g_2|.
\end{aligned} \tag{4.37}$$

$$\begin{aligned}
\rho(t)_{A_2 C_1} &= \text{Tr}_{A_1}(\rho(t)_{A_1 A_2 C_1}), \\
&= \frac{\cos^2 gt}{2} |g_2 0_1\rangle \langle g_2 0_1| + \frac{\sin^2 gt}{2} |g_2 1_1\rangle \langle g_2 1_1| \\
&+ \frac{1}{2} |e_2 0_1\rangle \langle e_2 0_1| + \frac{\sin gt}{2} |e_2 0_1\rangle \langle g_2 1_1| \\
&+ \frac{\sin gt}{2} |g_2 1_1\rangle \langle e_2 0_1|.
\end{aligned} \tag{4.38}$$

$$\begin{aligned}
\rho(t)_{A_1 C_1} &= \text{Tr}_{C_2}(\rho(t)_{A_1 A_2 C_1}), \\
&= \frac{\cos^2 gt}{2} |e_1 0_1\rangle \langle e_1 0_1| + \frac{\sin^2 gt}{2} |g_1 1_1\rangle \langle g_1 1_1| \\
&+ \frac{1}{2} |g_1 0_1\rangle \langle g_1 0_1| + \frac{\sin gt \cos gt}{2} |e_1 0_1\rangle \langle g_1 1_1| \\
&+ \frac{\sin gt \cos gt}{2} |g_1 1_1\rangle \langle e_1 0_1|.
\end{aligned} \tag{4.39}$$

The reduced density matrix of the pair of atoms $A_1 A_2$ is thus given by

$$\rho(t)_{A_1 A_2} = \begin{pmatrix} \frac{\sin^2 gt}{2} & 0 & 0 & 0 \\ 0 & \frac{1}{2} & \frac{\cos gt}{2} & 0 \\ 0 & \frac{\cos gt}{2} & \frac{\cos^2 gt}{2} & 0 \\ 0 & 0 & 0 & 0 \end{pmatrix} \tag{4.40}$$

in the basis of $|g_1 g_2\rangle$, $|g_1 e_2\rangle$, $|e_1 g_2\rangle$, and $|e_1 e_2\rangle$ states. Similarly,

$$\rho(t)_{A_2 C_1} = \begin{pmatrix} \frac{\cos^2 gt}{2} & 0 & 0 & 0 \\ 0 & \frac{\sin^2 gt}{2} & \frac{\sin gt}{2} & 0 \\ 0 & \frac{\sin gt}{2} & \frac{1}{2} & 0 \\ 0 & 0 & 0 & 0 \end{pmatrix} \tag{4.41}$$

and

$$\rho(t)_{A_1 C_1} = \begin{pmatrix} \frac{1}{2} & 0 & 0 & 0 \\ 0 & \frac{\sin^2 gt}{2} & \frac{\sin gt \cos gt}{2} & 0 \\ 0 & \frac{\sin gt \cos gt}{2} & \frac{\cos^2 gt}{2} & 0 \\ 0 & 0 & 0 & 0 \end{pmatrix} \tag{4.42}$$

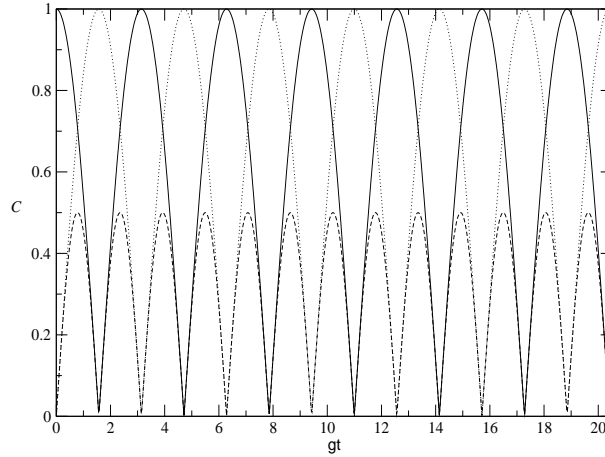


Figure 4.10: $C(\rho(t)_{A_1A_2})$ (solid line), $C(\rho(t)_{A_2C_1})$ (dotted line), $C(\rho_{A_1C_1})$ (broken line) plotted with respect to the Rabi angle gt .

Here also the CKW inequality [36] for the tripartite pure state $\rho(t)_{A_1A_2C_1}$, $C_{A_1A_2}^2 + C_{A_2C_1}^2 \leq C_{A_2(A_1C_1)}^2$ reduces to $\cos^2 gt + \sin^2 gt = 1$. We now compute the mixed-state bipartite entanglement measure (concurrence) [22, 23] for different pairs. These are given by

$$C(\rho(t)_{C_1C_2}) = |\cos gt|, \quad (4.43)$$

$$C(\rho(t)_{C_2A_1}) = |\sin gt|, \quad (4.44)$$

$$C(\rho(t)_{C_1A_1}) = |\cos gt \sin gt|, \quad (4.45)$$

and are plotted in Figure 4.10 for varying Rabi angle, clearly reflecting the monogamous nature of entanglement between A_1A_2 and A_2C_1 .

4.3.2 Effects of cavity dissipation on entanglement

In the same way as discussed in section 4.3.2 the tripartite (mixed) state of A_1 , A_2 and C_1 is obtained to be

$$\begin{aligned} \rho(t)_{A_1A_2C_1} &= |\Psi(t)_{A_1A_2C_1}\rangle\langle\Psi(t)_{A_1A_2C_1}| \\ &= \alpha_1|e_1g_20_1\rangle\langle e_1g_20_1| \\ &\quad + \alpha_2|g_1g_21_1\rangle\langle g_1g_21_1| \\ &\quad + \alpha_3|g_1e_20_1\rangle\langle g_1e_20_1| \end{aligned}$$

$$\begin{aligned}
& -\alpha_4|e_1g_20_1\rangle\langle g_1e_20_1| \\
& +\alpha_4|g_1e_20_1\rangle\langle e_1g_20_1| \\
& +\alpha_5|g_1g_21_1\rangle\langle g_1e_20_1| \\
& +\alpha_5|g_1e_20_1\rangle\langle g_1g_21_1| \\
& +\alpha_6|e_1g_20_1\rangle\langle g_1g_21_1| \\
& -\alpha_6|g_1g_21_1\rangle\langle e_1g_20_1|.
\end{aligned} \tag{4.46}$$

where the α_i are given by

$$\begin{aligned}
\alpha_1 &= \cos^2 gte^{-\kappa t}/2, \\
\alpha_2 &= \sin^2 gte^{-\kappa t}/2, \\
\alpha_3 &= (1 - e^{-\kappa t}/2), \\
\alpha_4 &= i\left(\frac{\cos gte^{-\kappa t/2}}{2} + \frac{\kappa e^{-\kappa t/2} \sin gt}{4g}\right), \\
\alpha_5 &= \frac{\sin gte^{-\kappa t/2}}{2}, \\
\alpha_6 &= i(e^{-\kappa t} \sin gt \cos gt)/2,
\end{aligned}$$

and κ is the leakage constant for cavity C_1 . The reduced density states of the pairs A_1A_2 , A_2C_1 , A_1C_1 are thus given by

$$\begin{aligned}
\rho(t)_{A_1A_2} &= \text{Tr}_{C_1}(\rho(t)_{A_1A_2C_1}), \\
&= \alpha_1|e_1g_2\rangle\langle e_1g_2| + \alpha_2|g_1g_2\rangle\langle g_1g_2| \\
&+ \alpha_3|g_1e_2\rangle\langle g_1e_2| - \alpha_4|e_1g_2\rangle\langle g_1e_2| \\
&+ \alpha_4|g_1e_2\rangle\langle e_1g_2|.
\end{aligned} \tag{4.47}$$

$$\begin{aligned}
\rho(t)_{A_2C_1} &= \text{Tr}_{A_1}(\rho(t)_{A_1A_2C_1}), \\
&= \alpha_1|g_20_1\rangle\langle g_20_1| + \alpha_2|g_21_1\rangle\langle g_21_1| \\
&+ \alpha_3|e_20_1\rangle\langle e_20_1| + \alpha_5|e_20_1\rangle\langle g_21_1| \\
&+ \alpha_5|g_21_1\rangle\langle e_20_1|.
\end{aligned} \tag{4.48}$$

$$\rho(t)_{A_1C_1} = \text{Tr}_{C_2}(\rho(t)_{A_1A_2C_1}),$$

$$\begin{aligned}
&= \alpha_1|e_10_1\rangle\langle e_10_1| + \alpha_2|g_11_1\rangle\langle g_11_1| \\
&+ \alpha_3|g_10_1\rangle\langle g_10_1| + \alpha_6|e_10_1\rangle\langle g_11_1| \\
&- \alpha_6|g_11_1\rangle\langle e_10_1|.
\end{aligned} \tag{4.49}$$

The reduced density matrix of the pair of atoms A_1A_2 is given by

$$\rho(t)_{A_1A_2} = \begin{pmatrix} \alpha_2 & 0 & 0 & 0 \\ 0 & \alpha_3 & -\alpha_4 & 0 \\ 0 & \alpha_4 & \alpha_1 & 0 \\ 0 & 0 & 0 & 0 \end{pmatrix} \tag{4.50}$$

in the basis of $|g_1g_2\rangle$, $|g_1e_2\rangle$, $|e_1g_2\rangle$, and $|e_1e_2\rangle$ states. Similarly,

$$\rho(t)_{A_2C_1} = \begin{pmatrix} \alpha_1 & 0 & 0 & 0 \\ 0 & \alpha_2 & \alpha_5 & 0 \\ 0 & \alpha_5 & \alpha_3 & 0 \\ 0 & 0 & 0 & 0 \end{pmatrix} \tag{4.51}$$

and,

$$\rho(t)_{A_1C_1} = \begin{pmatrix} \alpha_3 & 0 & 0 & 0 \\ 0 & \alpha_2 & \alpha_6 & 0 \\ 0 & -\alpha_6 & \alpha_1 & 0 \\ 0 & 0 & 0 & 0 \end{pmatrix}. \tag{4.52}$$

We again compute the concurrence for different pairs. These are functions of cavity dissipation, and are given by

$$C(\rho(t)_{A_1A_2}) = \left| \left(\cos gte^{-\kappa t/2} + \frac{\kappa e^{-\kappa t/2} \sin gt}{2g} \right) \right|, \tag{4.53}$$

$$C(\rho(t)_{A_2C_1}) = |\sin gte^{-\kappa t/2}|, \tag{4.54}$$

$$C(\rho(t)_{A_1C_1}) = |e^{-\kappa t} \cos gt \sin gt|. \tag{4.55}$$

The various concurrences are plotted in Figure 4.11 for varying Rabi angle, clearly reflecting the monogamous nature of entanglement between A_1A_2 and A_2C_1 . We see that the “monogamous” character or “complementarity” between $C(\rho(t)_{A_1A_2})$ and $C(\rho(t)_{A_2C_1})$ is maintained even with cavity leakage. The CKW inequality [36] for the tripartite pure state $\rho(t)_{A_1A_2C_1}$, $C_{A_1A_2}^2 + C_{A_2C_1}^2 \leq C_{A_2(A_1C_1)}^2$ reduces to $(\cos gte^{-\kappa t/2} + \frac{\kappa e^{-\kappa t/2} \sin gt}{2g})^2 +$

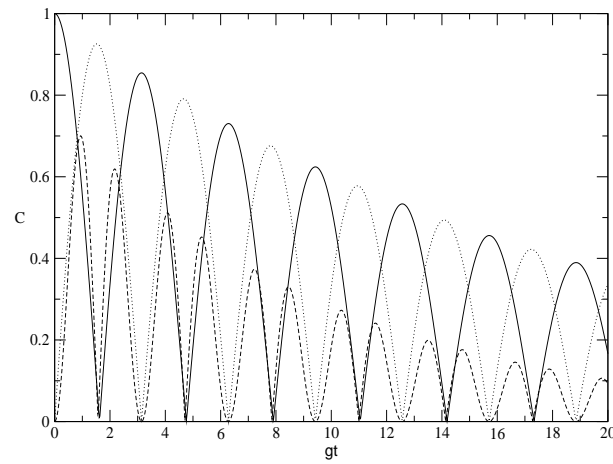


Figure 4.11: $C(\rho(t)_{A_1A_2})$ (solid line), $C(\rho(t)_{A_2C_1})$ (dotted line), $C(\rho_{A_1C_1})$ (broken line) plotted with respect to the Rabi angle gt . $\kappa/g = 0.1$

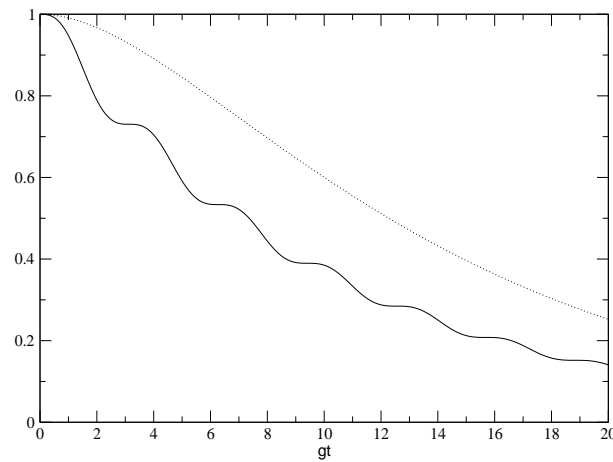


Figure 4.12: $C^2_{A_1A_2} + C^2_{A_2C_1}$ (solid line), $C^2_{A_2(A_1C_1)}$ (dotted line) plotted with respect to the Rabi angle gt .

$(\sin gte^{-\kappa t/2})^2 \leq 2e^{-\kappa t}(1 - e^{-\kappa t}/2)$ (since for small κ we take $C(\rho(t)_{A_2(A_1C_1)}) \approx 2\sqrt{\det\rho_{A_2}}$ which is equal to $2\sqrt{e^{-\kappa t}(1 - e^{-\kappa t}/2)}$). In Figure 4.12 we plot the left and the right hand sides ($C_{A_1A_2}^2 + C_{A_2C_1}^2$ and $C_{A_2(A_1C_1)}^2$, respectively) of the corresponding CKW inequality and here also we observe that it always holds under the above approximation.

4.4 Entanglement swapping in a system of two cavities and two atoms

4.4.1 Ideal case of four qubits

In this section we consider some aspects of entanglement swapping, or the transfer of entanglement from the two-cavity to the two-atom system. Such a scheme can be affected by sending two Rydberg atoms A_1, A_2 prepared in their ground states g_1, g_2 through two maximally entangled cavities C_1, C_2 (which can be prepared in the same way as stated in the earlier section) respectively. We will see how to get two maximally entangled atoms which never interacted in the past. The time of flights for the atoms through the cavities are the same. At $t = 0$, the state of the total system is

$$|\Psi(t=0)\rangle_{C_1C_2A_1A_2} = \frac{1}{\sqrt{2}}(|0_11_2\rangle + |1_10_2\rangle) \otimes |g_1g_2\rangle \quad (4.56)$$

When the atom A_1 passes through the cavity C_1 the evolved state at time t is

$$|\Psi(t)\rangle_{C_1C_2A_1} = \frac{1}{\sqrt{2}}(|0_11_2g_1\rangle + \cos gt|g_11_10_2\rangle) \quad (4.57)$$

$$- \sin gt|0_10_2e_1\rangle) \otimes |g_2\rangle \quad (4.58)$$

Now, considering the passage of both the atoms A_1 and A_2 through the respective cavities, C_1 and C_2 , the evolved state at time t is given by

$$\begin{aligned} |\Psi(t)\rangle_{C_1C_2A_1A_2} &= \frac{1}{\sqrt{2}}(\cos gt|0_11_2g_1g_2\rangle - \sin gt|0_10_2g_1e_2\rangle \\ &+ \cos gt|1_10_2g_1g_2\rangle - \sin gt|0_10_2e_1g_2\rangle) \end{aligned} \quad (4.59)$$

$$\rho(t)_{C_1C_2A_1A_2} = |\Psi(t)_{C_1C_2A_1A_2}\rangle\langle\Psi(t)_{C_1C_2A_1A_2}|$$

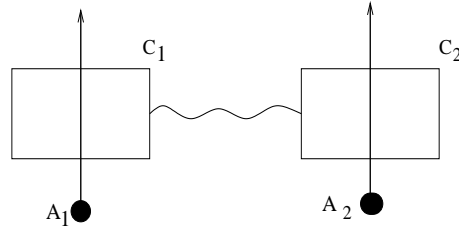


Figure 4.13: Two Rydberg atoms A_1 , A_2 prepared in the ground states g_1 , g_2 pass through two maximally entangled cavities C_1 , C_2 respectively.

$$\begin{aligned}
& \frac{\cos^2 gt}{2} |0_1 1_2 g_1 g_2\rangle \langle 0_1 1_2 g_1 g_2| \\
& + \frac{\sin^2 gt}{2} |0_1 0_2 g_1 e_2\rangle \langle 0_1 0_2 g_1 e_2| \\
& + \frac{\cos^2 gt}{2} |1_1 0_2 g_1 g_2\rangle \langle 1_1 0_2 g_1 g_2| \\
& + \frac{\sin^2 gt}{2} |0_1 0_2 e_1 g_2\rangle \langle 0_1 0_2 e_1 g_2| \\
& + \frac{\cos^2 gt}{2} |0_1 1_2 g_1 g_2\rangle \langle 1_1 0_2 g_1 g_2| \\
& + \frac{\cos^2 gt}{2} |1_1 0_2 g_1 g_2\rangle \langle 0_1 1_2 g_1 g_2| \\
& + \frac{\sin^2 gt}{2} |0_1 0_2 g_1 e_2\rangle \langle 0_1 0_2 e_1 g_2| \\
& + \frac{\sin^2 gt}{2} |0_1 0_2 e_1 g_2\rangle \langle 0_1 0_2 g_1 e_2| \\
& + \dots
\end{aligned} \tag{4.60}$$

Apart from the above eight terms no other term contributes to either of the reduced density states $\rho_{C_1 C_2}$ or $\rho_{A_1 A_2}$. The reduced density states of the pairs $C_1 C_2$, $A_1 A_2$ are given by

$$\begin{aligned}
\rho(t)_{C_1 C_2} &= \text{Tr}_{A_1 A_2}(\rho(t)_{C_1 C_2 A_1 A_2}), \\
&= \frac{\cos^2 gt}{2} |0_1 1_2\rangle \langle 0_1 1_2| + \frac{\cos^2 gt}{2} |1_1 0_2\rangle \langle 1_1 0_2| \\
&+ \sin^2 gt |0_1 0_2\rangle \langle 0_1 0_2| + \frac{\cos^2 gt}{2} |0_1 1_2\rangle \langle 1_1 0_2| \\
&+ \frac{\cos^2 gt}{2} |1_1 0_2\rangle \langle 0_1 1_2|.
\end{aligned} \tag{4.61}$$

$$\begin{aligned}
\rho(t)_{A_1A_2} &= \text{Tr}_{C_1C_2}(\rho_{C_1C_2A_1A_2}), \\
&= \cos^2 gt |g_1g_2\rangle\langle g_1g_2| + \frac{\sin^2 gt}{2} |g_1e_2\rangle\langle g_1e_2| \\
&+ \frac{\sin^2 gt}{2} |e_1g_2\rangle\langle e_1g_2| + \frac{\sin^2 gt}{2} |g_1e_2\rangle\langle e_1g_2| \\
&+ \frac{\sin^2 gt}{2} |e_1g_2\rangle\langle g_1e_2|.
\end{aligned} \tag{4.62}$$

The reduced density matrix of the pair of atoms C_1C_2 is given by

$$\rho(t)_{C_1C_2} = \begin{pmatrix} \sin^2 gt & 0 & 0 & 0 \\ 0 & \frac{\cos^2 gt}{2} & \frac{\cos^2 gt}{2} & 0 \\ 0 & \frac{\cos^2 gt}{2} & \frac{\cos^2 gt}{2} & 0 \\ 0 & 0 & 0 & 0 \end{pmatrix} \tag{4.63}$$

in the basis of $|0_10_2\rangle$, $|0_11_2\rangle$, $|1_10_2\rangle$, and $|1_11_2\rangle$ states. Similarly,

$$\rho(t)_{A_1A_2} = \begin{pmatrix} 0 & 0 & 0 & 0 \\ 0 & \frac{\sin^2 gt}{2} & \frac{\sin^2 gt}{2} & 0 \\ 0 & \frac{\sin^2 gt}{2} & \frac{\sin^2 gt}{2} & 0 \\ 0 & 0 & 0 & \cos^2 gt \end{pmatrix} \tag{4.64}$$

in the basis of $|e_1e_2\rangle$, $|e_1g_2\rangle$, $|g_1e_2\rangle$, and $|g_1g_2\rangle$ states. We now compute the concurrences for the pair of atoms A_1, A_2 and pair of cavities C_1, C_2 . These are given by

$$C(\rho(t)_{C_1C_2}) = \cos^2 gt, \tag{4.65}$$

$$C(\rho(t)_{A_1A_2}) = \sin^2 gt. \tag{4.66}$$

The concurrences for the pairs C_1-C_2 and A_1-A_2 are plotted in the Figure 4.14. One sees that the entanglement between two cavities are swapped by two atoms for the interaction times $gt = (2n + 1)\pi/2$, ($n = 0, 1, 2, \dots$), thus creating maximally entangled atomic pairs at these times.

4.4.2 Information transfer with cavity dissipation

Finally, we consider the effect of cavity leakage on the transfer of information from the two-cavity to the two-atom system. Under the secular approximation [27] and the approximation of a two-level cavity, one can solve the master equation [46] to obtain the

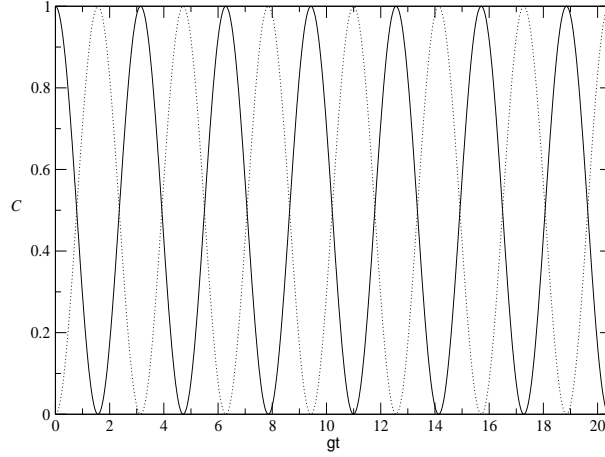


Figure 4.14: $C(\rho(t)_{C_1 C_2})$ (solid line), $C(\rho(t)_{A_1 A_2})$, (dotted line) plotted with respect to the Rabi angle gt .

four-party density matrix (the method of solving the master equation has been outlined in the section 2.2.1 of chapter 2) which can be formally expressed as

$$\begin{aligned}
 \rho(t)_{C_1 C_2 A_1 A_2} &= \alpha_1 |0_1 1_2 g_1 g_2\rangle \langle 0_1 1_2 g_1 g_2| \\
 &+ \alpha_2 |0_1 0_2 g_1 e_2\rangle \langle 0_1 0_2 g_1 e_2| \\
 &+ \alpha_3 |1_1 0_2 g_1 g_2\rangle \langle 1_1 0_2 g_1 g_2| \\
 &+ \alpha_4 |0_1 0_2 e_1 g_2\rangle \langle 0_1 0_2 e_1 g_2| \\
 &+ \alpha_5 |0_1 1_2 g_1 g_2\rangle \langle 1_1 0_2 g_1 g_2| \\
 &+ \alpha_5 |1_1 0_2 g_1 g_2\rangle \langle 0_1 1_2 g_1 g_2| \\
 &+ \alpha_6 |0_1 0_2 g_1 e_2\rangle \langle 0_1 0_2 e_1 g_2| \\
 &+ \alpha_6 |0_1 0_2 e_1 g_2\rangle \langle 0_1 0_2 g_1 e_2| \\
 &+ \dots
 \end{aligned} \tag{4.67}$$

where the α_i are given by

$$\begin{aligned}
 \alpha_1 &= \left(1 - \frac{e^{-\kappa_1 t}}{2}\right) e^{-\kappa_2 t} \cos^2 gt, \\
 \alpha_2 &= \sin^2 gte^{-\kappa_2 t} \left(1 - \frac{e^{-\kappa_1 t}}{2}\right), \\
 \alpha_3 &= \cos^2 gte^{-\kappa_1 t} \left(1 - \frac{e^{-\kappa_2 t}}{2}\right),
 \end{aligned}$$

$$\begin{aligned}
\alpha_4 &= \sin^2 g t e^{-\kappa_1 t} \left(1 - \frac{e^{-\kappa_2 t}}{2}\right), \\
\alpha_5 &= \frac{\cos^2 g t e^{-\kappa_1 t/2} e^{-\kappa_2 t/2}}{2}, \\
\alpha_6 &= \left(e^{-\kappa_1 t/2} \sin g t - \frac{\kappa_1 e^{-\kappa_1 t/2}}{2g} + \frac{\kappa_1}{2g}\right) \left(e^{-\kappa_2 t/2} \sin g t - \frac{\kappa_2 e^{-\kappa_2 t/2}}{2g} + \frac{\kappa_2}{2g}\right) / 2,
\end{aligned}$$

where κ_1 and κ_2 are the cavity leakage constants of cavities C_1 and C_2 respectively. Apart from the above eight terms no other term contributes to either of the reduced density states $\rho_{C_1 C_2}$ or $\rho_{A_1 A_2}$, which are given by

$$\begin{aligned}
\rho(t)_{C_1 C_2} &= \text{Tr}_{A_1 A_2}(\rho(t)_{C_1 C_2 A_1 A_2}), \\
&= \alpha_1 |0_1 1_2\rangle \langle 0_1 1_2| + \alpha_3 |1_1 0_2\rangle \langle 1_1 0_2| \\
&+ (\alpha_2 + \alpha_4) |0_1 0_2\rangle \langle 0_1 0_2| + \alpha_5 |0_1 1_2\rangle \langle 1_1 0_2| \\
&+ \alpha_5 |1_1 0_2\rangle \langle 0_1 1_2|.
\end{aligned} \tag{4.68}$$

$$\begin{aligned}
\rho(t)_{A_1 A_2} &= \text{Tr}_{C_1 C_2}(\rho(t)_{C_1 C_2 A_1 A_2}), \\
&= (\alpha_1 + \alpha_3) |g_1 g_2\rangle \langle g_1 g_2| + \alpha_2 |g_1 e_2\rangle \langle g_1 e_2| \\
&+ \alpha_4 |e_1 g_2\rangle \langle e_1 g_2| + \alpha_6 |g_1 e_2\rangle \langle e_1 g_2| \\
&+ \alpha_6 |e_1 g_2\rangle \langle g_1 e_2|.
\end{aligned} \tag{4.69}$$

The reduced density matrix of the pair of atoms $C_1 C_2$ is given by

$$\rho(t)_{C_1 C_2} = \begin{pmatrix} (\alpha_2 + \alpha_4) & 0 & 0 & 0 \\ 0 & \alpha_1 & \alpha_5 & 0 \\ 0 & \alpha_5 & \alpha_3 & 0 \\ 0 & 0 & 0 & 0 \end{pmatrix} \tag{4.70}$$

in the basis of $|0_1 0_2\rangle$, $|0_1 1_2\rangle$, $|1_1 0_2\rangle$, and $|1_1 1_2\rangle$ states. Similarly,

$$\rho(t)_{A_1 A_2} = \begin{pmatrix} 0 & 0 & 0 & 0 \\ 0 & \alpha_4 & \alpha_6 & 0 \\ 0 & \alpha_6 & \alpha_2 & 0 \\ 0 & 0 & 0 & (\alpha_1 + \alpha_3) \end{pmatrix} \tag{4.71}$$

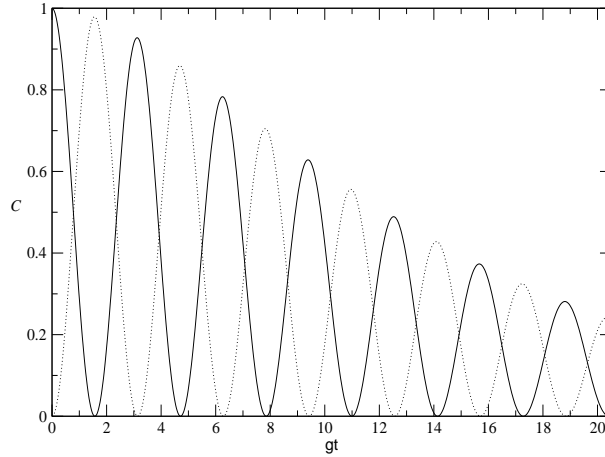


Figure 4.15: $C(\rho(t)_{C_1 C_2})$ (solid line), $C(\rho(t)_{A_1 A_2})$, (dotted line) plotted with respect to the Rabi angle gt . $\kappa_1/g = \kappa_2/g = 0.1$

in the basis of $|e_1 e_2\rangle$, $|e_1 g_2\rangle$, $|g_1 e_2\rangle$, and $|g_1 g_2\rangle$ states. We compute the concurrences for the pair of atoms A_1, A_2 and pair of cavities C_1, C_2 . These are

$$C(\rho(t)_{C_1 C_2}) = |\cos^2 gt e^{-\kappa_1 t/2} e^{-\kappa_2 t/2}|, \quad (4.72)$$

$$C(\rho(t)_{A_1 A_2}) = \left| \left(e^{-\kappa_1 t/2} \sin gt - \frac{\kappa_1 e^{-\kappa_1 t/2}}{2g} + \frac{\kappa_1}{2g} \right) \left(e^{-\kappa_2 t/2} \sin gt - \frac{\kappa_2 e^{-\kappa_2 t/2}}{2g} + \frac{\kappa_2}{2g} \right) \right|. \quad (4.73)$$

We plot them versus the Rabi angle in Figure 4.15. Though the concurrences $C(\rho(t)_{C_1 C_2})$ and $C(\rho(t)_{A_1 A_2})$ are reduced by the loss of cavity photons, one sees that perfect swapping is still obtained. One of the basic features of information exchange between bipartite systems, represented by entanglement swapping, is thus seen to be preserved for mixed states too.

4.5 Summary

In this chapter we have considered two important and interesting features of quantum entanglement, viz., “monogamy”, and entanglement swapping. We have used the set-up of (i) two initially entangled cavities [70, 71, 72] and a single Rydberg atom passing through one of them and, (ii) two initially entangled atoms [6] with one of these atoms passing through a single-mode vacuum cavity, to study the quantitative manifestations

of a “monogamy” inequality [36] in atom-photon interactions. The unavoidable photon leakage exists in cavities used for the practical realization of quantum information transfer. The effects of such dissipation have been investigated on the “monogamous” nature of the entanglement between the two cavities and an atom, and in between two atoms and the cavity. We have found that the essential “monogamous” character is preserved even with cavity dissipation.

We have further shown that the entanglement between the atom and the cavity through which it passes increases with larger dissipation, a feature that could be understood by invoking the “monogamous” character of entanglement in the first system. We have then considered a set-up involving two entangled cavities and two Rydberg atoms. Entanglement swapping between the two cavities and the two atoms which never interact directly with each other is observed in this system. Cavity dissipation reduces the total amount of information exchange. Moreover, here we have verified that the property of swapping is preserved with dissipation. Further studies on different quantitative manifestations of information transfer in the presence of dissipative effects might be useful for the construction of realistic devices implementing various protocols.

Chapter 5

Effects of cavity field statistics on entanglement

5.1 Introduction

The utility of entangled atomic qubits for quantum information processing has prompted several new methods for their generation [73]. Many of these schemes assume a vacuum cavity field to generate atomic entanglement. However, the process of atom-atom entanglement usually involves the transfer of entanglement between two different Hilbert spaces, i.e., from the photons to the atoms [9, 10, 11, 12, 74]. The properties of the radiation field involved, thus govern the quantitative nature of atomic entanglement generated through such transfers. In the present chapter we study the dynamical generation of entanglement between two two-level atoms mediated by various cavity fields. Since the atoms do not interact directly with each other, the properties of the radiation field encountered by them bears crucially on the nature of atomic entanglement. Our main purpose is to focus on the effect of different field statistics on the magnitude of two-atom entanglement.

The motivation for this work [12, 13] is to investigate the role of various radiation fields inside a cavity on the atomic entanglement mediated by it. We focus on a micromaser type system [9, 20, 33, 75] in which two-level Rydberg atoms are sent into the cavity at such a rate that the probability of two atoms being present there is negligibly small. We take the initial state of the two atoms as separate or product state, and the emergent two-qubit state is of a mixed entangled type [9]. Here we consider the cavity to be of a non-leaky type, i.e., $Q = \infty$. We quantify the two-atom entanglement by computing the entanglement of formation [22, 23]. We present a detailed and comparative study of two atom entanglement for low and high average photon number cases corresponding to the

different cavity fields.

The structure of the chapter is as follows. In Section 5.2 we give a description of various radiation fields and show how the entanglement between two spatially separated atoms is generated. We observe robust atom-atom entanglement mediated by the Fock state field, the thermal field, and the coherent field respectively [12]. We demonstrate how the various field statistics are reflected in two-atom entanglement as a function of the average photon number of the cavity fields and the Rabi angle. Several distinctive characteristics of the entanglement generated by the different fields through the Jaynes-Cummings interaction are discussed in comparison with some earlier results obtained for the Tavis-Cummings interaction [76]. A common feature that is observed is that for the cavity low photon number case, the entanglement between the two atoms decreases with increasing average photon number of the field. In section 5.3 we investigate an interesting relation between squeezing of the cavity field and the atomic entanglement generated [13]. We find the conditions in which squeezing can lead to the increase in the magnitude of entanglement.

5.2 Cavity field statistics and atomic entanglement

As discussed in chapter 2 the interaction picture Hamiltonian of the joint atom-field system can be written in the rotating wave approximation [46] as,

$$H_I = g(\sigma^+ a + \sigma^- a^\dagger). \quad (5.1)$$

where a^\dagger and a are the usual creation and destruction operators of the radiation field. Here we consider the quality factor of the cavity $Q = \infty$, which is a reasonable approximation since the cavity-QED related experiments are carried out with cavities with very high Q [6]. We consider a micromaser-type system discussed in details in chapter 3 in which atoms are sent into the cavity at such a rate that the probability of two atoms being present there is negligibly small. Our purpose here is to show the influence of the photon statistics of the driving fields (radiation field with which the atoms interact) on atomic entanglement. In the following analysis, we consider four different kinds of radiation fields, i.e., the Fock state field, the thermal field, the coherent state field, and the squeezed state field, respectively.

5.2.1 Fock state cavity field

A Fock state is written as $|n\rangle$ with n an integer value, signifying that there are n quanta of excitation in the mode. $|0\rangle$ corresponds to the ground state (no excitation). The amplitudes c_n s of these states obey the delta function relation $c_n = \delta_{m,n}$ where m is the photon number of the Fock state. The variance, defined in Eq.(2.6) is $V = 1 - \frac{1}{m}$ for a Fock state $|m\rangle$. So, for small values of m , $V < 1$ and field has a non-classical character. For large m , V tends towards the classical limit. This feature is reflected in the entanglement generated between the two atoms, as we see later.

Let us first consider the passage of the first atom, initially in the excited state $|e\rangle$, through the cavity. The joint atom-field state is given by

$$|\Psi(t=0)\rangle_{a-f} = |e\rangle \otimes |n\rangle. \quad (5.2)$$

The atom-field state evolves with the interaction given by Eq.(5.1) to

$$|\Psi(t)_{a-f}\rangle = \cos(\sqrt{n+1}gt)|e, n\rangle + \sin(\sqrt{n+1}gt)|g, n+1\rangle \quad (5.3)$$

The next atom which enters the cavity interacts with this “changed” field and thus a correlation develops between the two atoms via the cavity field. The joint state of the two atoms and the field is given by

$$|\Psi(t)\rangle_{a-a-f} = \alpha_1|e_1, e_2, n\rangle + \alpha_2|e_1, g_2, n+1\rangle + \alpha_3|g_1, e_2, n+1\rangle + \alpha_4|g_1, g_2, n+2\rangle \quad (5.4)$$

where

$$\begin{aligned} \alpha_1 &= \cos^2(\sqrt{n+1}gt), \quad \alpha_2 = \cos(\sqrt{n+1}gt) \sin(\sqrt{n+1}gt), \\ \alpha_3 &= \cos(\sqrt{n+2}gt) \sin(\sqrt{n+1}gt), \quad \alpha_4 = \sin(\sqrt{n+1}gt) \sin(\sqrt{n+2}gt). \end{aligned} \quad (5.5)$$

The reduced mixed density state of the two atoms after tracing over the field is given by (we display the non-vanishing terms only)

$$\begin{aligned} \rho(t)_{a-a} &= \text{tr}_f(\rho(t)_{a-a-f}) = \alpha_1^2|e_1e_2\rangle\langle e_1e_2| + \alpha_2^2|e_1g_2\rangle\langle e_1g_2| \\ &+ \alpha_3^2|g_1e_2\rangle\langle g_1e_2| + \alpha_2\alpha_3|e_1g_2\rangle\langle g_1e_2| + \alpha_2\alpha_3|g_1e_2\rangle\langle e_1g_2| + \alpha_4^2|g_1g_2\rangle\langle g_1g_2|. \end{aligned} \quad (5.6)$$

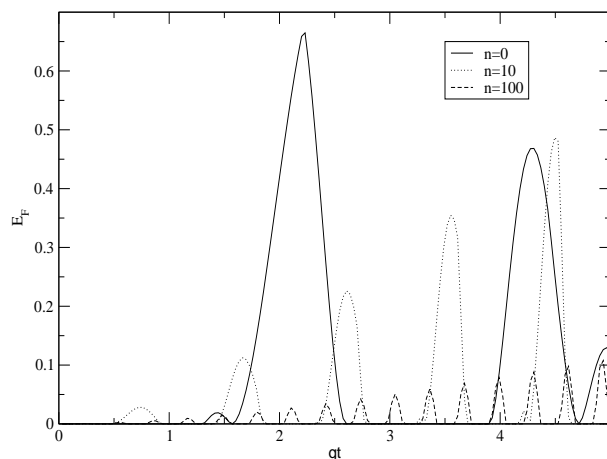


Figure 5.1: Atom-atom entanglement versus gt . Solid line, dotted line, and dashed line indicate E_F between two atoms when the cavity Fock states are $n = 0$, $n = 10$, and $n = 100$ respectively.

The corresponding reduced density matrix is obtained to be

$$\rho_{a-a} = \begin{pmatrix} \alpha_1^2 & 0 & 0 & 0 \\ 0 & \alpha_2^2 & \alpha_2\alpha_3 & 0 \\ 0 & \alpha_2\alpha_3 & \alpha_3^2 & 0 \\ 0 & 0 & 0 & \alpha_4^2 \end{pmatrix} \quad (5.7)$$

in the basis of $|e_1e_2\rangle$, $|e_1g_2\rangle$, $|g_1e_2\rangle$ and $|g_1g_2\rangle$ states.

We compute the entanglement of formation E_f for this bipartite two-atom state. In Figure 5.1 E_F is plotted versus the Rabi angle gt for different values of n . The peaks of the entanglement of formation are reflective of the photon statistics that are typical in micromaser dynamics[75]. We see that E_F falls off sharply as n increases. The non-classical character of the field for small values of the average photon number n , is reflected in larger entanglement between the two atoms. An interesting comparison can be made with the case of the Tavis-Cummings model[76] which is employed when two atoms are present simultaneously inside the cavity. Although the simultaneous interaction of two excited atoms with Fock state field never results in two-atom entanglement as was shown by Tessier et al.[7], the notable difference here is that in the JC dynamics modelling the micromaser one always gets two-atom entanglement mediated by the Fock state cavity field, as we see in Figure 5.1.

5.2.2 Thermal state cavity field

The thermal field is the most easily available radiation field, and so, its influence on the entanglement of spins (two-level atoms) is of interest [10]. The field at thermal equilibrium obeying Bose-Einstein statistics has an average photon number at temperature $T^0 K$, given by

$$\langle n \rangle = \frac{1}{e^{\hbar\omega/kT} - 1}. \quad (5.8)$$

The photon statistics is governed by the distribution P_n given by

$$P_n = \frac{\langle n \rangle^n}{(1 + \langle n \rangle)^{n+1}}. \quad (5.9)$$

We plot the probability distribution function P_n versus the photon number n for different values of the average photon number. This distribution function always peaks at zero, i.e., $n_{peak} = 0$ (Figure 5.2). We also observe that the peak of the distribution function at photon number zero reduces with increasing average photon number $\langle n \rangle$. We consider the scheme of two two-level atoms are passing through a cavity filled with a thermal radiation field one after the other. We assume the time of flight of each atom through the cavity to be the same. For a thermal field distribution function for the cavity field, the joint two-atom-cavity state is obtained by summing over all n , and is given by

$$\begin{aligned} |\Psi(t)\rangle_{a-a-f} = & \sum_n A_n [\cos^2(\sqrt{n+1}gt)|e_1, e_2, n\rangle + \cos(\sqrt{n+1}gt)\sin(\sqrt{n+1}gt)|e_1, g_2, n+1\rangle \\ & + \cos(\sqrt{n+2}gt)\sin(\sqrt{n+1}gt)|g_1, e_2, n+1\rangle \\ & + \sin(\sqrt{n+1}gt)\sin(\sqrt{n+2}gt)|g_1, g_2, n+2\rangle] \end{aligned} \quad (5.10)$$

where $P_n = |A_n|^2$ is the photon distribution function of the thermal field. The reduced mixed density state of two atoms after passing through the thermal cavity field can be written as

$$\begin{aligned} \rho(t)_{a-a} = \text{tr}_f(\rho(t)_{a-a-f}) = & \beta_1|e_1e_2\rangle\langle e_1e_2| + \beta_2|e_1g_2\rangle\langle e_1g_2| \\ & + \beta_3|g_1e_2\rangle\langle g_1e_2| + \beta_4|e_1g_2\rangle\langle g_1e_2| \\ & + \beta_4|g_1e_2\rangle\langle e_1g_2| + \beta_5|g_1g_2\rangle\langle g_1g_2|, \end{aligned} \quad (5.11)$$

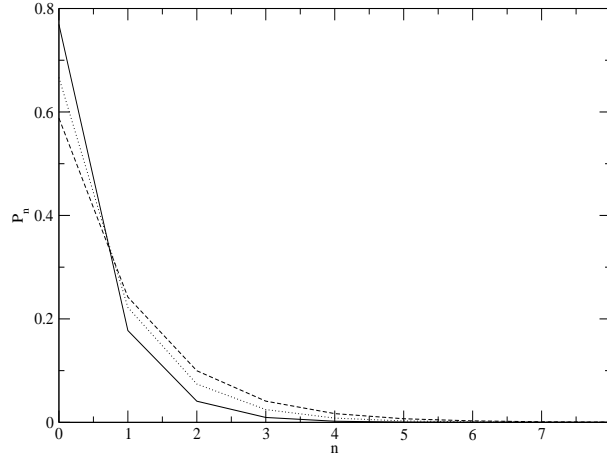


Figure 5.2: Thermal field distribution function P_n is plotted vs photon number n when (i) average photon number $\langle n \rangle = 0.3$ (solid line), (ii) $\langle n \rangle = 0.5$ (dotted line) and (iii) $\langle n \rangle = 0.7$ (dashed line).

where

$$\begin{aligned}
 \beta_1 &= \sum_n P_n \cos^4(\sqrt{n+1}gt), \\
 \beta_2 &= \sum_n P_n \cos^2(\sqrt{n+1}gt) \times \sin^2(\sqrt{n+1}gt), \\
 \beta_3 &= \sum_n P_n \cos^2(\sqrt{n+2}gt) \times \sin^2(\sqrt{n+1}gt), \\
 \beta_5 &= \sum_n P_n \sin^2(\sqrt{n+1}gt) \times \sin^2(\sqrt{n+2}gt), \\
 \beta_4 &= \sum_n P_n \sin^2(\sqrt{n+1}gt) \times \cos(\sqrt{n+1}gt) \cos(\sqrt{n+2}gt).
 \end{aligned} \tag{5.12}$$

The corresponding reduced density matrix can thus be written as

$$\rho_{a-a} = \begin{pmatrix} \beta_1 & 0 & 0 & 0 \\ 0 & \beta_2 & \beta_4 & 0 \\ 0 & \beta_4 & \beta_3 & 0 \\ 0 & 0 & 0 & \beta_5 \end{pmatrix} \tag{5.13}$$

in the basis of $|e_1e_2\rangle$, $|e_1g_2\rangle$, $|g_1e_2\rangle$ and $|g_1g_2\rangle$ states.

We compute the entanglement of formation E_F for the above two-atom state and plot it versus the Rabi angle gt for different values of the average photon number $\langle n \rangle$ in

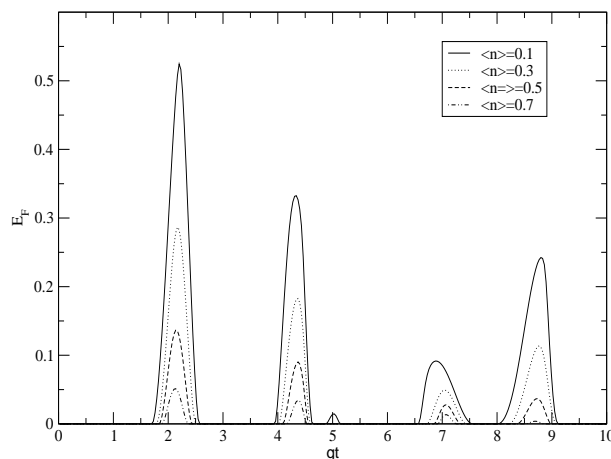


Figure 5.3: Atom-atom entanglement of formation mediated by the thermal cavity field is plotted versus gt .

Figure 5.3. It is interesting to note that the thermal field which has minimal information can nevertheless entangle qubits that are prepared initially in a separable state. In the context of the Tavis-Cummings framework when both the atoms interact simultaneously with the radiation field, Kim et al. [10] have noticed similar trends in the entanglement mediated by the thermal field. Thus both the Jaynes-Cummings and the Tavis-Cummings models of atom-photon interaction generate similar entanglement when the radiation field is thermal. However, a micromaser-like dynamics based on Janes-Cummings interaction is more realistic from the point of view of cavity-QED experiments.

5.2.3 Coherent state cavity field

A coherent states is a minimum uncertainty state[77] standing at the threshold of the classical-quantum limit. These states are parametrised by a single complex number α as follows:

$$|\alpha\rangle = \sum_n \frac{\alpha^n}{\sqrt{n!}} |n\rangle. \quad (5.14)$$

A coherent state is an eigenstate of the annihilation operator a

$$a|\alpha\rangle = \alpha|\alpha\rangle \quad (5.15)$$

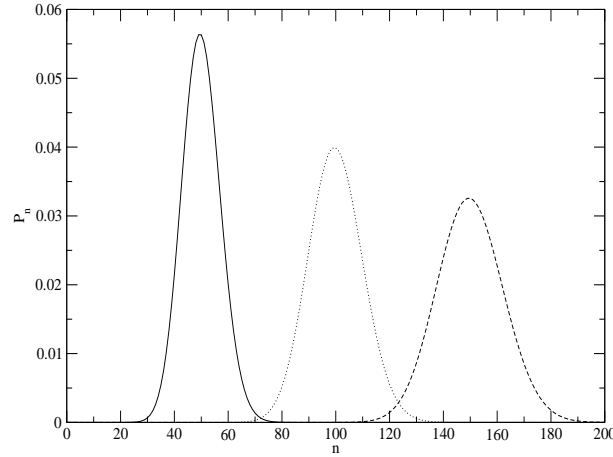


Figure 5.4: Coherent field distribution function P_n is plotted vs photon number n when (i) average photon number $\langle n \rangle = 50$ (solid line), (ii) $\langle n \rangle = 100$ (dotted line) and (iii) $\langle n \rangle = 150$ (dashed line).

and obeys a Poissonian distribution function in the photon number representation

$$P_n = \frac{e^{-\langle n \rangle} \langle n \rangle^n}{n!} \quad (5.16)$$

with the average photon number $\langle n \rangle = |\alpha|^2$. We plot the probability distribution function P_n of the coherent state field versus photon number n for different values of the average photon number $\langle n \rangle$ (Figure 5.4). It is clearly seen from Figure 5.4 that the distribution function P_n peaks at non-zero values of the photon number, i.e., $n_{peak} \neq 0$. We see that the peaks of the coherent distribution function shift to the right as the average photon number increases in contrast to the case of the thermal field.

The Jaynes-Cummings interaction[26] leads to a tripartite joint state of the cavity field and the two atoms passing through it given by

$$\begin{aligned} |\Psi(t)\rangle_{a-a-f} = & \sum_n A_n [\cos^2(\sqrt{n+1}gt) |e_1, e_2, n\rangle \\ & + \cos(\sqrt{n+1}gt) \sin(\sqrt{n+1}gt) |e_1, g_2, n+1\rangle \\ & + \cos(\sqrt{n+2}gt) \sin(\sqrt{n+1}gt) |g_1, e_2, n+1\rangle \\ & + \sin(\sqrt{n+1}gt) \sin(\sqrt{n+2}gt) |g_1, g_2, n+2\rangle] \end{aligned} \quad (5.17)$$

where $P_n = |A_n|^2$. Since we are interested in calculating the entanglement of the joint two-atom state after the atoms emerge from the cavity, we consider the reduced density

state $\rho(t)_{a-a}$ of the two atoms obtained after taking trace over the field variables

$$\begin{aligned}
\rho(t)_{a-a} &= \text{Tr}_{\text{field}}(|\Psi(t)\rangle_{a-a-f,a-a-f}\langle\Psi(t)|) \\
&= \gamma_1|e_1e_2\rangle\langle e_1e_2| + \gamma_2|e_1g_2\rangle\langle e_1g_2| \\
&\quad + \gamma_3|g_1e_2\rangle\langle g_1e_2| + \gamma_4|e_1g_2\rangle\langle g_1e_2| \\
&\quad + \gamma_4|g_1e_2\rangle\langle e_1g_2| + \gamma_5|g_1g_2\rangle\langle g_1g_2| \\
&\quad + \gamma_6|e_1e_2\rangle\langle g_1g_2| + \gamma_6|g_1g_2\rangle\langle e_1e_2| \\
&\quad + \gamma_7|e_1g_2\rangle\langle e_1e_2| + \gamma_7|e_1e_2\rangle\langle e_1g_2| \\
&\quad + \gamma_8|g_1e_2\rangle\langle e_1e_2| + \gamma_8|e_1e_2\rangle\langle g_1e_2| \\
&\quad + \gamma_9|g_1g_2\rangle\langle e_1g_2| + \gamma_9|e_1g_2\rangle\langle g_1g_2| \\
&\quad + \gamma_{10}|g_1e_2\rangle\langle g_1g_2| + \gamma_{10}|g_1g_2\rangle\langle g_1e_2|,
\end{aligned} \tag{5.18}$$

where

$$\begin{aligned}
\gamma_1 &= \sum_n P_n \cos^4(\sqrt{n+1}gt), \\
\gamma_2 &= \sum_n P_n \cos^2(\sqrt{n+1}gt) \sin^2(\sqrt{n+1}gt), \\
\gamma_3 &= \sum_n P_n \cos^2(\sqrt{n+2}gt) \sin^2(\sqrt{n+1}gt), \\
\gamma_4 &= \sum_n P_n \sin^2(\sqrt{n+1}gt) \cos(\sqrt{n+1}gt) \cos(\sqrt{n+2}gt), \\
\gamma_5 &= \sum_n P_n \sin^2(\sqrt{n+1}gt) \sin^2(\sqrt{n+2}gt), \\
\gamma_6 &= \sum_n \sqrt{P_n P_{n-2}} \cos^2(\sqrt{n+1}gt) \sin(\sqrt{n}gt) \sin(\sqrt{n-1}gt), \\
\gamma_7 &= \sum_n \sqrt{P_n P_{n-1}} \cos^2(\sqrt{n+1}gt) \cos(\sqrt{n}gt) \sin(\sqrt{n}gt), \\
\gamma_8 &= \sum_n \sqrt{P_n P_{n-1}} \cos^3(\sqrt{n+1}gt) \sin(\sqrt{n}gt), \\
\gamma_9 &= \sum_n \sqrt{P_n P_{n-1}} \sin^2(\sqrt{n+1}gt) \cos(\sqrt{n+1}gt) \sin(\sqrt{n}gt), \\
\gamma_{10} &= \sum_n \sqrt{P_n P_{n-1}} \sin^2(\sqrt{n+1}gt) \cos(\sqrt{n+2}gt) \sin(\sqrt{n}gt).
\end{aligned} \tag{5.19}$$

This state can be written in the matrix form in the basis of $|e_1e_2\rangle$, $|e_1g_2\rangle$, $|g_1e_2\rangle$ and

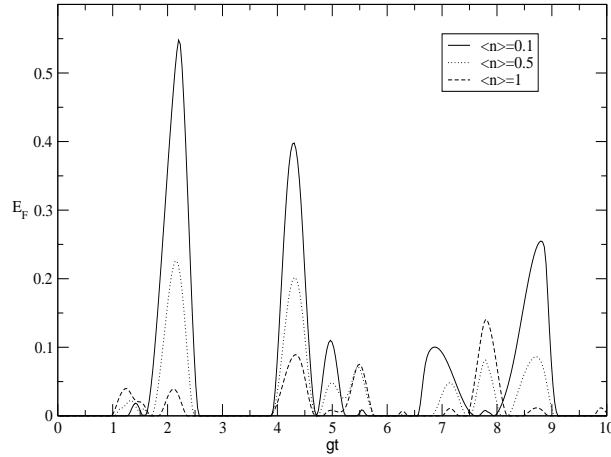


Figure 5.5: Two-atom entanglement mediated by the coherent state cavity field at low average photon number is plotted versus gt .

$|g_1g_2\rangle$ states as

$$\rho_{a-a} = \begin{pmatrix} \gamma_1 & \gamma_7 & \gamma_8 & \gamma_6 \\ \gamma_7 & \gamma_2 & \gamma_4 & \gamma_9 \\ \gamma_8 & \gamma_4 & \gamma_3 & \gamma_{10} \\ \gamma_6 & \gamma_9 & \gamma_{10} & \gamma_5 \end{pmatrix}. \quad (5.20)$$

The entanglement of formation E_F is computed separately for low and high photon numbers as the two cases have distinctive features for the coherent state field. E_f is plotted versus the Rabi angle gt for low average photon number $\langle n \rangle$ in Figure 5.5. The peaks of the entanglement of formation are reflective of the photon statistics that are typical in micromaser dynamics[75]. We see that E_F falls off sharply as $\langle n \rangle$ increases. For small photon numbers, $n_{peak} \approx 0$ and hence, the evolution of E_F is similar to the case when a thermal field is inside the cavity. For large $\langle n \rangle$, n_{peak} moves significantly to the right (Figure 5.6) and its influence is completely different compared to that for the low $\langle n \rangle$ case. Quantum effects which are predominant primarily when the photon number is low, help to increase the peak value of E_f . We note in Figure 5.6 that in general, E_F increases slightly with $\langle n \rangle$ with its time evolution being different for different $\langle n \rangle$. This is reflective of the collapse-revival characteristic in the Jaynes-Cummings model[26].

We further note that though E_F is higher for the low photon number category (Figure 5.5), this behaviour is reversed for the high photon number category (Figure 5.6). For

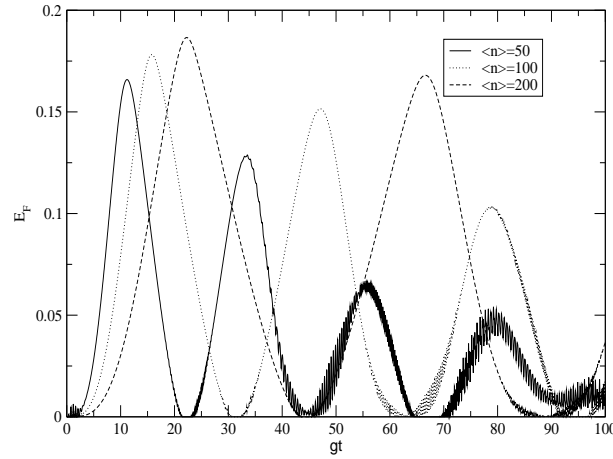


Figure 5.6: Atom-atom entanglement mediated by coherent state cavity field at high average photon number is plotted versus gt .

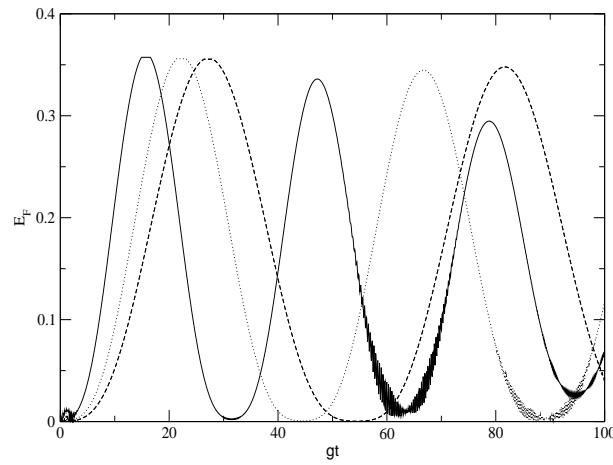


Figure 5.7: Atom-atom entanglement mediated by coherent state cavity field in the Tavis-Cummings model is plotted vs gt for average photon number (i) $\langle n \rangle = 100$ (solid line), (ii) $\langle n \rangle = 200$ (dotted line), and (iii) $\langle n \rangle = 300$ (dashed line).

high $\langle n \rangle$, the features of generated entanglement are thus significantly different from those in the case of the thermal field. In the context of the Tavis-Cummings framework when both the atoms interact simultaneously with the radiation field, Tessier et al. [7] have noticed similar trends in the entanglement mediated by the coherent field. In this framework where two two-level atoms prepared in the excited state simultaneously interact with the cavity field, one can get atom-atom entanglement mediated via by the coherent state field. In Figure 5.7 we plot the atom-atom entanglement in the Tavis-Cummings framework and see that it has similar trend in characteristics as entanglement in the Jaynes-Cummings framework (Figure 5.6).

5.3 Effects of squeezing on entanglement

A quantum mechanical cavity field such as the squeezed field[78] may assist in increasing the atomic entanglement. The squeezed radiation field has wide applications in many different arenas of quantum optics[78, 79, 80, 81, 82]. The relation between squeezing and entanglement in general, is itself an interesting issue which has been discussed through many approaches in the literature[80]. Squeezing has been used as a resource in several protocols of generating and distilling entanglement, and in information transfer[81]. In particular, it has been shown how atomic qubits can be entangled with the help of a squeezed radiation field using one or two optical cavities[82]. In this section we study the effects of squeezing parameters of a squeezed radiation field inside a microwave cavity on the quantitative entanglement of atomic qubits passing through it.

A squeezed state has less noise in one quadrature than a coherent state. To satisfy the uncertainty principle the noise in the other quadrature should be greater than that of a coherent state. Our purpose here is to study the effect of squeezing of the radiation field on the entanglement of a pair of atoms passing through it.

The single mode field inside the cavity can be written as

$$E(t) = a_1 \cos \omega t + a_2 \sin \omega t \quad (5.21)$$

where $a_1 = (a+a^\dagger)/2$ and $a_2 = (a-a^\dagger)/2i$ are the two quadratures satisfying $[a_1, a_2] = i/2$.

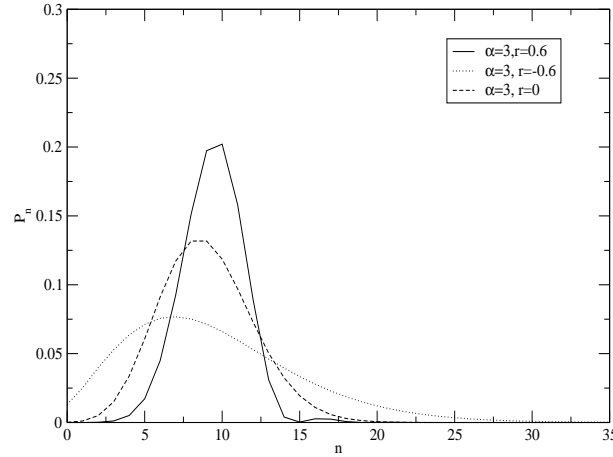


Figure 5.8: Probability distribution function P_n is plotted vs n for (i) sub-Poissonian field (solid line) (ii) super-Poissonian field (dotted line) (iii) coherent state field (dashed line).

The variances $\Delta a_1 = \sqrt{\langle a_1^2 \rangle - \langle a_1 \rangle^2}$ and $\Delta a_2 = \sqrt{\langle a_2^2 \rangle - \langle a_2 \rangle^2}$ satisfy

$$\Delta a_1 \Delta a_2 \geq \frac{1}{4}. \quad (5.22)$$

The coherent state or the minimum uncertainty state given by Eqs.(5.14-5.16) satisfy the equality sign along with

$$\Delta a_1 = \Delta a_2 = \frac{1}{2}. \quad (5.23)$$

Further, either of Δa_1 or Δa_2 can be reduced below $\frac{1}{2}$ at the expense of the other such that Eq.(5.22) is satisfied, and radiation fields having such properties are called squeezed fields.

The photon distribution function of the squeezed radiation field can be represented by [78, 83, 84, 85]

$$P_n = \frac{1}{n! \mu} \left(\frac{\nu}{2\mu}\right)^n e^{-\beta^2 \left(\frac{\nu}{\mu} - 1\right)} \left| H_n \left(\frac{\beta}{\sqrt{2\mu\nu}} \right) \right|^2, \quad (5.24)$$

where β is related to the coherent state amplitude α in Eq.(5.15) by $\beta = (\mu + \nu)\alpha$ for real α . μ and ν can be represented by the squeezing parameter r as $\mu = \cosh r$ and $\nu = \sinh r$. The average photon number can thus be written as

$$\langle n \rangle = |\alpha|^2 + \sinh^2 r. \quad (5.25)$$

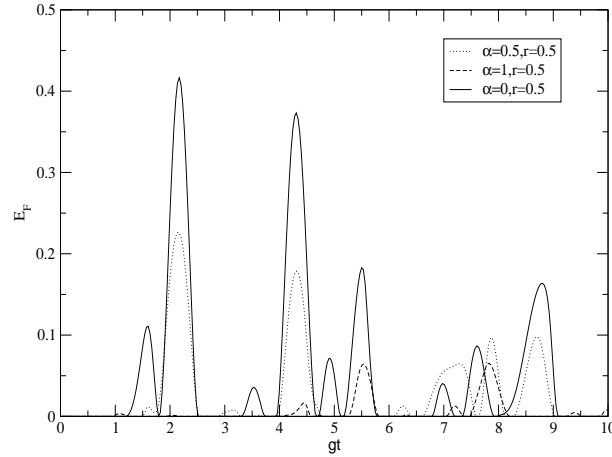


Figure 5.9: Atom-atom entanglement of formation mediated by the squeezed field for different values of α is plotted versus gt for the low photon number case.

In terms of the squeezing parameter, the variances of such fields are given by

$$\begin{aligned}\Delta a_1 &= \frac{1}{2}e^{-r}, \\ \Delta a_2 &= \frac{1}{2}e^r.\end{aligned}\tag{5.26}$$

Clearly, for $r = 0$, the statistics reduce to that for a coherent state given by Eq.(5.16). $r > 0$ gives rise to sub-Poissonian statistics, whereas $r < 0$ produces a super-Poissonian field. In Figure 5.8 we plot the probability distribution function for a sub-Poissonian field, a coherent state field, and a super-Poissonian field, respectively, keeping fixed $\alpha = 3$ [78, 83, 84, 85].

As in the earlier cases, we first obtain the reduced density matrix corresponding to the joint two-atom state after passing through a cavity with the squeezed field. The reduced density state has a similar form to that of the coherent state field given by Eq.(5.18) and Eq.(5.20), with γ^s also having the same form as given in Eq.(5.19). The difference in this case arises from the different photon statistics P_n obtained from the squeezed field distribution function as given in Eq.(5.24).

The effects of the photon statistics of the squeezed field on two-atom entanglement for low average photon number are displayed in the Figures 5.9 and 5.10, for varying α and r , respectively. We see that for low photon numbers the time evolution of E_F is similar to that for a coherent field. The effect of the squeezing parameter r enters

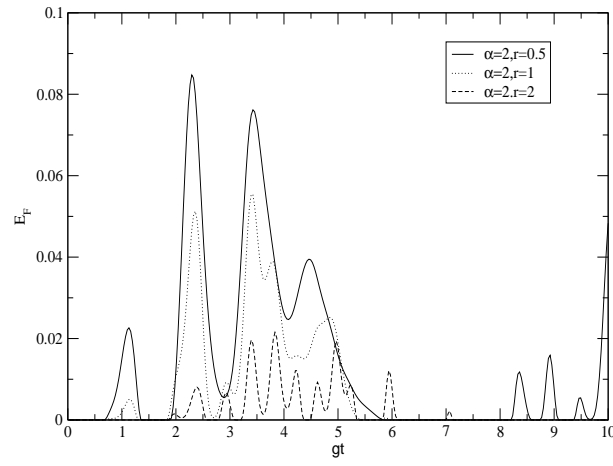


Figure 5.10: E_F mediated by the squeezed field is plotted versus gt for different values of the squeezing parameter r corresponding to the low average photon number case.

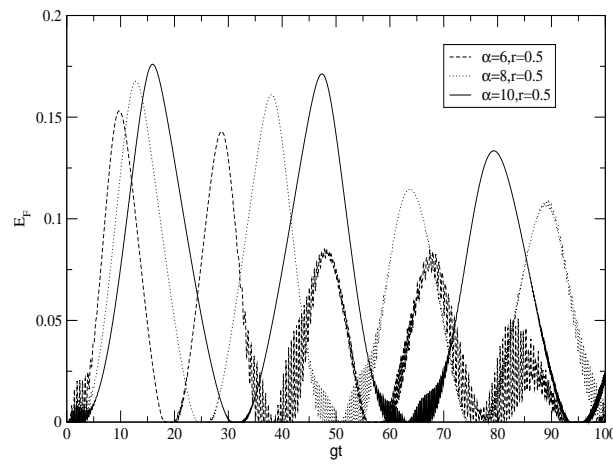


Figure 5.11: E_F mediated by squeezed field for different values of α is plotted versus gt for the high average photon number case.

through $\langle n \rangle$ in Eq.(5.25). An increase in r increases $\langle n \rangle$ and thus E_F diminishes accordingly. The influence of $\langle n \rangle$ on the quantum mechanical field statistics was observed also in Ref.[79] where it was shown that the strength of squeezing decreases faster for lower photon numbers. Here it might appear from Figure 5.10 that squeezing of the radiation field is anti-correlated with the generated atomic entanglement, but what is actually reflected is the decrease of E_F caused by the increase of the average photon number $\langle n \rangle$. This is seen in Figure 5.11 where a larger value of α corresponds to a larger $\langle n \rangle$, and causes E_F to be slightly increased with increasing n or α . The situation for the high photon number case resembles that for the coherent state field.

In Figures 5.12 and 5.13 we plot the two-atom entanglement of formation E_F versus the Rabi angle gt separately for the coherent state and the squeezed state keeping the average cavity photon number fixed. In Figure 5.12 we see that for small $\langle n \rangle$, the dynamics of E_F are similar for both kinds of cavity fields. But the striking feature of Figure 5.12 is in the peaks of E_F for various values of gt . Note that E_F for the squeezed field (dotted line) is higher compared to the coherent state field (dashed line). Thus squeezing of the radiation field as represented by the non-vanishing value of the squeezing parameter r , leads to a notable increase in the magnitude of atomic entanglement over the case the coherent state field ($r = 0$; no squeezing). This trend is also visible in the high photon number case (Figure 5.13), though not for all values of gt . In Figure 5.14 we plot two-atom entanglement of formation E_F versus the Rabi angle gt mediated by the squeezed state field for different squeezing parameter r with same average cavity photon number.

5.4 Summary

In this chapter we have investigated a micromaser-type model focussing on the consequences of cavity field statistics. The entanglement between the two separate atoms builds up via atom-photon interactions inside the cavity, even though no single atom interacts directly with another. We have computed the two-atom entanglement as measured by the entanglement of formation E_F , for the case of four different types of radiation fields, i.e., the Fock state field, the thermal field, the coherent state field, and the squeezed field

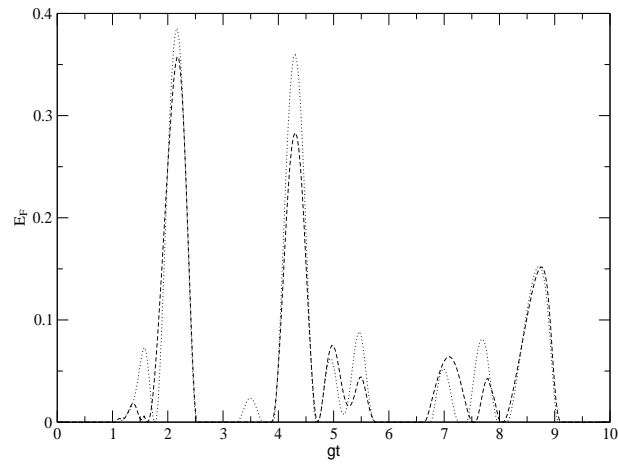


Figure 5.12: Atom-atom entanglement mediated by (i) squeezed cavity field (dotted line) when $\langle n \rangle = 0.3$ and $r = 0.5$, and (ii) coherent state field (dashed line) when $\langle n \rangle = 0.3$, plotted vs gt .

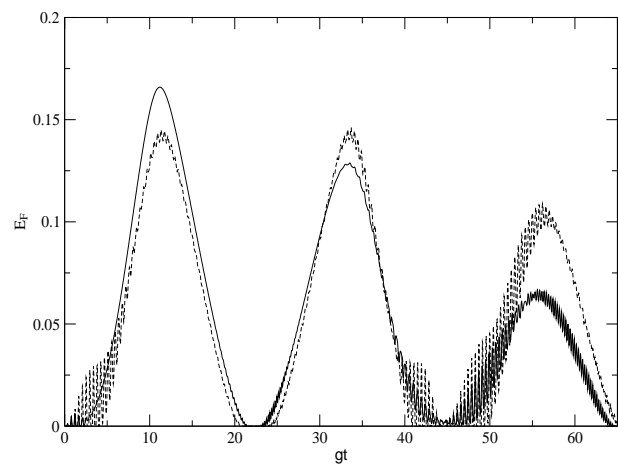


Figure 5.13: Atom-atom entanglement mediated by (i) squeezed cavity field (dashed line) for $\langle n \rangle = 50$ and $r = 1$, and (ii) coherent state field (solid line) for $\langle n \rangle = 50$ plotted vs gt .

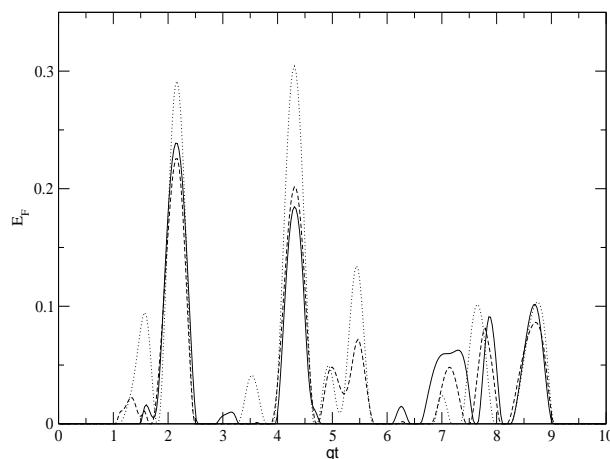


Figure 5.14: Atom-atom entanglement mediated by squeezed cavity field for (i) $\langle n \rangle = 0.5$ and $r = 0.5$ (solid line), (ii) $\langle n \rangle = 0.5$ and $r = 0$ (dashed line), and (iii) $\langle n \rangle = 0.5$ and $r = -0.5$ (dotted line) plotted vs gt .

respectively. Our purpose has been to study the effects of the statistics of the bosonic radiation field on the dynamics of the entanglement of two atomic qubits, i.e., two fermionic systems. Several interesting features of atomic entanglement are observed.

We first showed that for the Fock state cavity field, entanglement between two successively passing atoms can be generated as a consequence of Jaynes-Cummings (JC) dynamics. This is in contrast to the case when both the atoms reside together inside the cavity when Tavis-Cummings (TC) dynamics for atom-photon interactions is unable to generate atomic entanglement[7]. In our case we have got two-atom entanglement which decreases with increasing photon number. We then study the entanglement mediated by the thermal radiation field. It is interesting to note that the thermal field which carries minimum information is still able to produce atomic entanglement through the JC interaction. However, the thermal field having a high value of the average photon number loses its ability to entangle atomic qubits passing through it.

Next we computed the two-atom entanglement as measured by the entanglement of formation E_F for the cases of the coherent state field and the squeezed radiation field inside the cavity. We have performed a quantitative study of the effects of squeezing of the bosonic radiation field on the mediation of the mixed state entanglement of two atomic qubits. Two distinct patterns of entanglement are seen to emerge for the cases

corresponding to low and high average cavity photon numbers, respectively. In the former case the quantum nature of the radiation field plays a prominent role in enhancing atomic entanglement with the decrease of $\langle n \rangle$. The situation reverses for high $\langle n \rangle$ case where actually the increase of $\langle n \rangle$ leads to a slight increase of E_F . The key feature prominently observed for the low $\langle n \rangle$ case is that the two-atom entanglement can be increased with squeezing of the cavity field if the average cavity photon number is held fixed.

Chapter 6

Environment induced entanglement

6.1 Introduction

In the previous chapters, we have discussed various interesting features of entanglement obtained in devices involving microwave cavities[6]. In all these schemes interaction with the surrounding heat bath and cavity leakage has to be monitored such that rapid decoherence[86] is unable to destroy the created entanglement within the time-frame required for observation. Though most proposals of entanglement generation rely on methods to reduce the coupling with the environment, there have been some suggestions[10, 37, 38, 39, 41] for creating entanglement between two or more parties by their collective interactions with a common environment.

Though the effectiveness of collective interactions in the dynamics of quantum optical systems has been appreciated much earlier[47], specific examples of environment induced entanglement have been worked out recently. Schemes of using the decay of the cavity field to induce atom-atom or cavity-cavity entanglement have been proposed[37]. Braun has shown that entanglement can be created between two qubits which do not interact directly with each other, but interact with a common heat bath[41]. A corollary of this result is the mediation of atomic entanglement by a thermal field inside a cavity[10, 12]. Other proposals involving the collective dynamics of trapped ions, squeezed and thermal fields, and quantum-reservoir engineering have also been suggested[38, 39].

In this chapter we show that entanglement in atom-cavity devices can be quantitatively increased by increasing the cavity damping rate. We illustrate our point by first consid-

ering two examples of tripartite systems ((i) two cavities and a single atom, and (ii) one cavity and two atoms) where we obtain analytically the expressions for the atom-cavity and two-atom concurrences, respectively, as functions of the cavity leakage parameter κ . It is seen explicitly that the concurrences are maximized for intermediate values of κ/g . Plenio and Hulega[39] have earlier shown numerically that entanglement between two optical cavities driven by an external optical white noise field can be maximised for intermediate values of the cavity damping rates. In this chapter we derive analytically a similar result, using simple but practically realizable systems with above two examples.

The purpose of the present chapter is to show not just the creation of entanglement with environmental assistance, but to demonstrate the feasibility of actual enhancement of entanglement in real workable devices. To this end, we finally consider again the experimentally workable micromaser [31, 32]. The micromaser device is well known for its utility in the generation of entangled atomic states [52]. The controlled monitoring of dissipative effects makes it possible to study fundamental aspects like nonlocality and information transfer through the micromaser [9, 20] as we have shown in chapter 3. Many of these features have been demonstrated in several experiments performed using the micromaser [31, 32]. Here we choose certain experimentally achieved range of values for the micromaser parameters and show through numerical analysis that the entanglement between a pair of atoms can be increased with the increase of cavity damping κ up to a certain range of its values.

6.2 Enhancement of entanglement in tripartite systems

6.2.1 A two-level atom interacting with one of two maximally entangled cavities

We first consider two initially maximally entangled single-mode cavities (C_1 and C_2). Such a system can be prepared by sending a single circular Rydberg atom in its excited state through two identical and initially empty high-Q microwave cavities[70] discussed in details in chapter 4. A two-level Rydberg atom A_1 prepared in the ground state $|g\rangle$ passes through the cavity C_1 (see Figure 6.1). In the chapter 4 we have studied such a tripartite system to show the monogamous nature of entanglement. The resonant

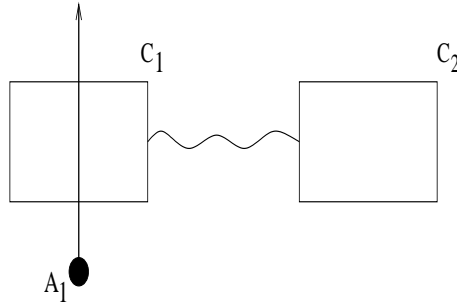


Figure 6.1: A two-level Rydberg atom prepared in the ground state is passing through one of two maximally entangled cavities C_1 (same as Figure 4.3)

interaction between the two-level atom and the cavity mode frequency takes place with the Rabi angle gt . In presence of the cavity dissipation, the dynamics of the flight of the atom is governed by the evolution equation (as we have seen in Eq.(3.4) in chapter 3)

$$\dot{\rho} = \dot{\rho}|_{\text{atom-field}} + \dot{\rho}|_{\text{field-reservoir}}, \quad (6.1)$$

At temperature $T \cong 0$ K, usually the case in cavity-QED experiments, the average thermal photon number can be taken to be zero. Since we are working with a two-level Rydberg atom, its lifetime is much larger compared to the atom-cavity interaction time and hence we can neglect the atomic dissipation. The first term on the r.h.s. of Eq.(6.1) evolves under the usual Jaynes-Cummings interaction, and the second term is given by (as we have seen in Eq.(3.3) in chapter 3)

$$\dot{\rho}|_{\text{field-reservoir}} = -\kappa(a^\dagger a \rho - 2a \rho a^\dagger + \rho a^\dagger a). \quad (6.2)$$

where κ is the cavity leakage constant. We consider the approximation of a two-level cavity, i.e., the probability of getting a two-or more than two-photon number state of the cavities is zero. Under the secular approximation[27] the time-evolved density matrix of the tripartite two-cavity-atom system $\rho_{C_1 C_2 A_1}$ is given in section 4.2.2. We reproduce them here for the sake of completeness in this chapter.

$$\begin{aligned} \rho(t)_{C_1 C_2 A_1} &= \alpha_1 |0_1 1_2 g_1\rangle \langle 0_1 1_2 g_1| \\ &+ \alpha_2 |1_1 0_2 g_1\rangle \langle 1_1 0_2 g_1| \\ &+ \alpha_3 |0_1 0_2 e_1\rangle \langle 0_1 0_2 e_1| \end{aligned}$$

$$\begin{aligned}
& +\alpha_4|1_10_2g_1\rangle\langle 0_10_2e_1| \\
& -\alpha_4|0_10_2e_1\rangle\langle 1_10_2g_1| \\
& +\alpha_5|0_11_2g_1\rangle\langle 1_10_2g_1| \\
& +\alpha_5|1_10_2g_1\rangle\langle 0_11_2g_1| \\
& +\alpha_6|0_10_2e_1\rangle\langle 0_11_2g_1| \\
& -\alpha_6|0_11_2g_1\rangle\langle 0_10_2e_1|,
\end{aligned} \tag{6.3}$$

where where $|0\rangle$ and $|1\rangle$ represent the 0-photon and the 1-photon number basis states of the cavities, respectively, and α_i are given by

$$\begin{aligned}
\alpha_1 &= \left(1 - \frac{e^{-\kappa_1 t}}{2}\right)e^{-2\kappa_2 t}, \\
\alpha_2 &= \cos^2 gt e^{-\kappa_1 t} \left(1 - \frac{e^{-2\kappa_2 t}}{2}\right), \\
\alpha_3 &= \sin^2 gt e^{-\kappa_1 t} \left(1 - \frac{e^{-2\kappa_2 t}}{2}\right), \\
\alpha_4 &= i \sin gt \cos gt e^{-\kappa_1 t} \left(1 - \frac{e^{-2\kappa_2 t}}{2}\right), \\
\alpha_5 &= \frac{\cos gt e^{-\frac{\kappa_1 t}{2}} e^{-\kappa_2 t}}{2}, \\
\alpha_6 &= i \left(\frac{e^{-\frac{\kappa_1 t}{2}} \sin gt}{2} - \frac{\kappa_1 e^{-\frac{\kappa_1 t}{2}} \cos gt}{4g} + \frac{\kappa_1}{4g} \right) e^{-\kappa_2 t},
\end{aligned} \tag{6.4}$$

where κ_1 and κ_2 are the leakage constants for cavity C_1 and C_2 respectively.

The reduced state of the first cavity and the atom ($\rho(t)_{C_1 A_1}$) is given by

$$\begin{aligned}
\rho(t)_{C_1 A_1} &= \text{Tr}_{C_2}(\rho_{C_1 C_2 A_1}), \\
&= \alpha_1|0_1g_1\rangle\langle 0_1g_1| + \alpha_2|1_1g_1\rangle\langle 1_1g_1| \\
&+ \alpha_3|0_1e_1\rangle\langle 0_1e_1| + \alpha_4|1_1g_1\rangle\langle 0_1e_1| \\
&- \alpha_4|0_1e_1\rangle\langle 1_1g_1|,
\end{aligned} \tag{6.5}$$

corresponding to the density matrix

$$\rho(t)_{C_1 A_1} = \begin{pmatrix} \alpha_1 & 0 & 0 & 0 \\ 0 & \alpha_3 & -\alpha_4 & 0 \\ 0 & \alpha_4 & \alpha_2 & 0 \\ 0 & 0 & 0 & 0 \end{pmatrix} \tag{6.6}$$

in the basis of $|0_1g_1\rangle, |0_1e_1\rangle, |1_1g_1\rangle,$ and $|1_1e_1\rangle$. We quantify the entanglement using the measure concurrence (defined in Eq. (1.29) of chapter 1). We compute the concurrence for $\rho(t)_{C_1A_1}$, which is given by

$$C(\rho(t)_{C_1A_1}) = \left| 2 \cos gt \sin gte^{-\kappa_1 t} \left(1 - \frac{e^{-2\kappa_2 t}}{2} \right) \right| \quad (6.7)$$

If we take $\kappa_1 = \kappa_2 = \kappa$, one gets

$$C(\rho(t)_{C_1A_1}) = 2C_{ideal}(e^{-\kappa t} - e^{-3\kappa t}/2) \quad (6.8)$$

For small κ , we can write

$$C(\rho(t)_{C_1A_1}) \approx C_{ideal}(1 + \kappa t). \quad (6.9)$$

where $C_{ideal} = |\cos gt \sin gt|$ (see Eq.(4.33) in chapter 4) is the value of the concurrence in the case of ideal cavities ($Q = \infty$) with no dissipation. It follows from Eq.(6.8) that for large κ one gets $C(\rho(t)_{C_1A_1}) \rightarrow 0$, as expected. However, for small values of κ , one sees from Eq.(6.9) that the concurrence can be increased by increasing κ . This feature of dissipation assisted increase of entanglement is observed for a range of values of κ , and the maximum of concurrence given by Eq.(6.8) is obtained for fixed gt from the condition

$$\frac{dC}{d(\kappa/g)} = 0. \quad (6.10)$$

So the entanglement for a particular interaction time (or Rabi angle) can be maximized by choosing the value of the cavity dissipation corresponding to

$$\text{or } \frac{\kappa}{g} = \frac{1}{2gt} \ln(3/2). \quad (6.11)$$

It is interesting to note that the entanglement between the two cavities C_1 and C_2 falls off with increasing κ , thus providing a manifestation of the monogamous nature of entanglement [34] between the pairs C_1A_1 and C_1C_2 . These aspects of bipartite entanglement in a three party system have been displayed in Figures 4.5-4.7 in chapter 4. The increase of atom-cavity entanglement with κ as seen in Eq.(6.9) follows from the collective nature of the dynamics of the two cavities, as is apparent from the structure of the elements of the atom-cavity state given in Eqs.(6.4) where the α_i 's are the sums of two terms involving κ_1 and κ_2 respectively. This motivates us to look for similar collective effects in other simple tripartite systems such as the one involving the interaction of a single cavity with two successive atoms, considered below.

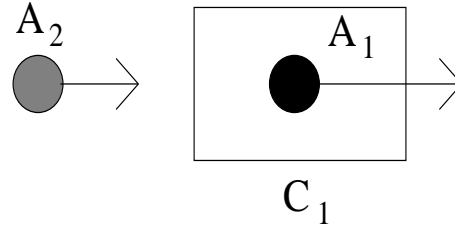


Figure 6.2: Two two-level atoms, the first prepared in the excited state and the second prepared in the ground state, traverse an empty cavity one after the other (same as Figure 2.9).

6.2.2 A single cavity and two two-level atoms

We now investigate a system where two two-level atoms A_1 and A_2 , the first prepared in the excited state $|e\rangle$, and the second prepared in the ground state $|g\rangle$, are sent into a vacuum cavity one after the other, i.e., there is no spatial overlap between the two atoms (see Figure 6.2). We have used this system to show the atom-atom entanglement in chapter 2. Our purpose here is to demonstrate analytically the increase of two-atom entanglement in this model with the increase of cavity damping rate. We compute the time-evolved density state for the tripartite system of the two atoms and the cavity under the same secular approximation, and the approximation of a two level (zero or one photon) cavity, given in section 4.3.2. We reproduce them here for the sake of completeness in this chapter.

$$\begin{aligned}
\rho(t)_{A_1 A_2 C_1} &= \gamma_1 |e_1 g_2 0_1\rangle \langle e_1 g_2 0_1| \\
&+ \gamma_2 |g_1 g_2 1_1\rangle \langle g_1 g_2 1_1| \\
&+ \gamma_3 |g_1 e_2 0_1\rangle \langle g_1 e_2 0_1| \\
&- \gamma_4 |e_1 g_2 0_1\rangle \langle g_1 e_2 0_1| \\
&- \gamma_4 |g_1 e_2 0_1\rangle \langle e_1 g_2 0_1| \\
&+ \gamma_5 |g_1 e_2 0_1\rangle \langle g_1 g_2 1_1| \\
&- \gamma_5 |g_1 g_2 1_1\rangle \langle g_1 e_2 0_1| \\
&+ \gamma_6 |g_1 g_2 1_1\rangle \langle e_1 g_2 0_1| \\
&- \gamma_6 |e_1 g_2 0_1\rangle \langle g_1 g_2 1_1|,
\end{aligned} \tag{6.12}$$

where γ_i are given by

$$\begin{aligned}
\gamma_1 &= (1 - \sin^2 gte^{-\kappa t}), \\
\gamma_2 &= \cos^2 gt \sin^2 gte^{-2\kappa t}, \\
\gamma_3 &= \sin^4 gte^{-2\kappa t}, \\
\gamma_4 &= \left(\sin gte^{-\kappa t/2} - \frac{\kappa}{2g} \cos gte^{-\kappa t/2} + \frac{\kappa}{2g} \right) \cos gt \sin gte^{-\kappa t}, \\
\gamma_5 &= i \sin^3 gt \cos gte^{-2\kappa t} \\
\gamma_6 &= i \cos^2 gt \sin gte^{-3\kappa t/2}.
\end{aligned} \tag{6.13}$$

The reduced density state of the pair of atoms A_1A_2 is given by

$$\begin{aligned}
\rho(t)_{A_1A_2} &= \text{Tr}_{C_1}(\rho_{A_1A_2C_1}) \\
&= \gamma_1 |e_1g_2\rangle\langle e_1g_2| \\
&\quad + \gamma_2 |g_1g_2\rangle\langle g_1g_2| \\
&\quad + \gamma_3 |g_1e_2\rangle\langle g_1e_2| \\
&\quad - \gamma_4 |e_1g_2\rangle\langle g_1e_2| \\
&\quad - \gamma_4 |g_1e_2\rangle\langle e_1g_2|,
\end{aligned} \tag{6.14}$$

with the corresponding density matrix

$$\rho(t)_{A_1A_2} = \text{Tr}_{C_1}(\rho_{A_1A_2C_1}) = \begin{pmatrix} \gamma_2 & 0 & 0 & 0 \\ 0 & \gamma_3 & -\gamma_4 & 0 \\ 0 & -\gamma_4 & \gamma_1 & 0 \\ 0 & 0 & 0 & 0 \end{pmatrix} \tag{6.15}$$

in the basis of $|g_1g_2\rangle$, $|g_1e_2\rangle$, $|e_1g_2\rangle$, and $|e_1e_2\rangle$ states.

The concurrence for the joint two-atom state $\rho(t)_{A_1A_2}$ is given by (see, also, Eq.(2.88))

$$C(\rho(t)_{A_1A_2}) = |2 \sin^2 gte^{-\kappa t} \sqrt{(1 - \sin^2 gte^{-\kappa t})}| \tag{6.16}$$

For values of κ/g and gt such that $(\tan^2 gt)(gt)(\kappa/g) \ll 1$, we can write

$$C(\rho(t)_{A_1A_2}) \approx C_{ideal} \left(1 + \frac{1}{2} \kappa t \tan^2 gt - \kappa t \right), \tag{6.17}$$

where C_{ideal} (no dissipation) in this case is given by $C_{ideal} = |2 \cos gt \sin^2 gt|$ (see Eq.(2.85) in chapter 2). Thus, enhancement of $C(\rho(t)_{A_1A_2})$, i.e., the increase of the atom-atom

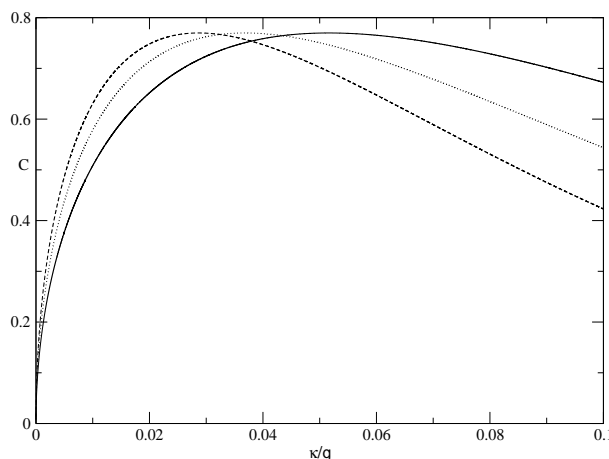


Figure 6.3: The two-atom concurrence $C_{A_1A_2}$ is plotted versus the κ/g for the atom-field interaction time (i) $gt = 5\pi/2$ (solid line) (ii) $gt = 7\pi/2$ (dotted line) (iii) $gt = 9\pi/2$ (dashed line).

mixed-state entanglement over its value in the ideal cavity case is possible if we choose the interaction time judiciously, such that $\tan(gt) > \sqrt{2}$. For fixed gt , the concurrence $C(\rho(t)_{A_1A_2})$ can be maximized with respect to κ/g . The maximum of concurrence is obtained at fixed gt from the condition $\frac{dC}{d(\kappa/g)} = 0$, which using Eq.(6.16) leads to

$$\kappa/g = [\ln((3/2) \sin^2 gt)]/(gt). \quad (6.18)$$

From the above expression one can see that the atom-atom entanglement maximises, for example, at $\kappa/g = 0.051$, 0.036 and 0.028 for atom-field interaction time $gt = 5\pi/2$, $7\pi/2$, and $9\pi/2$, respectively, as shown in Figure 6.3. It may be recalled from sections 4.2.1 and 4.2.2 that the entanglement oscillates as a function of gt and here we show that the reservoir of the cavity photons aids in the entanglement up to a certain value of cavity dissipation, given a particular interaction time. Further increase of cavity damping κ , causes the two-atom entanglement to fall off.

6.3 The one-atom micromaser

We now consider the real micromaser which has been experimentally operational [31, 32]. The mathematical model for the micromaser has been discussed in chapter 3. We have also

Table 6.1: Steady state photon statistics for the micromaser with the parameter values $n_{th} = 0.033$, $N = 1$, and $gt = 3\pi/4$.

κ/g	P_0	P_1	P_2	$\langle n \rangle$
0.1	0.771	0.220	0.007	0.236
0.01	0.664	0.316	0.014	0.359
0.005	0.655	0.324	0.015	0.370
0.0000807	0.645	0.332	0.016	0.382

described the dissipative dynamics of the micromaser there. Further we showed there how the entanglement is generated between two spatially separated atoms via the steady-state micromaser field. We display the steady state photon statistics $P_n^{ss} = \langle n | \rho_f^{ss} | n \rangle$ (Eq.(3.15) in chapter 3) for experimentally realizable values[31, 32] of the parameters N ($N = R/2\kappa$, where R denotes the number of atoms passing through the cavity per second), n_{th} and gt in Table 1. The probability of getting two (P_2) or more photons inside the cavity is negligible. The photon statistics thus provides a justification for our earlier assumption of a two-level cavity (P_0 and P_1) used for obtaining our analytical results of entanglement enhancement in the presence of dissipation in the previous examples. However, our present analysis for the real micromaser does not employ this assumption.

We compute the atomic entanglement generated between two experimental atoms that pass successively through the micromaser cavity. The tripartite joint state of the cavity and the two atoms is obtained by summing over all n . The reduced density state of the two atoms after passing through the the cavity field is given by after tracing over the field (we display the non-vanishing terms only)

$$\begin{aligned}
\rho(t)_{A_1 A_2} &= \text{tr}_f(\rho(t)_{A_1 A_2 f}) \\
&= \beta_1 |e_1 e_2\rangle \langle e_1 e_2| + \beta_2 |e_1 g_2\rangle \langle e_1 g_2| \\
&\quad + \beta_3 |g_1 e_2\rangle \langle g_1 e_2| + \beta_4 |e_1 g_2\rangle \langle g_1 e_2| \\
&\quad + \beta_4 |g_1 e_2\rangle \langle e_1 g_2| + \beta_5 |g_1 g_2\rangle \langle g_1 g_2|,
\end{aligned} \tag{6.19}$$

where the β_i are given by

$$\beta_1 = \sum_n P_n^{ss} \cos^4(\sqrt{n+1}gt),$$

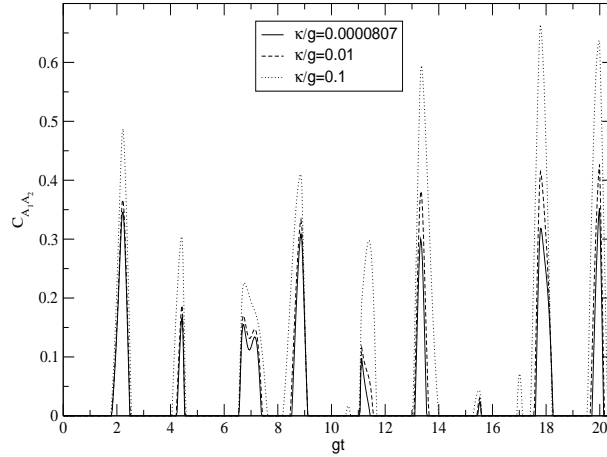


Figure 6.4: The two-atom concurrence $C_{A_1 A_2}$ is plotted versus the Rabi angle gt for various values of the cavity leakage parameter κ . Here we choose $N = 1$ and $\bar{n}_{th} = 0.033$

$$\begin{aligned}
 \beta_2 &= \sum_n P_n^{ss} \cos^2(\sqrt{n+1}gt) \sin^2(\sqrt{n+1}gt), \\
 \beta_3 &= \sum_n P_n^{ss} \cos^2(\sqrt{n+2}gt) \sin^2(\sqrt{n+1}gt), \\
 \beta_4 &= \sum_n P_n^{ss} \sin^2(\sqrt{n+1}gt) \cos(\sqrt{n+1}gt) \cos(\sqrt{n+2}gt), \\
 \beta_5 &= \sum_n P_n^{ss} \sin^2(\sqrt{n+1}gt) \sin^2(\sqrt{n+2}gt).
 \end{aligned} \tag{6.20}$$

The corresponding reduced density matrix is obtained to be

$$\rho(t)_{A_1 A_2} = \begin{pmatrix} \beta_5 & 0 & 0 & 0 \\ 0 & \beta_3 & \beta_4 & 0 \\ 0 & \beta_4 & \beta_2 & 0 \\ 0 & 0 & 0 & \beta_1 \end{pmatrix} \tag{6.21}$$

in the basis of $|g_1 g_2\rangle$, $|g_1 e_2\rangle$, $|e_1 g_2\rangle$ and $|e_1 e_2\rangle$ states.

The concurrence of the two-atom state is plotted with respect to the Rabi angle gt in Fig. 6.4 choosing the cavity temperature as in the operational micromaser[31]. We see that the entanglement between the two atoms increases as we increase the cavity dissipation parameter κ/g from the experimental values (solid curves in Fig. 6.4) at a fixed values of the Rabi angle gt . Increased damping of the micromaser cavity causes the average cavity photon number $\langle n \rangle$ to go down, as displayed in Table 1. The collective dynamics of the system causes the magnitude of two-atom entanglement to rise with

decreasing $\langle n \rangle$. This anti-correlation of the two-atom entanglement with the cavity photon number $\langle n \rangle$ has also been observed in chapter 5 (see Figures 5.3, 5.5 and 5.9). It is expected that further increase of κ/g beyond the values shown in the figure would make the concurrence to fall. However, the validity of the micromaser theory that we have used [33] is itself limited to low dissipation values.

6.4 Summary

In this chapter we have presented concrete examples of the increase of entanglement caused by an interaction of a part of a composite system with its environment. We have first considered the atom-cavity entanglement in a system comprised of two entangled cavities and a two-level atom [70]. The derived expression for the atom-cavity concurrence clearly shows the maximization of entanglement for intermediate values of the cavity damping. A similar analytical result is also obtained for two-atom entanglement in the case of a micromaser-type system involving a single cavity and two atoms. It is important to note that the environment cannot help to increase the entanglement for every kind of systems. For example, it can be verified for a system in which two two-level atoms pass respectively through two maximally entangled cavities (see section 4.4 in chapter 4), that cavity dissipation does not help to enhance the atomic entanglement.

We have finally again considered a model for the real micromaser [31, 32] and demonstrated the increase of atomic entanglement with cavity damping for fixed atom-cavity interaction times for experimentally operational values of the micromaser parameters. With further development, it may be possible to utilize this effect of environment assisted entanglement enhancement in information processing involving multipartite systems where the interactions times may not be easily controllable. In conclusion, we highlight that atom-cavity systems provide much scope for the quantitative tests of several manifestations of environment induced entanglement [10, 12, 37, 41] in experimentally realizable situations.

Chapter 7

Conclusions

Quantum entanglement has been widely observed within the framework of quantum optical systems such as in cavity quantum electrodynamics. Many beautiful experiments have been carried out in recent years and several types of entangled states have been created. The preparation and manipulation of these entangled states that have nonclassical and nonlocal properties leads to a better understanding of basic quantum phenomena. For example, complex entangled states, such as the Greenberger, Horne, and Zeilinger triplets of particles [87] are used for tests of quantum nonlocality [88]. Practical realization of various features of quantum entanglement are obtained in atom-photon interactions in optical and microwave cavities[6]. An example that could be highlighted is the generation of a maximally entangled state between two modes in a single cavity using a Rydberg atom coherently interacting with each mode in turn[72].

For practical implementation of quantum information protocols useful in communication and computation[4], entanglement has to be created and preserved between qubits that are well separated. A recent experimental breakthrough has been obtained by entangling two distant atomic qubits by their interaction with the same photon[89]. From the viewpoint of information processing, quantification of entanglement is an important aspect, and recently some studies have been performed to quantify the entanglement that is obtained in atom-photon interactions in cavities[7, 8, 9, 10]. In addition to pedagogical aspects, entanglement has become a fundamental resource in quantum information processing[68] and there has been rapid development of this subject in recent years[4].

In this thesis we have studied the generation of various types of entanglement via direct

or indirect atom-photon interactions. We have investigated the characteristic properties of entanglement in cavity-QED systems under dissipative dynamics. To quantify the generated entanglement we have used the well-known measures of the concurrence or the entanglement of formation [22, 23]. They are monotones of each other and are good entanglement measures for bipartite mixed states in $2 \otimes 2$ Hilbert space dimension. A basic tool in quantum optics to generate various types of entanglement is the Jaynes-Cummings model [26] which we have discussed in chapter 2. A two-level atom and a single mode cavity field get entangled under the Jaynes-Cummings interaction as a rule and we can quantify this entanglement. We have shown how atom-cavity, atom-atom, and cavity-cavity entanglements can be generated in atom-photon interactions, in the presence of cavity dissipation.

The generation of quantum entanglement between two spatially separated atoms can be achieved by a practical device, the one-atom micromaser [29, 30] which we have discussed in chapter 3. The micromaser is an experimentally operational [31] real physical device where abstract quantum information theoretic concepts can be revealed in the presence of dissipative interactions. The micromaser cavity field is maintained in a steady state by streaming of two-level Rydberg atoms passing one at a time through it. We have shown [9] that it is possible to monitor the robust entanglement generated between two successive experimental atoms passing through the micromaser by the control decoherence parameters. We computed the entanglement of formation (E_F) as a function of the micromaser pump rate D for different values of the mean thermal photon number \bar{n}_{th} keeping the cavity dissipation parameter κ/g fixed. We have shown that E_F decreases with increasing \bar{n}_{th} . Quantum information transfer can be studied in a quantitative manner using the micromaser. To see how information from the micromaser cavity field is transported to construct the entangled atomic states, we have computed the Shannon entropies of micromaser field before and after the passage of the two experimental atoms. This difference exhibits some correspondence with the magnitude of atomic entanglement for certain values of the Rabi angle. An important new direction that has emerged from our analysis is the possibility to formulate experimental proposals to test several theoretical concepts of quantum channel capacity [21], using the micromaser.

Entanglement is endowed with certain curious features. Unlike classical correlations,

quantum entanglement cannot be freely shared among many quantum systems. It has been observed that a quantum system being entangled with another one limits its possible entanglement with a third system. This behaviour of entanglement is known as “monogamous nature of entanglement” [36]. We have shown [35] in chapter 4 this “monogamous nature of entanglement” quantitatively in the ideal case and also in the presence of cavity dissipation for two tripartite systems. Another distinctive property of quantum entanglement for multipartite systems is the possibility of entanglement swapping [67] between two or more pairs of qubits. Entanglement swapping is observed between the two-cavity and the two-atom system in our study. Cavity dissipation leads to the quantitative reduction of information transfer, though preserving the basic swapping property [35]. Further studies regarding different quantitative manifestations of information transfer in the presence of dissipative effects might be useful for the construction of realistic devices to implement various communication protocols.

The role of the cavity field in mediating atomic entanglement cannot be overemphasized. The nature and properties of the radiation field have a crucial bearing on the magnitude of the generated atomic entanglement. In chapter 5 we have presented a detailed investigation of the effects of cavity field statistics on atomic entanglement by considering the cases of three different types of radiation fields, i.e., the Fock state field, the thermal field, and the coherent state field respectively. We have shown [12] how the statistics of the various fields are reflected on the atomic entanglement produced when two atoms pass through the cavity one after another. A comparative study of the two-atom entanglement has been presented for the low and the high mean photon number cases corresponding to the different field statistics. Several interesting analogies, and certain notable differences too, have been found with the results obtained in similar investigations performed by using the Tavis-Cummings model [76] of atom-photon interactions. The relationship of squeezing with entanglement is by itself a rather interesting direction of study [79]. In chapter 5, we further investigate the consequences of squeezing of the cavity radiation field on the atomic entanglement mediated via it. We show [13] that in certain cases the magnitude of entanglement can be increased by increasing the value of squeezing parameter. Our approach has opened up prospects for further investigations in this direction such as on the connection of squeezing with other features of entanglement

like its monogamous nature.

The effects of dissipation in reducing the magnitude of entanglement has been discussed throughout the thesis. However, some interesting examples have been found recently [10, 37, 39, 41] where it was shown how entanglement can be generated from the reservoir itself under certain conditions. This formed the motivation for our study in chapter 6 where we have discussed some new examples in atom-cavity interactions [42] in which entanglement is not only created out of the cavity reservoir, but is shown to increase with increase of the cavity damping rate. The role of the collective dynamics of the photon modes interacting with the atomic levels towards assisting atomic entanglement up to certain intermediate values of the cavity dissipation parameter has been highlighted for the first time in these examples. Here we also demonstrate [42] how such an example of environment induced entanglement could be experimentally verified using the micromaser with operational values of the micromaser parameters. The study of more such examples could be of much practical importance in quantum information processing and computing devices.

Finally, we would like to reemphasize that the quantitative study of entanglement produced in various types of atom-photon interactions is a very relevant arena for investigations. Atom-photon interactions and the generation of entanglement mediated through them are expected to play an important role in possible future practical realizations in the field of quantum communications[89, 90]. Recently, the possibility of entanglement of a thermal radiation field with high temperature phonons associated with moving mirrors of a cavity has been shown[91], brightening the prospects for creating macroscopic entanglement. Even from a purely pedagogical perspective, investigations of quantitative entanglement in atom-photon interactions could lead to interesting insights on the curious properties of entanglement such as its ‘monogamous’ nature. Further interesting directions could be to investigate the possibility of generating maximally entangled mixed atomic qubits[92] using squeezing of the bosonic field as a resource.

Appendix 1 : Derivation of master equation

We derive the so-called master equation governing the damping of the cavity mode field or its interaction with its reservoir [46, 47]. We represent the reservoir by an infinite number of modes of the radiation field of frequency ω_i , with annihilation and creation operators b_i and b_i^\dagger respectively. They satisfy the commutation relation

$$[b_i, b_j^\dagger] = \delta_{ij}. \quad (A_1)$$

The interaction Hamiltonian of the cavity mode of frequency ω_c , represented by the annihilation (creation) operators a (a^\dagger), with the reservoir can be written as

$$H_{int} = \sum_i g(\omega_i)(a + a^\dagger)(b_i + b_i^\dagger) \quad (A_2)$$

where $g(\omega_i)$ is the coupling constant between the cavity mode and the reservoir mode ω_i . The density operator ρ_{C-R} of the composite cavity-reservoir system obeys the equation of motion, in the interaction picture,

$$i\hbar\dot{\rho}_{C-R} = [H_{int}, \rho_{C-R}]. \quad (A_3)$$

Formally integrating Eq.(A₃) with respect to time, we have

$$\rho_{C-R}(t) = \rho_{C-R}(t=0) + \frac{1}{i\hbar} \int_0^t dt' [H_{int}(t'), \rho_{C-R}(t')]. \quad (A_4)$$

This integral equation can be solved by successive substitution in the form of an absolutely and uniformly convergent series. Substitution of Eq.(A₄) in the right hand side of Eq.(A₂) gives

$$i\hbar\frac{\partial}{\partial t}\rho_{C-R}(t) = [H_{int}, \rho_{C-R}(t=0)] + \frac{1}{i\hbar} \int_0^t dt' [H_{int}(t), [H_{int}(t'), \rho_{C-R}(t')]]. \quad (A_5)$$

We can continue the same substitution procedure and obtain an infinite series of integral terms which can be regarded an exact solution for $\rho_{C-R}(t)$. We however, confine ourselves to the second order as the coupling constants g_i are weak. (In fact, going beyond the second order means taking into account the back reactions in the cavity-reservoir systems.) This is known as the Born approximation in the literature. In this approximation, the

reduced density operators for the cavity mode and the reservoir donot change appreciably. Hence, we can write

$$\rho_{C-R}(t') = \rho_C(t')\rho_R(0) \quad (A_6)$$

where ρ_C and ρ_R are the reduced density operators for the cavity and reservoir respectively. Also at $t = 0$, we have

$$\rho_{C-R}(0) = \rho_C(0)\rho_R(0). \quad (A_7)$$

Since the reservoir is in thermal equilibrium, we can write

$$\langle b_i \rangle = \langle b_i^\dagger \rangle = 0 \quad (A_8)$$

$$\langle b_i^\dagger b_j \rangle = \bar{n}_{th} \delta_{ij}. \quad (A_9)$$

We substitute Eqs.(A₆ – A₉) in Eq.(A₅), and in order to solve the integral on its RHS, we change the time variable to $\tau = t - t'$. The resulting integro-differential equation describes the time evolution of $\rho_C(t)$ which depends on its past value, that is, $\rho_C(t - \tau)$. The cavity-QED at microwave frequencies that we deal in the thesis, involves the cavity parameter which varies in $\sim 10^{-5}$ seconds. But the exponents in the integrals that are involved vary in 10^{-12} seconds, which is much shorter compared to the time scale at which ρ_C changes appreciably. Hence, we can safely take $\rho_C \cong \rho_C(t - \tau)$ which is known as the Markov approximation in the literature. This eliminates the integrals on the RHS in Eq.(A₅) giving us finally,

$$i\hbar \frac{\partial \rho_C}{\partial t} = -\kappa(\bar{n}_{th} + 1)(a^\dagger a \rho - 2a \rho a^\dagger + \rho a^\dagger a) - \kappa \bar{n}_{th}(a a^\dagger \rho - 2a^\dagger \rho a + \rho a a^\dagger) \quad (A_{10})$$

where $\kappa = 2\pi |g(\omega_c)|^2 f(\omega_c)$ with $f(\omega_c)$ being the mode distribution function of the densely occupied infinite modes of the reservoir. The thermal photons \bar{n}_{th} is related to the reservoir (cavity) temperature by the relation

$$\bar{n}_{th} = \frac{1}{e^{\frac{\hbar\omega_c}{k\beta T}} - 1}. \quad (A_{11})$$

For a cavity in vacuum, $\bar{n}_{th} = 0$, Eq.(A₁₀) reduces to

$$i\hbar \frac{\partial \rho_C}{\partial t} = -\kappa(a^\dagger a \rho - 2a \rho a^\dagger + \rho a^\dagger a) \quad (A_{12})$$

which is Eq.(2.31) and elsewhere in the thesis.

Bibliography

- [1] A. Einstein, B. Podolsky and N. Rosen, Phys. Rev. **47**, 777 (1935).
- [2] J. S. Bell, Physics **1**, 195 (1964). A text book presentation is given by L. E. Ballentine, *Quantum Mechanics*, (World Scientific, 2002).
- [3] E. Schrödinger, Proc. Camb. Phil. Soc. **31**, 555 (1935).
- [4] M. A. Nielsen and I. L. Chuang, *Quantum Computation and Information* (Cambridge University Press, Cambridge, England, 2000).
- [5] C. H. Bennett, and P. W. Shor, IEEE Trans. Inform. Theory **44**, 2724 (1998).
- [6] J. M. Raimond, M. Brune, and S. Haroche, Rev. Mod. Phys. **73**, 565 (2001).
- [7] T. Tessier, A. Delgado, I. Fuentes-Guridi, and I. H. Deutsch, Phys. Rev. A **68**, 062316 (2003).
- [8] P. Masiak, Phys. Rev. A **66**, 023804 (2002).
- [9] A. Datta, B. Ghosh, A. S. Majumdar and N. Nayak, Europhys. Lett. **67**, 934 (2004).
- [10] M. S. Kim, Jinhyoung Lee, D. Ahn and P. L. Knight, Phys. Rev. A **65**, 040101(R) (2002).
- [11] L. Zhou, H. S. Song and C. Li, J. Opt. B: Quantum Semiclass. Opt. **4**, 425 (2002).
- [12] B. Ghosh, A. S. Majumdar and N. Nayak, Int. J. Quant. Inf. **5**, 169 (2007).
- [13] B. Ghosh, A. S. Majumdar and N. Nayak, quant-ph/0605191 (to appear in Int. J. Theo. Phys., Group Theo., and Nonl. Opt. **12**, Issue 2 (2007)).

- [14] A. Peres, Phys. Rev. Lett. **77**, 1413 (1996).
- [15] M. Horodecki, P. Horodecki, and R. Horodecki, Phys. Rev. Lett. **80**, 5239 (1998).
- [16] J. F. Clauser, M. A. Horne, A. Shimony and R. A. Holt, Phys. Rev. Lett. **23**, 880 (1969).
- [17] N. Gisin, Phys. Lett. A **154**, 201 (1991).
- [18] R. F. Werner, Phys. Rev. A **40**, 4277 (1989).
- [19] A. Aspect, P. Grangier, and G. Roger, Phys. Rev. Lett. **49**, 91 (1982).
- [20] A. S. Majumdar and N. Nayak, Phys. Rev A **64**, 013821 (2001).
- [21] M. Keyl, Phys. Rep. **369**, 431 (2002).
- [22] S. Hill and W. K. Wootters, Phys. Rev. Lett. **78**, 5022, (1997).
- [23] W. K. Wootters, Phys. Rev. Lett. **80**, 2245 (1998).
- [24] W. K. Wootters, Quantum Inf. Comput. **1**, 2744, (2001).
- [25] G. Vidal, J. Mod. Opt. **47**, 355, (2000).
- [26] E. T. Jaynes, F. W. Cummings, Proc. IEEE **51**, 89 (1963).
- [27] S. Haroche and J. M. Raimond, in “*Advances in atomic and molecular physics*”, Vol. 20, eds. D. R. Bates and B. Bederson (Academic, New York, 1985).
- [28] L. Allen and J. H. Eberly, *Optical Resonance and Two-level Atoms* (Dover Publications, 1987).
- [29] D. Meschede, H. Walther and G. Muller, Phys. Rev. Lett. **54**, 551, (1985).
- [30] Filipowicz, J. Javanainen and P. Meystre, Phys. Rev. A **34**, 3077, (1986).
- [31] G. Rempe, F. Schmidt-Kaler and H. Walther, Phys. Rev. Lett. **64**, 2783, (1990).

- [32] M. Brune, E. Hagley, J. Dreyer, X. Matre, A. Maali, C. Wunderlich, J. M. Raimond, and S. Haroche, Phys. Rev. Lett. **77**, 4887 (1996); M. Weidinger, B. T. H. Varcoe, R. Heerlein, and H. Walther, Phys. Rev. Lett. **82**, 3795 (1999).
- [33] N. Nayak, Opt. Commun. **118** 114 (1995).
- [34] Bennett C. H., Lecture course in the School on Quantum Physics and Information Processing, TIFR, Mumbai, 2002 (<http://qip-server.tcs.tifr.res.in/qpip/HTML/Courses/Bennett/TIFR2.pdf>).
- [35] B. Ghosh, A. S. Majumdar, and N. Nayak, Int. J. Quant. Inf. **4**, 665 (2006).
- [36] V. Coffman, J. Kundu and W. K. Wootters, Phys. Rev. A **61**, 052306 (2000).
- [37] M. B. Plenio, S. F. Huelga, A. Beige, and P. L. Knight, Phys. Rev. A **59**, 2468 (1999).
- [38] S. Schneider and G. J. Milburn, Phys. Rev. A **65**, 042107 (2002); B. Kraus and J. I. Cirac, Phys. Rev. Lett. **92**, 013602 (2004); S.-B. Li and J.-B. Xu, quant-ph/0505216.
- [39] M. B. Plenio and S. F. Hulega, Phys. Rev. Lett. **88**, 197901 (2002).
- [40] A. Beige, D. Braun, B. Tregenna and P. L. Knight, Phys. Rev. Lett. **85**, 1762 (2000).
- [41] D. Braun, Phys. Rev. Lett. **89**, 277901 (2002).
- [42] B. Ghosh, A. S. Majumdar, and N. Nayak, Phys. Rev. A **74**, 052315 (2006).
- [43] S. J. D. Phoenix and P. L. Knight Phys. Rev. A **44**, 6023 (1991).
- [44] S. Furuichi, and M. Ohya, Lett. Math. Phys. **49**, 279 (1999).
- [45] S. Bose, I. Fuentes-Gurudi, P. L. Knight, and V. Vedral, Phys. Rev. Lett. **87**, 050401 (2001).
- [46] See, for instance, W. H. Louisell, *Quantum Statistical Properties of Radiation* (Wiley, New York, 1973).
- [47] G. S. Agarwal, in *Springer Tracts in Modern Physics*, Vol.70, (Springer-Verlag, Berlin & New York, 1974).

- [48] C. Cabrillo, J. I. Cirac, P. G-Fernandez and P. Zoller, Phys. Rev. A **59**, 1025 (1999); S. Bose, P. L. Knight, M. B. Plenio and V. Vedral, Phys. Rev. Lett. **83**, 5158 (1999); M. B. Plenio, S. F. Huelga, A. Beige and P. L. Knight, Phys. Rev. A **59**, 2468 (1999); J. Hong and H. W. Lee, Phys. Rev. Lett. **89**, 237901, 2002; L. M. Duan, H. J. Kimble, Phys. Rev. Lett. **90**, 253601, (2003).
- [49] L. M. Duan, M. D. Lukin, J. I. Cirac and P. Zoller, Nature **414**, 413 (2001); L. M. Duan, Phys. Rev. Lett. **88**, 170402 (2002).
- [50] E. Solano, G. S. Agarwal and H. Walther, Phys. Rev. Lett. **90**, 027903 (2003); P. Lougovsky, F. Casagrande, A. Lulli, B.-G. Englert, E. Solano and H. Walther, Phys. Rev. A **69**, 023812 (2004).
- [51] B. Tregenna, A. Beige and P. L. Knight, Phys. Rev. A **65**, 032305 (2002); A. S. Sorensen and K. Molmer, Phys. Rev. A **66**, 022314 (2002), A. S. Sorensen and K. Molmer, Phys. Rev. Lett. **91**, 097905 (2003); C. Marr, A. Beige and G. Rempe, Phys. Rev. A **68**, 033817 (2003); S. Clark, A. Peng, M. Gu, S. Parkins, Phys. Rev. Lett. **91**, 177901 (2003).
- [52] S. J. D. Phoenix and S. M. Barnett, J. Mod. Opt. **40**, 979 (1993); J. I. Cirac and P. Zoller, Phys. Rev. A **50**, R2799 (1994).
- [53] E. Hagley, X. Maitre, G. Nogues, C. Wunderlich, M. Brune, J. M. Raimond, and S. Haroche, Phys. Rev. Lett. **79**, 1 (1997); M. Loffler, B. G. Englert and H. Walther, Appl. Phys. B **63**, 511 (1996); S. B. Zheng and G. C. Guo, Phys. Rev. Lett. **85**, 2392 (2000).
- [54] N. Nayak and D. Das, Phys. Rev. A **48**, 2475, (1993).
- [55] B. G. Englert, P. Lougovski, E. Solano, H. Walther, Laser Phys. **13**, 355 (2003).
- [56] C. E. Shannon, Bell System Technical Journal, **27**, 379 (1948).
- [57] R. Horodecki, P. Horodecki and M. Horodecki, Phys. Lett. A **200**, 340 (1995).
- [58] T. J. Osborne and F. Verstraete, Phys. Rev. Lett. **96**, 220503 (2006).

- [59] V. Buzek, V. Vedral, M. B. Plenio, P. L. Knight and M. Hillery, *Phys. Rev. A* **55**, 3327 (1997).
- [60] D. Bruß, *Phys. Rev. A* **60**, 4344 (1999).
- [61] W. Dür, G. Vidal and J. I. Cirac, *Phys. Rev. A* **62**, 062314 (2000).
- [62] M. Koashi, V. Buzk and N. Imoto, *Phys. Rev. A* **62**, 050302 (2000).
- [63] K. A. Dennison and W. K. Wootters, *Phys. Rev. A* **65**, 010301R (2001).
- [64] B. M. Terhal, quant-ph/0307120.
- [65] M. Koashi and A. Winter, *Phys. Rev. A* **69**, 022309 (2004).
- [66] E. S. Guerra and C. R. Carvalho, *J. Mod. Opt.* **53**, 865 (2006).
- [67] J. W. Pan, D. Bouwmeester, H. Weinfurter, and A. Zeilinger, *Phys. Rev. Lett.* **80**, 3891 (1998).
- [68] C. H. Bennett, G. Brassard, C. Crpeau, R. Jozsa, A. Peres, and W. K. Wootters, *Phys. Rev. Lett.* **70**, 1895 (1993); M. Zukowski, A. Zeilinger, M. A. Horne and A. K. Ekert, *Phys. Rev. Lett.* **71**, 4287 (1993).
- [69] B. Yurke and D. Stoler, *Phys. Rev. Lett.* **68**, 1251 (1992).
- [70] L. Davidovich, N. Zagury, M. Brune, J.M. Raimond, and S. Haroche, *Phys. Rev. A* **50**, R895 (1994).
- [71] V. Giovannetti, D. Vitali, P. Tombesi, and A. Ekert, *Phys. Rev. A* **62**, 032306 (2000).
- [72] A. Rauschenbeutel, P. Bertet, S. Osnaghi, G. Nogues, M. Brune, J. M. Raimond and S. Haroche, *Phys. Rev. A* **64**, 050301 (2001).
- [73] K. Hammerer, K. Molmer, E. S. Polzik and J. I. Cirac, *Phys. Rev. A* **70**, 044304 (2004); K. Hammerer, E. S. Polzik and J. I. Cirac, *Phys. Rev. A* **72**, 052313 (2005); D. N. Matsukevich, T. Chanelire, S. D. Jenkins, S.-Y. Lan, T. A. B. Kennedy, and A. Kuzmich, *Phys. Rev. Lett.* **96**, 030405 (2006).

- [74] P. Masiak, Phys. Rev. A **66**, 023804 (2002); A. Biswas and G. S. Agarwal, Phys. Rev. A **69**, 062306 (2004); P. K. Pathak and G. S. Agarwal, Phys. Rev. A **70**, 043807 (2004).
- [75] N. Nayak, A. S. Majumdar and V. Bartzis, Nonlinear Optics **24**, 319 (2000).
- [76] M. Tavis and F. W. Cummings, Phys. Rev. **170**, 379 (1968).
- [77] E. Schrödinger, Naturwiss. **14**, 664 (1926); R. J. Glauber Phys. Rev. Lett. **10** 84 (1963); E. C. G. Sudarshan, Phys. Rev. Lett. **10** 277 (1963).
- [78] D. F. Walls, Nature **306**, 141 (1983).
- [79] F.-li Li, X.-shen Li, D. Lin and T. F. George, Phys. Rev. A **40**, 5129 (1999); Phys. Rev. A **45**, 3133 (1992).
- [80] L.-M. Duan, A. Sorensen, J. I. Cirac and P. Zoller, Phys. Rev. Lett. **85**, 3991 (2000); A. Sorensen, L.-M. Duan, J. I. Cirac and P. Zoller, Nature **409**, 63 (2001); X. Wang and B. C. Sanders, Phys. Rev. A **68**, 012101 (2003); J. Korbicz, J. I. Cirac and M. Lewenstein, Phys. Rev. Lett. **95**, 120502 (2005).
- [81] G. Giedke, M. M. Wolf, O. Krüger, R. F. Werner, and J. I. Cirac, Phys. Rev. Lett. **91**, 107901 (2003); J. Eisert, D. E. Browne, S. Scheel, and M. B. Plenio, Annals of Physics (NY) **311**, 431 (2004); J. Eisert, M. B. Plenio, S. Bose and J. Hartley, Phys. Rev. Lett. **93**, 190402 (2004).
- [82] W. Son, M. S. Kim, J. Lee and D. Ahn, J. Mod. Opt. **49**, 1739 (2002); S. G. Clark and A. S. Parkins, Phys. Rev. Lett. **90**, 047905 (2003); M. Paternostro, W. Son and M. S. Kim, quant-ph/0310031.
- [83] D. Stoler, Phys. Rev. D **1**, 3217 (1970).
- [84] H. P. Yuen, Phys. Rev. A **13**, 2226 (1976).
- [85] C. M. Caves, Phys. Rev. D **23**, 1693 (1981).
- [86] W. H. Zurek, Phys. Rev. D **26**, 1862 (1982); E. Joos and H. D. Zeh, Z. Phys. B **59**, 223 (1985).

- [87] D. M. Greenberger, M. A. Horne, and A. Zeilinger, *Am. J. Phys.* **58**, 1131 (1990).
- [88] J. W. Pan, D. Bouwmeester, M. Daniell, H. Weinfurter and A. Zeilinger, *Nature (London)* **403**, 515 (2000).
- [89] D. N. Matsukevich, T. Chanelire, S. D. Jenkins, S.-Y. Lan, T. A. B. Kennedy, and A. Kuzmich, *Phys. Rev. Lett.* **96**, 030405 (2006).
- [90] J. Volz, M. Weber, D. Schlenk, W. Rosenfeld, J. Vrana, K. Saucke, C. Kurtsiefer, and H. Weinfurter, *Phys. Rev. Lett.* **96**, 030404 (2006).
- [91] A. Ferreira, A. Guerreiro, and V. Vedral, *Phys. Rev. Lett.* **96**, 060407 (2006).
- [92] W. J. Munro, D. F. V. James, A. G. White and P. G. Kwiat, *Phys. Rev. A* **64**, 030302 (2001); T.-C. Wei, K. Nemoto, P. M. Goldbart, P. G. Kwiat, W. J. Munro and F. Verstraete, *Phys. Rev. A* **67**, 022110 (2003).